Flood modelling using data available on the Internet

M.J. Pretorius

Dissertation presented for the degree of M.Sc. (Eng.)
In the Department of Geomatics
University of Cape Town
August 2011

Plagiarism declaration

I know the meaning of plagiarism and declare that all the work in the document, save for that which is properly acknowledged, is my own.

Abstract

The aim of this study was to determine if sufficient data at no charge is available on the Internet to use as input to a free and open source hydrological model for use in a flood monitoring system. As such, the monitoring system would be SensorWeb enabled. The study area is the C83A quaternary catchment (746 km^2) in the Northern Free State, part of the Vaal primary catchment in South Africa. The catchment has a response time of approximately 13 hours and so sub daily calculation steps were required in the hydrological model. The data that were available on the Internet to use as input to a hydrological model were: catchment boundaries, river lines, a digital elevation model, soil texture, land use, evaporation rates, flow rates and rainfall estimates from the Tropical Rainfall Measurement Mission (TRMM) 3B42 data product. Data from off-line sources were also used and all data were free for research purposes. After determining the requirements for the model and evaluating a number of models, the Storm Water Management Model (SWMM) was chosen as hydrological model. The coarseness of the available input data necessitated a coarser model than is the norm for SWMM. Nevertheless, the calibrated model performed well overall. It had Nash-Sutcliffe (N-S) correlations of 0.80 and 0.73 for the calibration and evaluation periods respectively. The model performed best during dry periods and inadequately during the rainy season (N-S correlation of 0.31) and was therefore not suitable for use in a flood monitoring system. An additional investigation into the model and the TRMM 3B42 rainfall estimates indicated that the SWMM model follows physical principles and that it can model total flow volumes to within 0.31% of measured values using physically realistic parameters. However, it cannot adequately model the shape and amplitude of the outflow hydrograph during rainy periods. Therefore, the inadequate model performance during wet periods is most likely due to the coarse time and spatial resolution of the 3B42 rainfall estimates relative to the size of the catchment. Such smaller catchments do need to be studied though, because it is the under-resourced authorities in charge of small catchments who may benefit from a flood monitoring system that uses free data from the Internet and open source software.

Acknowledgements

I would to thank the following people and institutions who helped during this project:

Computational Hydraulics International, especially Bill James, who provided the PCSWMM software free of charge and who gave generously of his time to help me along the steep learning curve of hydrological modelling.

Dr. Julian Smit, my supervisor, for all his help and suggestions.

UCT and The Meraka Institute at the CSIR for financial assistance.

Scott Sinclair for advice on how to get started, providing the TOPKAPI model, and some Python assistance.

David Townsend (Aurecon), Neil Armitage (UCT), Kevin Winter (UCT) and Dylan Kime (DHI) for advice on models and their possibilities and some source code (David).

For providing data free of charge: NASA, USGS, SAWS (Elsa de Jager and Estelle deConing in Pretoria), DWA (Juanita Jacobs and Nicolene Fourie in Pretoria and Chris Lloyd in Bloemfontein) and CD:NGI in Mowbray, Cape Town.

My partner Karin, for lending me her chair.

Table of Contents

List of Tables

List of Figures

List of Abbreviations

3B42	TRMM 3-hourly satellite rainfall estimates data product (research product)
3B42RT	TRMM 3-hourly satellite rainfall estimates data product (real-time product)
AMSR-E	Advanced Microwave Scanning Radiometer-Earth Observing System
AMSU-B	Advanced Microwave Sounding Unit-B
AVHRR	Advanced Very High Resolution Radiometer
BWO	Bethlehem Weather Office
CHI	Computational Hydraulics International
cm	centimetre
CPC	Climate Prediction Center
CSIR	Council for Scientific and Industrial Research
db	decibel
DEM	Digital Elevation Model
DWA	Department of Water Affairs
EPA	Environmental Protection Agency
FAO	Food and Agricultural Organisation
FAR	False Alarm Rate
GB	Gigabyte
GCRD	Global Composite Runoff Data
GDS	Global Daily Summary (climate data from the US National Climate Data Center)
GeoSFM	Geospatial Streamflow Model
GHz	Giga Hertz
GIS	Geographical Information System
GPCP	Global Precipitation Climatology Project
GPS	Global Positioning Satellite
GRASS	Geographical Resources Analysis Support System
GSOD	Global Surface Summary of the Day (climate data from the US National Climate Data Center)
GTOPO30	USGS DEM for the world with 30 arc second resolution
h	hour
ha	hectare
HEC-HMS	Hydrologic Engineering Center's – Hydraulic Modeling System
HEC-RAS	Hydrologic Engineering Center's – River Analysis System
HQ	High Quality
HTML	Hyper-Text Mark-up Language
HWSD	Harmonised World Soil Database

IHACRES	Identification of unit Hydrographs And Component flows from Rainfall, Evaporation and Streamflow data
ILLUDAS	Illinois Urban Drainage Area Simulator
IR	Infrared
ISO	Input Storage Output
Kineros2	KINematic runoff and EROSion
km	kilometre
LIDAR	Light Detection and Ranging
m	metre
MAE	Mean Absolute Error
MB	Megabyte
min	minute
mm	millimetre
MODIS	Moderate Resolution Imaging Spectrometer
N.A.	Not Applicable
NASA	North American Space Administration
NCDC	National Climatic Data Centre
NOAA	National Oceanic and Atmospheric Administration
N-S	Nash-Sutcliffe
PERSIANN	Precipitation Estimation from Remotely Sensed Information using Artificial Neural Networks
PM	Passive Microwave
POD	Probability Of Detection
RMS	Root Mean Square
RMSE	Root Mean Square Error
RT	Real Time
s	second
SAWS	South African Weather Service
SBRE	Satellite-Based Rainfall Estimates
SCS-CN	Soil Conservation Science – Curve Number (the previous name of the USDA-NRCS-CN method)
SHE	Système Hydrologique Europeen
SLURP	Semi-Distributed Land-Use Runoff Process
SRTM	Shuttle Radar Topography Mission
SSM/I	Special Sensor Microwave Imager
SWMM	Storm Water Management Model
TCI	TRMM Combined Instrument
TIN	Triangulated Irregular Network
TMI	TRMM Microwave Imager

TMPA	TRMM Multisatellite Precipitation Analysis
TOPMODEL	TOPographic Index MODEL
TRMM	Tropical Rainfall Measurement Mission
TSDIS	TRMM Science Data and Information System
UK	United Kingdom
US	United States
USDA-NRCS-CN	United States Department of Agriculture, Natural Resources Conservation Service Curve Number
USGS	United States Geological Survey
UTM	Universal Transverse Mercator
WERRD	Water and Ecosystem Resources in Regional Development
WO	Weather Office
μm	micrometer

1. Introduction

1.1 Problem statement

Floods are one of the common natural disasters occurring all over the world and they can be very destructive. The South African Risk and Vulnerability Atlas indicates that parts of all South Africa's provinces are at risk of floods (Department of Science and Technology, 2010, p.5). Gauteng, the Northern Cape, the Free State and Kwa-Zulu Natal experienced damaging floods in the summers of 2010 and 2011. The 2011 floods killed more than 100 people (Smith, 2011) and damaged infrastructure to the value of R 160 billion (Vecchiato, 2011). In Australia , floods submerged Brisbane in dirty brown water in January 2011 (Greer, 2011), killed at least 17 people and caused billions of dollars' worth of damage (Davies, 2011). Pakistan experienced its worst floods in history in August 2010, affecting 18 million people and killing 2 000 (Alertnet, 2011). The Organization for Economic Cooperation and Development found that coastal flooding alone caused US $3 trillion damage worldwide in 2007. China's Yellow River valley has claimed millions of lives during the last century (National Geographic, n.d.).

Floods can take hours or days to develop, depending on the size of the catchment and the extent of the rainfall, and so a flood monitoring system that can use a model to predict in a few minutes what may happen in the next few hours, would be very useful to help reduce deaths and damage from floods. Such a system should ideally automatically run the hydrological model as new rainfall data becomes available and display the computed results graphically for decision makers. The result display should include some form of warning when the computed flows and flood extents are extraordinary.

This project forms part of the Meraka Institute's research theme to use earth observation and SensorWeb technologies for disaster management. The Meraka Institute is part of the Council for Scientific and Industrial Research (CSIR).

1.2 Research objectives

This research evaluates if is possible to construct a real-time flood monitoring system using only free data available from the Internet and free software. The system should consist of a hydrological model that calculates runoff from rainfall input, and an inundation model that determines the extents of rivers as the flow through them changes. The output should be visualised on a map.

1.3 Research questions

This project aims to answer the following research questions:

a) Is sufficient hydrological data for the study area available on the Internet to use as input to a hydrological model?

b) Is a hydrological model available that is free and open source and that can use the available data as input?

c) Can the hydrological model predict the stream flow in the study area with a Nash-Sutcliffe (N-S) correlation between observed and calculated flow of 0.8 or better?

d) Can the output of the hydrological model be used to determine the extents of rivers in the study area based on their calculated water levels?

e) Can these models and data be combined in a real-time flood monitoring system?

1.4 Hypotheses

This project will test the following hypotheses:

a) Sufficient hydrological data for the study area are available for free on the Internet to use as input to a free and open source hydrological model.

b) The hydrological model can predict the flow at the outlet of the catchment with a Nash-Sutcliffe (N-S) correlation of 0.8 or better between observed and calculated flow.

1.5 Scope and methods

1.5.1 Study area

This study focuses on South Africa's quaternary catchment C83A (746 km^2), shown in Figure 1 on page 5, which is part of the Vaal primary catchment. C83A was selected on the advice of an expert in the field who noted that this area of the country is relatively well gauged and its terrain is relatively uniform. Satellite-based rainfall estimates (SBRE) tend to perform badly in complex terrain (Sinclair, S (2010), pers. comm., March 5). This study area is covered in agricultural fields and grass lands.

The nearest town, Bethlehem, received on average 638 mm rain per year between 1993 and 2009, with most of it occurring during midsummer[1]. Rain falls generally in the form of convective thunderstorms. The elevation in the catchment ranges from about 1 600 m to 2 500 m above sea level with an average slope of 10.22%. The slope ranges from very steep in the mountains bordering on Lesotho (78.56%) to very flat on the plains near the outlet (0.22%)[2].

Midgley et al. (1994) give the mean annual precipitation for this catchment as 600 mm to 800 mm (Map 1.1 in Midgley et al., 1994) and they give the mean annual runoff as 20 mm to 50 mm (Map 9.1 in Midgley et al., 1994). Therefore, the proportion of rainfall that becomes runoff in this catchment ranges from 0.033 to 0.063. This is also called the runoff coefficient.

[1] Calculated from data ranging from 1 March 1993 to 31 March 2010, received from the South African Weather Service.
[2] All elevation and slope values from Shuttle Radar Topography Mission 90 m Digital Elevation Model.

In the western part of the catchment is the Ash river, which receives water from the Katse dam in Lesotho through a tunnel transfer (see Figure 1 on page 5 for the location and Figure 2 (a) on page 6 for a photograph of the tunnel outlet). At the outlet of the transfer tunnel the Department of Water Affairs (DWA) has a flow meter, C8H036, that measures the inflow from Lesotho. This inflow has a marked daily and weekly cycle, probably because the water flows through a hydro-electric power station in Lesotho and the flow cycle reflects changes in electricity demand through the work day and the work week (Lloyd, C, 2010, pers. comm., November 25).

In the North West corner of the catchment is the Saulspoort dam (surface area of 443 ha and capacity of 16 million cubic metres at full service level), just before the outlet to the catchment. The Katse inflow is attenuated by the time it reaches the Saulspoort dam (see Figure 2 (b) on page 6), where DWA gauge C8R004 measures the outflow from the dam just behind the dam wall. C8R004 also measures the water level in the dam. The inflow from Lesotho ensures that significant amounts of water flow through the catchment outlet, even during the dry winter months. In Figure 2 (b) the green line represents the measured flow at the Katse inflow and the red line represents the measured flow at the Saulspoort dam.

The coordinate system used in this project is South African Longitude (SA Lo) 29° East. It is a Transverse Mercator projected coordinate system, centred on longitude 29° E and latitude the equator. It uses metres as unit and the WGS84 ellipsoid as the datum.

1.5.2 Study period

The model in this study covers the period from 1 November 2004 to 31 October 2005 (calibration) and 1 November 2005 to 31 October 2006 (evaluation). Section 7.1 on page 73 explains the reasons for choosing this period. Some of the other data available and used for statistical analysis cover wider periods, for example the rainfall record at the Bethlehem Weather Office (BWO).

1.5.3 Data

Most of the data used in this project comes from the Internet sources and all the data is free for use in research projects. Table 1 lists the major data used in this project and their sources. Chapter 5 on page 58 gives more detail on all the data used. It should be noted that radar rainfall data would have been ideal for this project, but the South African Weather Service (SAWS) does not make real-time radar data available to projects such as this one and it does not have a system set up to make historical radar rainfall available (DeConing, E, (2011) pers. comm., August 10).

Table 1: Major data sources used in this project

Description	Source	On Internet?	Free?
Tropical Rainfall Measurement Mission (TRMM) 3B42 rainfall (v.6)[3]	North American Space Administration (NASA)	Yes	Yes
Bethlehem Weather Office rainfall	SAWS	No	Yes, but only for research.
Shuttle Radar Topography Mission (SRTM) 90 m Digital Elevation Model (DEM)	NASA Jet Propulsion Laboratory	Yes	Yes
Rivers	DWA	Yes	Yes
Catchments	DWA	Yes	Yes
Evaporation rates	DWA	Yes	Yes
1:50 000 topographic data	Chief Directorate: National Geospatial Information (CD:NGI)	No	Yes

1.5.4 Hydrological model

The model chosen for this project is the Storm Water Management Model (SWMM). SWMM is available for free from the United States (US) Environmental Protection Agency (EPA) and it can model overland flow as well as channel flow. Engineers and researchers all over the world use it to model both urban and rural study areas. Section 4.3 on page 56 explains further the reasons for choosing this model and Section 3.10 on page 36 describes how SWMM works.

1.5.5 Real-time monitoring system

Figure 3 shows a high-level design for a real-time flood monitoring system. The controlling program could run in Python, since this language easily interfaces with Geographical Information System (GIS) packages, such as GRASS, ArcGIS and QuantumGIS. Both GRASS and QuantumGIS can publish maps to the web. The system would only simulate real-time monitoring since the study period is in the past. The TRMM SBRE become available nine hours after the measurements took place (Huffman, 2007), so any implementation of such a system can be quasi real time at best. The implementation of this system depends on whether the models can adequately represent the measured values.

An initial investigation into the DEMs available to this project (the STRM 90 m DEM and, later on, a 20 m DWA DEM) indicated that neither of these two DEMs had fine enough spatial resolutions to find the river cross section profiles required for inundation modelling. Without inundation modelling the results of a hydrological model are difficult to visualise in GIS and therefore the real-time monitoring system was not pursued.

[3] The version number refers to the version of the algorithm that generated the SBRE.

Inundation modelling is still presented in the review of previous work and the theory to indicate why the DEM plays such an important role in this type of modelling.

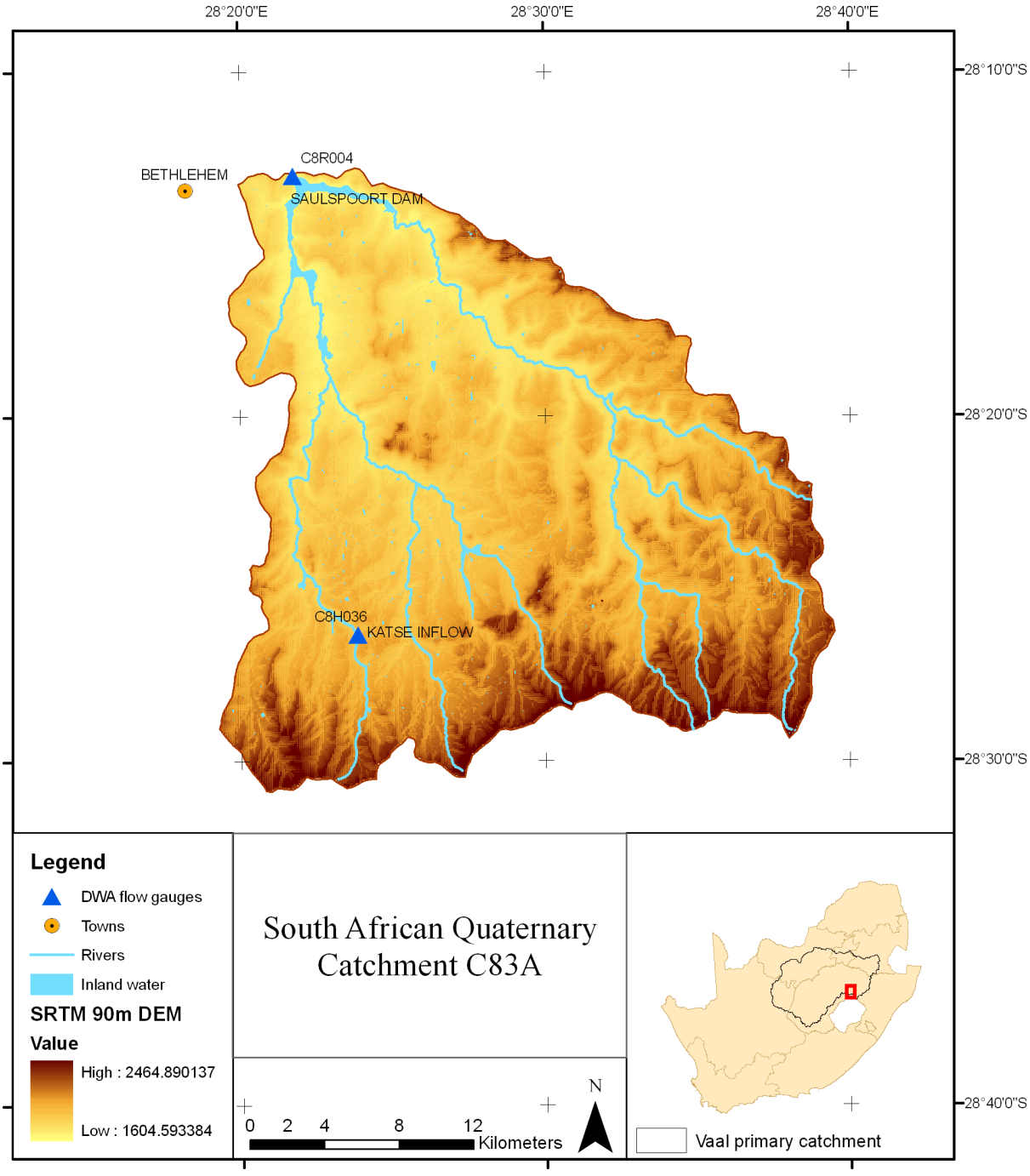

Figure 1: Study area overview

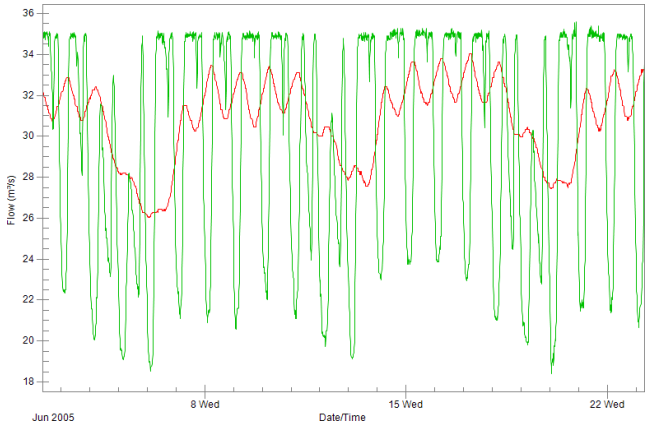

(a) Katse outlet tunnel[4]

(b) Flow attenuation from the Katse outlet (green) to the Saulspoort dam (red)

Figure 2: Water transfer from Lesotho to the C83A catchment

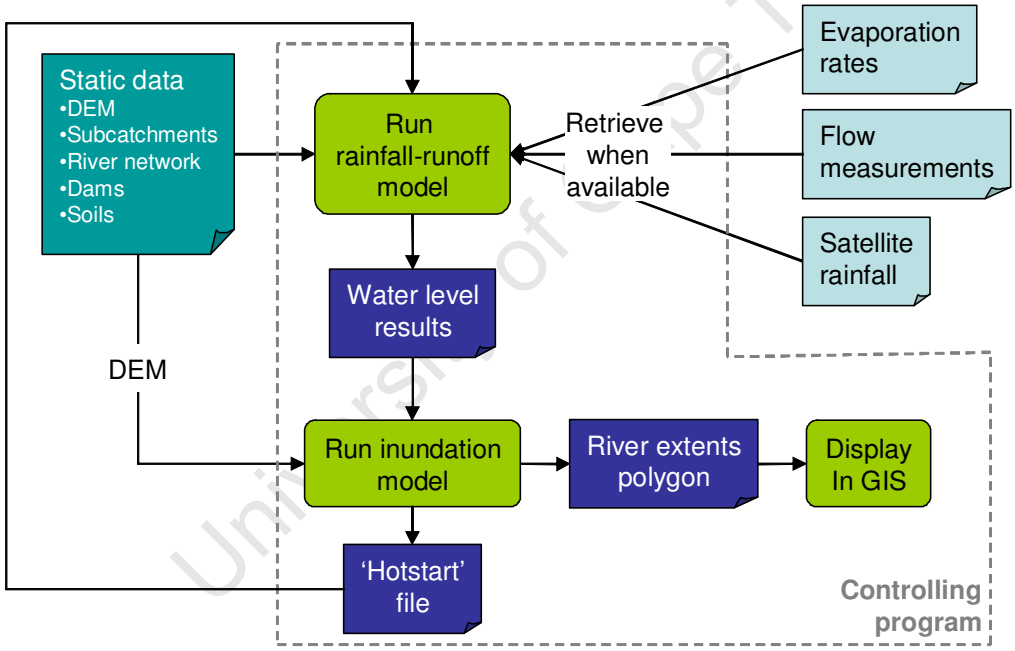

Figure 3: Real-time flood monitoring system overview

The 'hotstart' file in the monitoring system enables the model to use the result of the previous model run as a starting point for the next run. This drastically cuts down run time as the amount of data in the model increases over time. An example of such a system implemented using PCSWMM is available online[5]. This downloads radar rainfall as input every five minutes and calculates the predicted flow and inundation extents in less than two minutes.

[4] Image retrieved from http://www.dwaf.gov.za/Hydrology/RTGraphImage.aspx?Station=C8H036&Type=Photo on 11 July 2011.
[5] http://www.chiwater.com/pcswmmrtdemo/. Retrieved 15 July, 2011.

1.5.6 Software

A variety of software packages were used in this study. Table 2 lists the software, their versions and uses.

Table 2: Software used in this project

Name	Version	Free?	Use
ArcMap	9.3	No	Making presentation maps for this document.
GRASS GIS	6.4.0 6.4.1	Yes	Testing r.sim.water module. Subcatchment delineation, surface interpolation, generating profiles.
PCSWMM	4.2.915	No	Data processing, visualisation, SWMM model calibration and evaluation. (PCSWMM uses SWMM as its computational engine.)
Python	2.6.x 2.7	Yes	Scripts to download and process data from Internet sources. Read SWMM output files.
QuantumGIS	1.7.0	Yes	Data visualisation and vector analysis.
SWMM	5.0.018	Yes	Hydrological modelling.

1.6 Beneficiaries of the research

South Africa's rain gauge network is in decline because of poor maintenance (Lynch, 2004) and rainfall measurements are crucial to flood monitoring. Many South African municipalities (especially the smaller ones) don't have the financial or human resources to set up or maintain a flood monitoring system. Such authorities would benefit greatly from a system that could be set up once and then use rainfall data from the Internet as input from there on. Thus only an Internet connection would be needed for local authorities to monitor imminent floods.

A further advantage of using SBRE in flood monitoring is that the sensor itself doesn't risk being destroyed in the flood, as ground-based gauges do.

1.7 Structure of this document

The rest of this document describes the research conducted and project executed to evaluate the research questions and to evaluate the hypotheses.

Section 2 describes previous studies that are relevant to this project because they used similar data, models or methods. Section 3 describes the theory of the models, methods and data relevant to this project. Section 4 describes the requirements for the hydrological model, the models reviewed and the one selected. Section 5 lists the data sources selected and used as input to the hydrological model. Section 6 describes the methods used to prepare the data and to construct the hydrological model. This includes selecting periods to model. Section 7 presents the results of the SBRE analysis and the model runs. Section 8 discusses the results and suggests possible future avenues of research.

2. Review of previous work

Researchers use the term 'flood' in a variety of senses: a) river *flow volumes* greater than a selected statistical measure; b) river *stages* above a selected statistical measure; and c) the areas that river waters cover after heavy rains, or *inundation*. Excess rainfall causes overland flow that runs into rivers. Along with exfiltration from groundwater, these two sources generate river flow. In a flood, the river bursts its banks and inundates the adjacent land. A complete flood model therefore consists of three sections: overland flow modelling, channel flow modelling and flood inundation modelling. Rainfall-runoff modelling usually covers only overland flow modelling and channel flow modelling.

The following sections focus on the models that researchers used and the results that they found. Section 2.4 on page 16 lists studies that used remotely sensed data in some form. Since SWMM was chosen as the model for this project, Section 2.1.1 on page 10 and Section 2.1.2 on page 12 describe studies that used SWMM in rural and urban settings respectively. (Model selection for this project is discussed in Section 4 on page 54.)

2.1 Rainfall-runoff modelling

Beven (2001, p. *x*) notes in the preface to his book that the number of rainfall-runoff models available already exceeded 100 in the 1970s. He also quotes Robin Clarke who stated in 1974 that water resources modelling is subject to inflation: the number of models is increasing all the time. This text therefore covers only the models found during the literature search, which was aimed at studies relevant to this project.

Lacroix et al. (2000) used the Semi-Distributed Land-Use Runoff Process (SLURP) rainfall-runoff model in their model of the Küçük Menderes Basin (3 617 km^2), Turkey. They used only data available from the Internet and a model time step of 1 day. To verify their model, they compared the computed monthly flows to measured monthly flows for four years of data. The first three years gave a mean flow error that was 73% of the observed mean. Adding the last year, the error increased to 121% of the mean. They attribute the poor results in the last year to changes in weather patterns or to that fact that the precipitation stations no longer adequately represented the basin precipitation.

McIntyre and Al-Qurashi (2009) compared the performance of adaptations of the Identification of unit Hydrographs And Component flows from Rainfall, Evaporation and Streamflow data (IHACRES) model, a physics-based model, a KINematic runoff and EROSion (Kineros2) model and a 2-parameter regression model applied to a 734 km^2 arid catchment in Oman. They achieved a best error in time of peak flow of 53% (using the 4-parameter event-based IHACRES model) and in flow volume of 36% (using the 3-parameter event-based IHACRES model). They concluded that none of the models gave impressive performances for time of peak flow or flow volume predictions. However, they note that hydrological modelling is much more

difficult in arid regions than in humid regions and, in this context, the models' performances were 'not disappointing'.

Using the Xinanjiang rainfall-runoff model, Li et al. (2008) modelled the runoff in the Nzoia River basin (12 696 km^2) in East Africa with TRMM SBRE as rainfall input. The Xinanjiang model dates from the 1970s and is appropriate for humid and semi-humid regions (Li et al., 2008). These modellers achieved an N-S correlation of 0.67 in the evaluation period and 0.84 in the calibration period; they call these results "reasonable". They used a model time step of one day and calibrated the model separately using ground-based rain gauge data and SBRE before evaluating the model using satellite rainfall. They found that the model performed better when they calibrated it with the SBRE.

Jia et al. (2009) developed their own precipitation-runoff correlation curve method to predict runoff in Beijing (16 400 km^2 catchment). They developed a distributed model with a 1 km by 1 km grid cell size. The model calculates surface runoff using a runoff coefficient dependent on land cover. It also calculates subsurface runoff and evaporation. Surface runoff, subsurface runoff and evaporation combine to give precipitation-runoff curves for three types of areas: urban, mountainous and plain. The results from the rainfall-runoff model were integrated into a real-time web-based GIS system used for water resource assessment and flood regulation. They achieved a best relative error in calculated flow of 3%. This system has been operational in Beijing since 2005.

Using the TOPographic Index MODEL (TOPMODEL), Hossain et al. (2006) simulated the runoff in the Posina catchment in Italy (116 km^2) and used it to determine a satellite rainfall error model. They do not provide numerical accuracy assessments in their article, but the calculated vs. observed hydrographs look reasonably accurate.

To develop a flood monitoring system for the Limpopo basin (400 000 km^2), Asante et al. (2007) used the Geospatial Streamflow Model (GeoSFM), an extension of ArcView and TRMM rainfall data. They used the SBRE as input to the rainfall-runoff model to establish baseline climatology for identifying 'extreme' events (events in which the flow was 1.5 standard deviations above the short-term mean annual flow). They found that the climatology stabilised after five years of data. Since they did not verify the model results against stream flow measurements, they used the streamflow forecasts primarily as a trigger to verify a forecasted extreme event from field sources.

Ye et al. (1998) extended the IHACRES model for use in an ephemeral, low-yielding Australian catchment of 544 km^2 by adding two parameters to this conceptual model. The extended IHACRES model achieved a best N-S correlation in calculated flow of 0.86 during the verification period, compared to the standard IHACRES model's best result of 0.57. Aggregating the flow calculations from daily to monthly values improved the extended IHACRES model's performance to 0.96.

To research the usability of remotely sensed data to improve results from run-off models, Schultz (1996) used various rainfall-runoff models, but gives numerical accuracy for one only: a nonlinear reservoir model using hydrologically similar units in the Alsdorf/Nims catchment (264 km^2) in Germany. He used Landsat imagery to classify land uses, which contributes to model the water storage capacity of the soil in the study area. This model achieved an N-S correlation of 0.90 for its validation period.

Melesse et al. (2003) also investigated using remotely sensed data to estimate changes in runoff for three watersheds in Florida – Etonia (114 km^2), Econlockhatchee (size not given), and S-65A (size not given). They used the United States Department of Agriculture, Natural Resources Conservation Service Curve Number (USDA-NRCS-CN) method to determine the run-off and integrated it with a GIS to create a distributed model. For individual storm events their model achieved N-S correlations ranging from 0.75 to 0.99.

Hong et al. (2007) used the NRCS-CN method to estimate runoff from rainfall for the whole world between 50°N and 50°S. They used only data available on the Internet: TRMM rainfall, Food and Agricultural Organization (FAO) soil data, Moderate Resolution Imaging Spectrometer (MODIS) land classification, the Global Composite Runoff Data (GCRD) and data from HYDRO1k[6] for routing information. They calculated the runoff per day and achieved a 0.75 correlation between the calculated runoff and GCRD values. Artan et al. (2007) also assessed satellite rainfall to predict runoff in large basins: the Nile river basin in Africa (6 000 km^2) and the Mekong river basin in Asia (22 000 km^2). They used the GeoSFM model and achieved a best N-S correlation of 0.81.

Using TOPMODEL as a starting point for two models and the Xinanjiang model as a starting point for another, Li and Zhang (2008) developed three rainfall-runoff models and compared their performance in a sub-basin of the Yellow River, China (4 716 km^2). Ground-based rain gauges provided the rainfall data. All the models performed 'well', but a gridded model based on TOPMODEL performed the best, achieving an N-S correlation of 0.97 for one of the floods in the study.

Yang et al. (2004) coupled a distributed hydrological model with reservoir operations to create a flood management system for a 1 300 km^2 catchment in Japan. They adjusted the geomorphology-based hydrological model (GBHM) (that Yang had developed in an earlier study) to model rainfall-runoff. They give only graphical results for their model, but note that the coupled model 'successfully simulated releases from the reservoirs'.

2.1.1 SWMM models in rural areas

Jang et al. (2007) wanted to improve the method to study the hydrologic impact of urbanisation on three rural watersheds (8.51 km^2, 33.63 km^2 and 55.93 km^2) in Korea. Typically, engineers use synthetic hydrograph methods for pre-and post development conditions or they use a synthetic hydrograph for pre-development

[6] HYDRO1k is a geographic database that provides global coverage of topographically derived data sets, including streams, drainage basins and ancillary layers derived from the United States Geological Survey's 30 arc-second DEM.

and an urban hydrology model for the post-development condition. The synthetic hydrograph method doesn't adequately model the drainage structure in the post-development condition and the combination of a synthetic hydrograph and an urban hydrology model are difficult to compare because of the different model conceptualisations and parameterisations (Jang et al., 2007). To overcome these problems, Jang et al. (2007) modelled both the pre- and post-development conditions using SWMM. They found that an *uncalibrated* SWMM model calculated the flow rates pre-development usually to within 10% of the measured values, although one event had a 40% error. These researchers concluded that SWMM is equally as applicable to natural watersheds as the synthetic hydrograph method and that it performed better for some events.

Chung et al. (2011) used SWMM to study the impact of urbanisation on water quality. Their study area was a 56 km^2 Korean watershed with predominantly forest and agricultural land use (69%) and the rest urban. Their model had an N-S correlation of 0.65 in flow rate for the verification period of the pre-development scenario. In another pre-and post-development discharge study, Pomeroy et al. (2008) applied SWMM to a 93 ha study area consisting mostly of pasture land and natural prairie in Kansas, US. They do not give error estimates of the modelled results, only hydrographs of the increase in runoff for different development scenarios.

The City of Austin wanted to develop a tool that could explicitly represent the physical processes governing water quantity and quality in the Barton Creek watershed and so they commissioned a study by their Watershed Protection and Development Review Department (City of Austin, 1997). The study area was 311 km^2 of Texas Hill Country from the headwaters of Barton Creek to its confluence with the Colorado River near downtown Austin, Texas. The area was 11% urbanised at the time of the study. These researchers provide their results as hydrographs only, but they comment that the overall volume comparison is 'good' and that the peak comparison is 'satisfactory'. They conclude that the Barton Creek SWMM Model can accurately predict flow quantities above the recharge zone and that it can predict changes in base flow[7] and direct runoff quantities resulting from changes in impervious land cover.

Jun et al. (2010) used the SWMM Groundwater Edition to analyse the relationship between long-term stream discharge and the changes in groundwater use in the Gapcheon watershed (649 km^2), Korea. The subcatchments had an average percent impervious area of 12%. The SWMM model's calculated runoff in the catchment had a correlation coefficient of 0.81 with the observed runoff.

El-Sharif (1998) used SWMM to see if he could reproduce the results of an earlier, more complex hydrological and hydraulic model that was based on the solution of the gradually-varied unsteady flow equations (the St. Venant equations). The study area was the catchment of the Salmon and North rivers drainage area (730 km^2) in Nova Scotia, Canada. El-Sharif (1998) reports the results as graphs of river stages only and graphs of differences between the two models. Differences between the two models' calculated river stages

[7] Base flow refers to sustained or dry-weather runoff, including water draining from natural storage in groundwater bodies, lakes and marshes and delayed subsurface runoff.

range between –1 m and +1 m. The SWMM model results matched those of the earlier model better for the 20-year return period design storm than for the 100-year return period design storm. He concluded that SWMM successfully reproduced the maximum water profiles with an adequate accuracy.

2.1.2 SWMM models in urban areas

Barco et al. (2008) applied SWMM to an urban catchment (217 km^2) in Los Angeles for 10 storms. They found an average relative error of 28.5% in calculated total volume and 26.4% in peak flow. The SWMM model predicted these two parameters worst for the smaller storms.

In their study of criteria to compare models, Green & Stephenson (1986) applied three rainfall-runoff models (WITWAT, SWMM and Illinois Urban Drainage Area Simulator (ILLUDAS)) to an urban catchment in Pinetown (size not given), South Africa. The WITWAT model and SWMM models performed similarly (N-S correlation of 0.68 and 0.67 respectively), while the ILLUDAS model performed poorly with an N-S correlation of 0.33.

Chen and Adams (2007) used the results of a SWMM model as standard to evaluate their own analytical rainfall-runoff model. The study area was a 36.3 ha catchment in Toronto, Canada. The SWMM model's predicted runoff correlated to a value of 0.93 with the observed runoff. The analytical model's calculated annual runoff came within 2.1% of the SWMM model's value.

Xiong and Melching (2005) used a simulated urban watershed to determine the effect of different storm durations on the results from kinematic-wave and nonlinear reservoir routing of urban watershed runoff. SWMM uses non-linear reservoirs to calculate runoff and their SWMM model gave 'acceptable' results for storms with durations longer than the watershed time of concentration[8] (average N-S correlation of 0.88). However, for storms that are shorter than or equal to the time of concentration, they obtained poor results (average N-S correlation of 0.07). In general they achieved more accurate results with the Dynamic Watershed Simulation Model, which uses kinematic-wave routing, especially for the short storms (N-S correlation of 0.81).

Tsihrintzis and Sidan (2008) compared the performance of five rainfall-runoff models in four urban sites (5.97 to 23.57 ha): the ILLUDAS ILUDRAIN, Penn State Runoff Quality Model (PSRM-QUAL), the Santa Barbara urban hydrograph method (SCS-SBUH), the United States Geological Survey (USGS) Distributed Routing Rainfall–Runoff Model (DR3M) and SWMM. On the commercial land use site ILUDRAIN and SWMM gave the best peak flow results for the verification runs with correlations of 0.94 and 0.86 respectively. However, SWMM had the smaller mean percentage error: 6.54% compared to 14.88% for ILUDRAIN. On the high density residential site, SWMM predicted peak flow best with an R^2 of 0.99 and mean percentage error of –1.14%. The authors concluded that the predictions from all the models showed

[8] The time of concentration is the time between the start of a runoff event and the time when the entire watershed is contributing flow.

good agreement with the observed data but that predictions were generally better for the more impervious sites (commercial and high density residential).

In a study that compared the Soil Conservation Science – Curve Number (SCS-CN) method and SWMM, Solanki and Suau (1996) modelled the peak discharge rates for 15 urban watersheds in Florida, US. Imperviousness ranged from 0 to 85% and the sizes of the watersheds ranged from 0.36 km^2 to 40 km^2. The SWMM calculated peak discharge rates had errors ranging from –19% to 48% with a mean of 9%. The authors concluded that 'SWMM yielded fairly good agreement between observed and estimated runoff in urban and rural watersheds.

Schmidt et al. (1997) investigated if SWMM could be used for water resource conservation planning in Volusia County, Florida, USA. The study area was 116 km^2 and consisted of wetlands and urban areas. SWMM modelled the flow for the calibration month to within 7% of the measured flow and it computed annual flow to within 12% of the measured flow.

In a study to compute the effects of urbanisation on the water balance and water quality in a high recharge area, Graham et al. (1997) applied SWMM to a 4 834 km^2 study area that includes the Ohio River around Cincinnati, USA. The two hydrographs shown for two calibration events show that SWMM models the total volume in a 24 hour period to within 21% and 3%. Xie et al. (1997) modelled faecal coliform in Mill Creek, which has a 60 km^2 catchment in the Cleveland, US. During the 3-day evaluation event, SWMM modelled the flow to within 10% of the measured values.

Nye et al. (2005) used SWMM to create a continuous model of surface runoff, groundwater and water quality in a 105 km^2 basin in Florida, US. Their model computed flow volume to within 11.9%, peak flow to within 6% and peak stage to within 1.5% of the measured values for an eight-day event.

Using SWMM's Extended Transport (EXTRAN) module (the hydraulic modelling part of SWMM), Tsihrintzis et al. (1998) modelled the effect of wetlands on flood detention. Their study area was a 142 ha wetland mitigation bank in the city of Pembroke Pines, Florida, US. It consisted of mostly vegetated areas connected by culverts, channels and weirs. Their calibrated model had a correlation of 0.93 between measured and predicted flows and 0.85 between measured and predicted stages. Shamsi and Schneider (1993) created an SWMM hydraulic model of the sewage system in Alleghny County, Pennsylvania, US. During dry weather flow calibration, the model computed a flow and volume only 1.93% different from the observed volume and mean flow during a 24 hour period. During wet weather flow calibration, SWMM computed the flow volume to within 7.7% of the measured flow during a 24 hour period and it computed the peak flow to within 5.5% of the measured peak flow.

2.2 Inundation modelling

Using the Hydrologic Engineering Center's River Analysis System (HEC-RAS), Baldassarre et al. (2009), modelled the inundation around a 98 km reach of the river Po in Italy during a flood event. This river is up to 4 km wide in the study area. They verified the modelled flood extent using satellite radar imagery with a 100 m pixel size. HEC-RAS modelled the water level in the river to within 4% compared to a gauging station, and the inundation extent had a mean absolute error of 400 m. These modellers attributed the poor inundation prediction to the fact that the model had been calibrated against a high-magnitude flood event and evaluated against a low-magnitude flood event.

Matgen et al. (2007) conducted a similar study, also using HEC-RAS, on a 10 km stretch of the River Alzette in Luxembourg. This river has an average width of 300 m. These modellers used satellite radar imagery with a ground pixel size of 25 m to verify their model's water level rather than just the extent of the flood. They found that the radar data on its own is not accurate enough for hydraulic modelling, with errors of up to 2 m in water levels. They then applied a multiple linear regression model to water levels after classifying the original radar image using a thresholding and active contour model approach. In this way, they improved the accuracy of the calculated water level to a Root Mean Square Error (RMSE) of 41 cm.

Horritt and Bates (2002) used a statistical active contour model to delineate flood extent in a 60 km reach of the river Severn, UK, from satellite radar imagery. They then used this flood extent to determine how accurately three inundation models, namely TELEMAC-2D, LISFLOOD-FP and HEC-RAS could predict the same two flood events. The first two models are two-dimensional models while the third is a one-dimensional model. They found that HEC-RAS marginally out-performed TELEMAC-2D for the evaluation event. Both these models predicted at best around 65% of the inundation extent. LISFLOOD-FP performed worst, although not by much.

2.3 Complete flood modelling systems

Complete modelling systems (as defined in Section 2 on page 8 of this text) are scarce in literature. Two Water Research Commission reports (Sinclair and Pegram, 2004 and Makwananzi and Pegram, 2004) describe a full flood modelling system created for the Mgeni river's Mlazi Catchment (955 km^2) in the Ethekwini municipality (Durban). The project team had access to the following data:

- real-time SAWS rain gauge data
- real-time SAWS radar rainfall data
- real-time river flow data from DWA
- a detailed land use map created by an engineering firm
- measurements of hydraulic structures (such as bridges and culverts) from fieldwork
- channel cross-sections, vegetation cover and water flow depth from fieldwork

- 1:2 000 orthophotos of the river reach
- 2 m contours for the river reach
- an aerial laser survey of the full river corridor
- 5 m contours for the catchment

This complete flood modelling system merges the two sources of rainfall data and uses it as input to a rainfall-runoff model (a Hydrologic Engineering Center's – Hydraulic Modeling System (HEC-HMS) model). The hydrographs that HEC-HMS generates are input to a HEC-RAS hydraulic model that simulates the flow of the water in the Mgeni River. HEC-RAS also produces the water levels and inundation extent that results from the river flow.

The authors report the accuracy of the HEC-HMS model as a graph only, but mention that it 'generally correctly predicts the peak discharge' (Makwananzi and Pegram, 2004, p.80). The reports give no accuracy for the inundation modelling.

Whiteaker et al. (2006) describe a complete modelling system that they created for Rosillo Creek (73 km^2) in Texas, US. They used radar rainfall as input to a HEC-HMS model. The output hydrographs from HEC-HMS fed into a HEC-RAS hydraulic model and the water levels output from this model were input to a flood inundation model. These researchers wrote source code to automatically convert data between the different modelling systems and between ArcHydro and the modelling systems. Whiteaker et al. (2006) focus on the design of the system in their article and do not mention the accuracy of their models. Knebl et al. (2005) conducted a similar study using the same software combination on the San Antonio River Basin (about 10 000 km^2) in Central Texas, USA. They publish numerical results for the rainfall-runoff model only and they achieved an average correlation of 0.78 (ranging from 0.23 to 0.91) for 12 subbasins.

Chen et al. (2009) describe a case study for developing a GIS-based urban flood inundation model. The rainfall-runoff part of the model takes into account precipitation, infiltration and storm water conveyed through the sewer system. They developed their own rainfall-runoff model to provide the input for the inundation model. The inundation model used a 10 m DEM created from Light Detection and Ranging (LIDAR) data in their study area: the campus of the University of Memphis in Tennessee, US. Inundation modelling distributed the total volume of surface runoff inside the boundary starting from a number of topographic depressions, not just the lowest point in the catchment. Experimental threshold values of flow determined which starting points were chosen. The distribution procedure iteratively increases water depth of wet cells and simultaneously expands wet cells to surrounding low 'dry' cells. Their model achieved a best mean inundation depth error of –0.04% compared to field-recorded inundation depths.

2.4 Remotely sensed data and Internet data in hydromodelling

This section tabulates studies found that used remotely sensed data and data from the Internet in some way in hydromodelling. Hydromodelling refers to rainfall-runoff modelling, flood inundation modelling, complete flood modelling systems and water resource modelling. Remotely sensed data and Internet data used in hydromodelling include precipitation and other climate data, DEMs, soil types, and land cover types. Table 3 lists the data and models used, the numerical accuracy of the model (if available) and conclusions from the studies if they are relevant to this project. The table also includes the size of the study area and the topographic data used in the studies to serve as a comparison with the data available for this study.

Table 3: Studies that used remotely sensed data for hydrological, hydraulic and inundation modelling

Author(s)	Type and purpose of study	Remotely sensed data and Internet data	Size of study area	DEM resolution	Model(s)	Best accuracy achieved	Relevant conclusion(s)
Lacroix et al. (2000)	Rainfall-runoff: see if a hydrological model could successfully simulate the hydrology of a river basin using only data from the Internet.	a) USGS GTOPO30 DEM b) Derived land cover from Advanced Very High Resolution Radiometer (AVHRR) 1 km images and DEM c) Global Daily Summary (GDS) climate data (precipitation and temperature) d) Global Surface Summary of the Day (GSOD) climate data (precipitation, temperature dew point, wind velocity)	3 617 km^2	30 arc second (approximately 1 km)	SLURP	73% standard error in mean annual flow	Can apply a distributed hydrological model to a basin using only data from the Internet and using no calibration.
Yang et al. (2004)	Rainfall-runoff: couple a distributed hydrological model with reservoir operations for flood forecasting and control	a) Radar rainfall b) FAO global digital soil map	1 300 km^2	50 m	Own modified geomorphology-based hydrological model	Only available as hydrographs	Radar measurements captured the spatial pattern of rainfall better than the rain gauges.
Li et al. (2008)	Rainfall-runoff: evaluate the applicability of integrating NASA's standard satellite precipitation product with a flood prediction model for disaster management	a) TMPA (TRMM Multisatellite Precipitation Analysis) 3B42RT rainfall b) SRTM DEM c) River and basin data from HydroSHEDS d) FAO digital soil map of the world e) MODIS land classification map	12 696 km^2	30 m	Xinanjiang	N-S correlation of 0.67	Results suggest that TMPA 3B42RT can be acceptably used to drive hydrological models for flood prediction. However, the satellite-based rainfall estimates require further investigation into an optimal calibration strategy.

Author(s)	Type and purpose of study	Remotely sensed data and Internet data	Size of study area	DEM resolution	Model(s)	Best accuracy achieved	Relevant conclusion(s)
Asante et al. (2007)	Rainfall-runoff: develop a flood monitoring system	a) TRMM rainfall b) Global Land Cover Characteristics database c) FAO digital soil map of the world d) Global Data Assimilation System (potential evapotranspiration)	400 000 km^2	Unknown	GeoSFM	Not given	Satellite-derived precipitation, even with an uncalibrated model, can identify extreme events both in terms of relative intensity and spatial extent.
Hossain and Anagnostou (2004)	a) Rainfall-runoff: determine adequacy of current passive-microwave- and infrared-based satellite rainfall for flood prediction of a medium-sized watershed. b) Develop a satellite rainfall error model.	a) TRMM rainfall	116 km^2	20 m	TOPMODEL	Accuracy not given for rainfall-runoff calculation	As the space scales and timescales become smaller, the sensor's precipitation detection and retrieval accuracy become increasingly more complex.
Schultz (1996)	Rainfall-runoff: use remotely sensed data as model input data; to estimate model parameters	a) Meteosat infrared (IR) channel (derive precipitation) b) Landsat (derive land cover, leaf area index and normalised difference vegetation index)	16 000 km^2 and 264 km^2	50 m	Various, including a nonlinear reservoir model	N-S correlation of 0.90 for the validation period of the nonlinear reservoir model	Remote sensing data combined with in-situ measurements will provide opportunities for more efficient hydrological modelling in the future.
Hong et al. (2007)	Rainfall-runoff: approximate assessment of quasi-global runoff	a) TMPA 3B42RT rainfall b) Hydro1k DEM and routing information c) FAO digital soil map of the world d) MODIS land classification map e) GCRD runoff	Whole world between 50°N and 50°S	30 arc second (approximately 1 km)	NRCS-CN	0.75 correlation between calculated runoff and GCRD values	TRMM-CN performance is significantly better for larger basins (>10 000 km^2).
Artan et al. (2007)	Rainfall-runoff: evaluate a spatially distributed hydrologic model driven by daily satellite-based estimates of rainfall	a) National Oceanic and Atmospheric Administration (NOAA) Climate Prediction Center (CPC) satellite rainfall b) GTOPO30 DEM c) FAO digital soil map of the world	6 000 km^2 and 22 000 km^2	30 arc second (approximately 1 km)	GeoSFM	0.81	Satellite rainfall can be used to drive hydrologic models for streamflow prediction if the hydrologic model is calibrated with satellite rainfall.
Li and Zhang (2008)	Rainfall-runoff: develop and compare distributed hydrological models integrated with GIS	a) Global Land Cover Characteristics Data Base b) GOTOPO30 DEM c) Soil composition from NOAA remotely sensed image	4 716 km^2	30 arc second (approximately 1 km)	GTOP-MODEL GIS-Based TOPMODEL Xinanjiang	N-S correlation of 0.97	A finer DEM resolution should improve the models' performance.

Author(s)	Type and purpose of study	Remotely sensed data and Internet data	Size of study area	DEM resolution	Model(s)	Best accuracy achieved	Relevant conclusion(s)
Yang et al. (2004)	Rainfall-runoff: apply a coupled distributed hydrological model (with reservoir operations) to flood forecasting and control	a) Radar rainfall b) FAO digital soil map of the world	1 300 km^2	50 m	Modified GBHM	Only available as hydrographs	Radar rainfall measurements capture the spatial pattern of rainfall better than rain gauges do, leading to much more accurate simulations of the inflows into reservoirs.
Horritt and Bates (2002)	Inundation: compare 1D and 2D inundation models	a) Radar Satellite (RADARSAT) image, 25 m ground pixel size b) European Remote-Sensing Satellite 2 (ERS-2), 25 m ground pixel size	60 km reach of river	50 m	HEC-RAS LISFLOOD-FP TELEMAC 2D	65% of the inundation extent	-
Baldassarre et al. (2009)	Inundation: determine if model calibrated on high-magnitude event can model low-magnitude event	European Space Agency Environmental Satellite (ENVISAT) Advanced Synthetic Aperture Radar (ASAR), 100 m ground pixel size	98 km reach of river that is up to 4 km wide	2 m	HEC-RAS	Water level: within 4% Inundation extent: Mean Absolute Error (MAE) of 400 m.	A well-calibrated flood inundation model may perform very poorly when it is used to predict different events.
Matgen et al. (2007)	Inundation: develop image processing methodologies to extract water levels at any point of the floodplain	ENVISAT ASAR, 25 m ground pixel size	10 km reach of a river that is, 300 m wide on average	2 m	HEC-RAS	RMSE of 41 cm in flood height	Accurate inundation mapping depends on highly accurate topographic data.
Sinclair and Pegram (2004) and Makwananzi and Pegram (2004)	Complete flood modelling system: help metropolitan disaster managers to be proactive when floods are imminent	a) Radar rainfall b) Flow gauge data	955 km^2	2 m (river channel) 5 m (catchment)	HEC-HMS (hydrology) HEC-RAS (hydraulics and inundation)	Only available as hydrographs	Computing flood lines is a fairly laborious process that requires a large degree of human interaction. This does not encourage online computation of current and forecast inundation depths as a first choice of modus operandi.

2.5 Satellite rainfall assessment

Hughes (2006) evaluated satellite precipitation data (the Global Precipitation Climatology Project (GPCP) and Precipitation Estimation from Remotely Sensed Information using Artificial Neural Networks (PERSIANN) products) for input (along with gauge data) to monthly time step, rainfall-runoff models. The study covered four basins in Southern Africa: Okavango River basin (530 000 km^2 in Angola, Botswana and Namibia), Kafue Basin (156 995 km^2 in Zambia), Thukela River basin (29 046 km^2 in Kwa-Zulu Natal) and the Kat River basin (1 715 km^2 in the Eastern Cape). In the Okavango River basin, no ground-based gauge data was available for the period covered in Hughes' 2006 study, so he compared the GPCP and PERSIANN data to satellite data from the Water and Ecosystem Resources in Regional Development (WERRD) project[9], for which a non-linear correction equation that was determined from historical data. The average correlation for eight 1° x 1° grid cells was 0.57 between the WERDD data and the GPCP data and 0.63 between the WERDD data and the PERSIANN data. In the Kafue River basin, the average correlation for the rainfall estimates between four ground-based rain gauges and SBRE in 17 1° x 1° grid cells was 0.83 for the GPCP data and 0.82 for the PERSIANN data. In the Thukela River basin four 1° grid cells of GPCP data and 4 rain gauges had a correlation of 0.58. For this basin, the PERSIANN and gauge data overlapped poorly, so Hughes (2006) compared the PERSIANN data to the GPCP data and found an average correlation of 0.57. The Kat River basin had a similar problem with overlap between PERSIANN and gauge data and the correlation between the GPCP data and the PERSIANN data was 0.53. The correlation between one 1° grid GPCP cell and four rain gauges was 0.58[10]. Hughes (2006) concluded that satellite data are insensitive to topographic influences on precipitation and that SBRE should be processed to try and match the characteristics of the historical gauge rainfall before applying the SBRE in rainfall-runoff models that have already been calibrated with rain gauge data.

Sorooshian et al. (2000) evaluated their PERSIANN SBRE algorithm by comparing it to ground-based gauges and radar rainfall measurements. At a resolution of 5° x 5°, they found 36 grid cells that contain 5 or more ground based rain gauges for which data was available through the National Climatic Data Centre (NCDC). In these cells, the correlation between the monthly accumulated PERSIANN data and the rain gauge data was 0.77 or greater. In cells with more than 10 gauges, the correlation increased to 0.9 or greater. The TRMM 3B43 product had similar correlations to the ground-based gauges (at least 0.87 for cells with 5 or more gauges and 0.91 for cells with 10 or more gauges). The TRMM 3B42 product had a correlation of 0.72 for cells with 5 or more gauges and 0.87 for cells with 10 or more gauges. Comparing the daily rainfall that PERSIANN estimates to radar rainfall measurements in 36 1° x 1° grid cells, these researchers found an average correlation of 0.73 and an RMSE of 6.43 mm/day.

[9] The University of Sussex developed satellite rainfall estimates for 1991–1997 in the Okavango basin using TRMM and METEOSAT data. It was part of the Water and Ecosystem Resources in Regional Development project.
[10] One rain gauge seemed to have anomalous data and was excluded from the average.

Hossain and Anagnostou (2004) derived rain retrieval error parameters for the TRMM Passive Microwave (PM) (2A12) and IR (3B41RT) sensors. They compared the SBRE to the values that a dense network of rain gauges measured in the study area. They found that the PM sensor was significantly more sensitive to detecting rain than the IR sensor. The PM sensor's probability of detection (POD) approached 1 at a rain rate of about 2 mm/h. The IR sensor's POD tended to its best value of about 0.76 at rain rates of around 6 mm/h. The PM sensor's false alarm rate (FAR) became zero at rainfall rates of 5 mm/h and that of the IR at about 8 mm/h; the FAR of the IR sensor was almost twice that of the PM sensor. The successful no-rain detection probabilities were 93% for the PM sensor and 88% for the IR sensor.

Li et al. (2008) compared mean daily TRMM 3B42RT precipitation to ground-based gauges and found a correlation of 0.57. The POD was 0.996 and the FAR 0.19. The RMSE was 4.82 mm/day. They found that validation indices improved as the time intervals over which they are aggregated, increased. For example, the FAR reduced from 0.19 to 0.05 when they changed the time scale from 1 day to 5 days. They found that the SBRE had a positive bias of 15%.

Artan et al. (2007) used an NOAA SBRE available at daily intervals in a rainfall-runoff model and found that the model performed best when they calibrated it using the SBRE rather than using ground-based rain gauge measurements. The average N-S correlation (in three different basins) of the predicted streamflow improved from 0.50 to 0.65 when using SBRE to calibrate the model. This is compared to an average N-S correlation of 0.78 when the model used ground-based rainfall data as input. They concluded that SBRE can drive hydrologic models for streamflow prediction as long as the same data is used to calibrate the model. These authors also found that the two rainfall estimates (SBRE and ground-based) were weakly correlated at daily timescales, but the correlation between monthly accumulated rainfall values was excellent. Their SBRE product slightly underestimated the rainfall compared to the rainfall that the ground-based gauges measured.

In their study of coastal sediment plumes resulting from river runoff, Shaban et al. (2009) compared daily TRMM rainfall data to ground-based measurements. Over 22 days they found that ratio of ground-based rainfall measurements to SBRE was 1:35, so the TRMM values in general underestimated the rainfall.

Villarini and Krajewski (2007) compared six years' three-hourly TRMM 3B42 data from one pixel (0.25° x 0.25°) to the measurements of 23 ground-based rain gauges in the same area. They found a large spread between the satellite and the rain gauge data with relatively low correlation coefficients. Taking the ground-based measurements as the standard, they found that the TRMM product underestimates the rainfall by between 3% and 14% and that the satellite observations are not very sensitive to low rainfall values. The TRMM estimates are best during the hot season. From their statistical analysis they concluded that the TMPA should be considered as a 100-minute accumulation product, with the accumulation starting between 90 and 30 minutes before its nominal time. This also depends on the season, though, and they stress that their results are valid only for Oklahoma, where they conducted the study.

Huffman et al. (2007) cite a study by Ebert (2005) that compares the monthly TRMM data products to ground-based rain gauges in Australia. She found that the TRMM data available in 2004 in general performed best in relatively heavy, convective storms in warm seasons. They performed worse in light rain associated with the cool seasons in Australia. During the warm season, the TRMM data had a positive bias with a correlation coefficient around 0.50 between the SBRE and ground-based gauges. During the cool season, the TRMM data has a negative bias with a correlation coefficient around 0.30. Reworking the data with the current version of the TMPA algorithm (v.6) removed the seasonal cycle and improved the correlation coefficient to 0.90. The mean absolute monthly bias improved from 28% to 9%.

2.6 Concluding remarks

The previous work reviewed here indicate that various researchers have successfully applied SBRE as input to rainfall-runoff models in study areas ranging from hundreds of square kilometres to hundreds of thousands of square kilometres. However, no studies were found that used SBRE in rainfall-runoff models with calculation time steps shorter than a day. Section 5.1 on page 58 discusses the SBRE considered for this study and why TRMM 3B42 was selected.

Evaluation of SBRE show that their correlation with ground-based data is generally greater than 0.5 and that correlation improves with larger time scales and with larger numbers of ground-based gauges in the comparison. SBRE are better at detecting and estimating heavy rain than light rain.

Many researchers have applied SWMM in rural and urban settings with good results. Models such as SWMM that couple surface runoff with channel routing and that can model urban drainage are becoming especially important in studies that evaluate the impact of urbanisation on runoff. Section 4.3 on page 56 describes in detail why SWMM was chosen for this project.

Previous work on inundation modelling suggests that success depends to a large extent on the resolution of the DEM relative to the size of the river and to the expected changes in water levels.

3. Theory

This chapter describes the theory of the models, methods and data relevant to this project. It starts with general a discussion on rainfall-runoff modelling and the types of models available. Then it describes the components of rainfall-runoff models: precipitation (including a discussion of SBRE), evapotranspiration, interception, groundwater, infiltration, overland flow and channel flow. How SWMM implements these concepts then follows, along with a discussion on how to evaluate model performance. Finally, it describes two inundation models and how to evaluate results of inundation models.

3.1 What is a model?

All models are wrong, though some may be said to be useful.

G.E. Box

A model is a simplified version of reality. It helps us deal with complexity and to select the best among competing proposals (James 2005, p.2).

3.2 Rainfall-runoff modelling

Beven (2001, p.1) gives as the main reason for rainfall-runoff modelling that we cannot measure everything that we need to know about hydrological systems, so models enable hydrologists to extrapolate and interpolate hydrological variables in space and in time. Models also help hydrologists to understand and explore system behaviours and to check for inconsistencies and errors in their data (Silberstein, 2006).

Rainfall-runoff models read rainfall as input and account for abstractions (such as infiltration and evaporation) to produce a rainfall excess hyetograph[11]. The model then converts the excess rainfall to overland flow that moves to the drainage channels (gulleys or stream valleys) in the catchment. The catchment's size, infiltration rate, slope and surface roughness determine how much water will reach the channels and when it will reach them. The water then flows in the channels to the catchment outlet. The hydraulic characteristics of the drainage channels greatly influence how much and when the water in the channels reaches the outlet. Some factors that determine the runoff characteristics are drainage area, slope, hydraulic roughness, storage, and length (Mays 2001, p.248–253). Depending on the model used, it calculates hydrographs (relating stream flow to time) at the outlet of the catchment or at specific points in the channels in the catchments. Figure 4 on page 23 illustrates this process.

[11] A graph of rainfall vs. time.

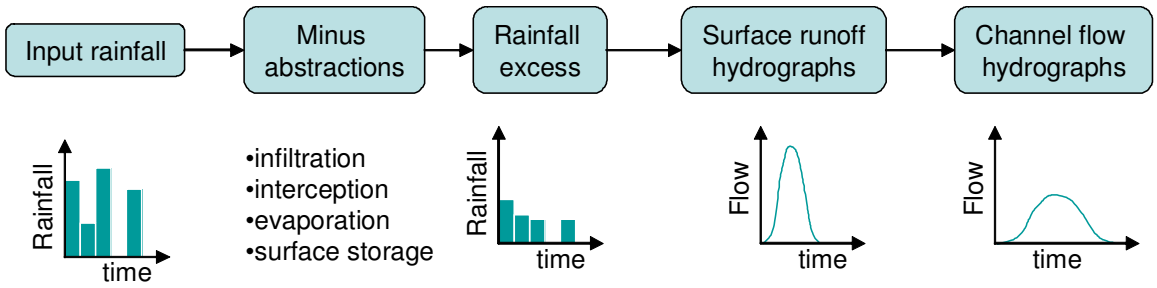

Figure 4: The rainfall-runoff modelling process

Since hundreds of rainfall-runoff models are available (Beven 2001, p.*x*), this text cannot examine them all and will instead look at them in broad categories. The boundaries between the categories are not absolute and models can combine elements from different categories. Beven (2001, p.18) identifies one characteristic for classifying rainfall-runoff models as *lumped* or *distributed* models. The latter vary state variables and hydrological characteristics in space while the former use average values for the whole catchment. Hydrologists can discretize distributed models to the desired level of complexity. SWMM can function as a lumped or a distributed model and the modeller can control the level of discretization by, for example, defining sub-catchments.

Another characteristic for classifying rainfall-runoff models is whether it is *deterministic* or *stochastic* (Beven 2001, p.18). Deterministic models allow only one set of outputs for a given set of inputs. Stochastic models allow some randomness or uncertainty in possible outcomes because the inputs are uncertain. The vast majority of rainfall-runoff models are deterministic. However, when a deterministic model is used in sensitivity, calibration or error analyses, it may produce a range of outputs.

Models can further be divided into physical models, statistical (also called empirical) or conceptual (Silberstein, 2006). Physical models try to reproduce the physical processes that take place in the catchment. These fully distributed models use partial differential equations to describe flow processes. Examples are the Système Hydrologique Europeen (SHE) and the Institute of Hydrology Distributed Model (IHDM). Physical models are complex and require detailed information on the state and characteristics of the catchment. They require skilled operators and, often, significant computing resources to run. The advantage of complex physical models is that they help researchers to understand the processes that produce streamflow (Pegram and Sinclair 2002 p.10). Statistical models use regression or machine learning algorithms, such as neural networks or support vector machines, to find a relationship between rainfall and runoff (Pegram and Sinclair 2002 p.11). They are 'black box' models that do not concern themselves with the physical processes that explain the rainfall-runoff relationship. Conceptual models are generally simplifications of physical models and they use mathematical techniques to reduce complexity while taking into account the physical processes that result in the streamflow (Pegram and Sinclair 2002, p.11). The majority of models are conceptual and they represent a catchment as a series of moisture stores (reservoirs) with fluxes between the stores (Silber-

setin, 2006). SWMM combines elements of physical, statistical and conceptual models, but it is classified as a physical model because most of its processes follow physical explanations (James 2005, p.3).

Sections 3.3 to 3.9 explain the theory of the components of rainfall-runoff models. Since SWMM was selected as the model for this project, the theory of how SWMM implements these components then follows.

3.3 Precipitation

Precipitation refers to any kind of solid or liquid water that falls or condenses from the atmosphere onto the earth's surface. Water molecules concentrate and condensate around nuclei such as smoke, dust or salt. When air cools, condensation increases and more clouds form. When the droplets or ice crystals in the clouds reach a sufficient size, they fall towards the earth's surface and so become precipitation (Ward and Trimble 2004, p.32).

Air cools mainly because it rises upward and three processes lift air masses: weather fronts, convection and orographic lift. These processes in turn give rise to the three types of precipitation of the same names. Frontal precipitation occurs at the boundary between two air masses of different temperature. The colder air mass causes the warmer air mass to lift and so increases condensation that leads to precipitation. Convection precipitation occurs when solar energy heats air directly or indirectly (heat radiated from the earth's surface) and the air expands. The expanded air is lighter than the surrounding air, so it lifts up to cooler regions where the water vapour in the air starts to condense. Thunderstorms are one form of convective precipitation, but air that moves into a low-pressure system can also cause convective precipitation. Orographic precipitation occurs when wind forces air up over mountains. The rise cools the air, which causes condensation (Ward and Trimble 2004, p.33).

3.3.1 Ground-based rain gauges

Ground-based rain gauges measure the depth of rain that falls on a horizontal surface during a certain period. The SAWS uses both recording and non-recording gauges. The former automatically log their readings on paper or electronically while volunteers read the latter (E. de Jager 2010, pers. comm., 9 April). Most recording gauges in South Africa are tipping bucket gauges. Rain falls through a collector funnel into one bucket that tips after 0.2 mm rain has fallen, aligns a contiguous bucket and empties (sometimes) into a cumulative bucket. The data logger records each tip and accumulates the rainfall for a set period (E. de Jager 2011, pers. comm., 12 April).

A ground-based rain gauge measures precipitation at one point in space and thus doesn't accurately reflect the amount of rain that falls over an area. However, it's the only measurement that directly gauges the actual amount of water that reaches the ground. Radar and satellite sensors estimate rainfall indirectly.

3.3.2 Ground-based radar

Ground-based weather radars emit a pulse of electromagnetic energy and detect how much of the energy is reflected back to the instrument. Water drops in the atmosphere reflect the radar's electromagnetic energy, so the greater the reflected energy, the greater the amount of water in the atmosphere. The Marshall-Palmer relationship relates reflected electromagnetic energy to the instantaneous rain rate:

$Z = AR^b$ (Sinclair 2007, p.46)

Where

Z ≡ reflectivity (dbZ)

R ≡ rain rate (mm/h)

A and b ≡ calibration parameters

South African weather radars scan in azimuth and elevation steps to produce a complete volume scan. The spatial resolution is 1 km^2 and the temporal resolution is 5 minutes (Sinclair 2007, p.46).

3.3.3 Satellite-based rainfall estimates

Precipitation is highly variable in time and space and its statistical behaviour deviates significantly from normal. It therefore requires frequent, closely spaced observations for adequate representation. Such fine-scale observations are possible from one type of sensor, but researchers are increasingly combining data from different sensors to improve accuracy, coverage, and resolution. Several such SBRE are now available and in quasi-operational production, including the TRMM data products, the CPC morphing algorithm (CMORPH), the Naval Research Laboratory Global Blended-Statistical Precipitation Analysis (NRLgeo), the Passive Microwave-Calibrated Infrared algorithm (PMIR), and PERSIANN (Huffman et al., 2007).

3.3.3.1 Infrared sensors

Infrared sensors detect radiation that objects emit in the wavelength range between 10.5 μm and 12.5 μm. In general, infrared estimates of precipitation assume that, the higher a cloud's reflectivity and the colder its tops, the more rain it produces. Users of these sensors also assume that the rain falls directly beneath the clouds. Data from such sensors are used to produce brightness temperatures, in other words, the temperature of the cloud is calculated from Planck's law that relates emissivity to temperature. Rainfall estimates from infrared sensors have good spatial and temporal resolutions. However, the properties that they measure have no direct, physical link to rainfall processes (Ba, 2008). Infrared-based precipitation estimates have the limitation that brightness temperatures correspond primarily to the temperature of the cloud top. This is poorly

correlated to precipitation at fine time and space scales but it is relatively well correlated at time scales larger than one day and at spatial scales larger than 2.5° × 2.5° (Huffman et al., 2007).

3.3.3.2 Passive microwave sensors

Passive microwave sensors (radiometers) detect the microwave radiation that objects emit after being heated by the sun. Passive Microwave radiometers that estimate precipitation usually work in the frequency range between 19.3 GHz and 85.5 GHz (wavelengths between 15 mm and 3.5 mm). Atmospheric particles emit radiation, which increases the signal that the sensor receives. At the same time, scattering due to hydrometeors[12] reduces the radiation. The type and size of the hydrometeor determine the frequency of the upwelling radiation. Scattering and emission happen at the same time and the radiation undergo multiple transformations in the cloud column that is in the sensor's field of view. Radiometers use different frequencies to observe the different parts of the rain column. Radiometers detect precipitation drops without the infrared biases because the drops interact so strongly with microwave radiation (Levizzani et al., 2002, pp.7–8).

The biggest disadvantage to using microwave radiation to detect precipitation is the poor spatial and temporal resolution. Diffraction limits the ground resolution for a satellite microwave antenna, so microwave sensors travel on polar satellites (Levizzani et al. 2002, p.8). More powerful antennas with better spatial resolutions would need geostationary satellites that can carry payloads heavier than is currently possible.

Since this project used the TRMM TMPA rainfall estimates, the following paragraphs describe this product in more detail.

3.3.3.3 TMPA

The primary TRMM data product, TMPA (also called 3B42), is a merged passive microwave and infrared product, computed every three hours on a 0.25° × 0.25° grid between the 50°N and 50°S latitudes. It combines estimates from various satellite systems and, where available, ground-based gauges. This SBRE is available as a quasi real-time (RT) product with a nine hour lag and as a research product computed 10 to 15 days after each month end. The research product is corrected using ground-based data while the real-time product is not (Huffman et al., 2007).

Table 4 lists the instruments from which TMPA gathers data and the satellites that carry them. The institutions in the 'Data processor' column convert the raw data to precipitation estimates (Huffman et al., 2007).

[12] Liquid water or ice in the atmosphere in various forms: rain, ice crystals, hail, fog, or clouds.

Table 4: TMPA data sources

Type of data	Instrument	Satellite	Data processor
Passive microwave	TRMM Microwave Imager (TMI)	TRMM	TRMM Science Data and Information System (TSDIS)
	Special Sensor Microwave Imager (SSM/I)	Defence Meteorological Satellite Program (DMSP) satellites	TSDIS
	Advanced Microwave Scanning Radiometer-Earth Observing System (AMSR-E)	NASA's *Aqua* satellite	TSDIS
	Advanced Microwave Sounding Unit-B (AMSU-B)	National Oceanic and Atmospheric Administration (NOAA) satellite series	National Environmental Satellite, Data, and Information Service (NESDIS)
Infrared	Various	International constellation of geosynchronous earth orbit satellites	CPC of the NOAA/National Weather Service
Radar	TMI and the TRMM precipitation radar (PR)	TRMM	TRMM Combined Instrument (TCI) estimate –TSDIS
Rain gauge	N.A.	N.A.	GPCP monthly rain gauge analysis
Rain gauge	N.A.	N.A.	Climate Assessment and Monitoring System (CAMS) monthly rain gauge analysis

The TMPA algorithm consists of four stages: 1) combine and calibrate passive microwave precipitation estimates, 2) create infrared precipitation estimates from the calibrated microwave precipitation, 3) combine the microwave and IR estimates, and 4) incorporate rain gauge data (research product only) (Huffman et al., 2007). Figure 5 illustrates the algorithm and the paragraphs that follow give more details.

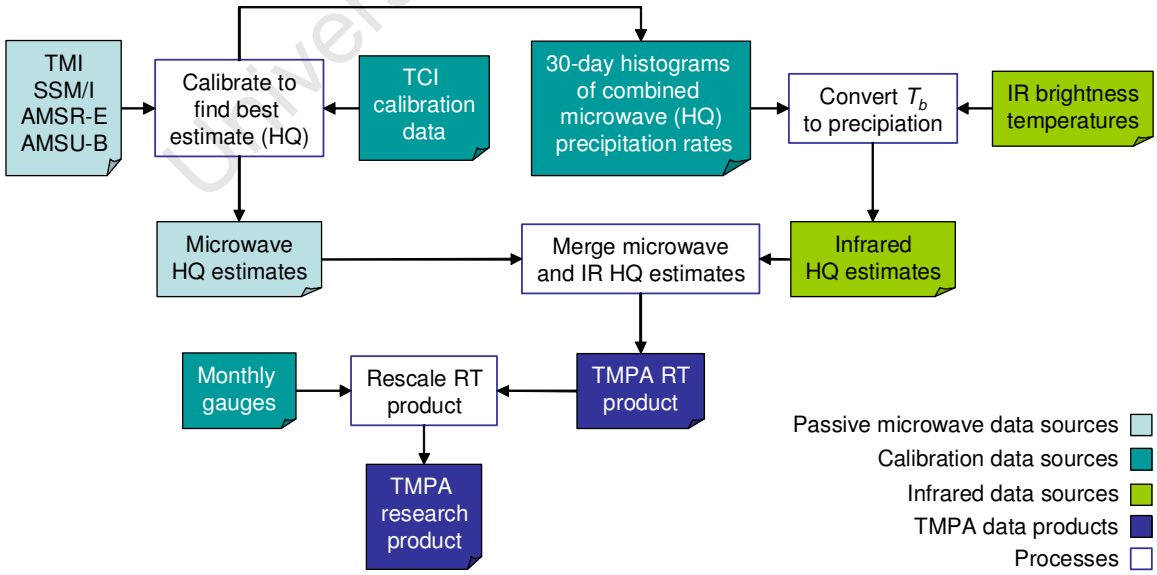

Figure 5: TRMM TMPA algorithm

In the first step of the data processing, the TMPA algorithm averages the passive microwave data to the 0.25° grid cells and adjusts the precipitation estimates from all the sensors to a best estimate using probability matching of precipitation rate to histograms of coincident data. The histograms are derived from the TCI estimate[13]. The algorithm averages overlapping data from multiple PM sensors (Huffman et al., 2007).

In the second step of the data processing, the TMPA algorithm averages the infrared brightness temperature values to 0.25° resolution. It then converts these values to precipitation using time-space matched histograms of combined microwave precipitation rates (calculated in the previous step) (Huffman et al., 2007).

In the third step of the data processing, the TMPA merges the microwave and infrared precipitation estimates. If the physically-based combined microwave estimate is available for a grid cell, it becomes the TMPA precipitation estimate for that cell. Otherwise, the microwave-calibrated IR estimate becomes the TMPA precipitation estimate for that cell (Huffman et al., 2007).

The final step in the data processing (reserved for the research TMPA product) uses rain gauge data to rescale the remotely sensed estimations. For this, the TMPA algorithm uses monthly rain gauge data to ensure that the gauge data is sufficiently dense and have consistent observation intervals. The result is the high resolution typical of satellite data and the small bias typical of gauge analyses (Huffman et al., 2007).

The TMPA data product includes a relative error estimate. This the RMSE error of each precipitation estimate compared to a probability distribution function of rainfall rates (Huffman, 1997).

3.3.4 Comparing precipitation measurements and satellite estimates

Section 2.5 on page 19 describes some studies that compared SBRE to ground-based rainfall measurements. Researchers use various statistical measures to compare precipitation values from different sources. Table 5 on page 29 lists the measures described in Li et al. (2008) and used in this study. In the table *G* denotes ground-based precipitation measurements and *S* denotes satellite precipitation estimates. The number of observations being compared is *n*. The term *hit* refers to times when the two time series both detect rainfall events and *miss* refers to times when the ground-based gauge detected a rainfall event, but the SBRE did not. The term *false alarm refers* to times when the SBRE detected rain, but the gauge measured none.

[13] The TCI estimate uses data from both TMI and the TRMM precipitation radar (Huffman et al., 2007).

Table 5: Statistical measures to compare ground-based precipitation measurements and satellite estimates

Name	Formula	Comments
Pearson correlation coefficient	$r = \frac{1}{n-1}\sum_{i=1}^{n}\left(\frac{G_i-\overline{G}}{\sigma_G}\right)\left(\frac{S_i-\overline{S}}{\sigma_S}\right)$ $= \frac{1}{n-1}\sum_{i=1}^{n}\left(\frac{G_i-\overline{G}}{\sqrt{\sum_{i=i}^{n}\left(G_i-\overline{G}\right)^2}}\right)\left(\frac{S_i-\overline{S}}{\sqrt{\sum_{i=i}^{n}\left(S_i-\overline{S}\right)^2}}\right)$ where $\overline{G}$ = mean of ground-based measurements; $\overline{S}$ = mean of SBRE; σ_G = standard deviation of ground measurements; σ_S = standard deviation of SBRE	Measures the linear dependence between two variables. If the ground-based measurements and the SBRE have the same values at each point in the time series, the correlation coefficient is 1. If there is no dependence between the two variables, the correlation coefficient is 0.
Probability of detection	$POD = \frac{hits}{hits + misses}$	The fraction of gauge-observed events that the SBRE detected as well.
False alarm rate	$FAR = \frac{false\,alarms}{hits + false\,alarms}$	The fraction of SBRE rainfall events that were non-events according to the ground-based gauge.
Critical success index	$CSI = \frac{hits}{hits + misses + false\,alarms}$	Overall fraction of events that the SBRE diagnosed correctly.
Bias	$Bias = \frac{\sum_{i=1}^{n} S_i - \sum_{i=1}^{n} G_i}{\sum_{i=1}^{n} G_i} \times 100\%$	Systematic bias of the SBRE.

3.4 Evapotranspiration

In the hydrological cycle water changes between all three phases of matter and molecules move continuously between these states. Evaporation occurs when water changes from the liquid to the vapour state. Evaporation happens when rain falls, once it has ponded on the surface or while it's flowing in rivers or stored in dams. Evaporation also happens via the transpiration of water from plants' leaves, hence the term evapotranspiration. Evaporation is usually quantified by measuring the amount of water that evaporates from a pan placed outside at a specified height on a specified surface during a specified period (Ward and Trimble 2004, p.92). Pans have a standard size and are made from standard materials. In South Africa the DWA uses Symons or S-pans, while the SAWS uses the A-class pans that the US Weather Bureau also uses (Haarhoff & Cassa 2009, p.108).

If the pan evaporation values are used to estimate the amount of water that evaporates from a dam, one needs to multiply the pan measurements by a pan factor to account for a higher water and air temperature in the pan and for the greater influence of wind over the dam. These pan factors depend on the time of year and are available in literature (Haarhoff & Cassa 2009, p.110).

3.5 Interception

Vegetation intercepts precipitation when the water adheres to leaves and branches. When enough rain falls, some water flows through to the ground (throughfall), some water flows down the stems of the vegetation (stemflow) and some of the intercepted precipitation evaporates. Hydrologists measure interception by placing rain gauges above the vegetation canopy or in open areas and under the canopy. They also place collars around tree trunks to measure stemflow. Hydrologists divide the volume of stemflow by the area of the study plot to estimate the depth of precipitation that the stemflow abstracts. Interception is then the difference between gross precipitation and the sum of the stemflow and the throughfall (Ward and Trimble 2004, p.295).

Another form of interception is depression storage, which is the water required to fill natural depressions to their overflow levels (James et al., 2008, p.777).

3.6 Infiltration

Infiltration is the process of water penetrating into soil. Once in the soil, the water becomes soil moisture that generates (unsaturated) subsurface flow in response to a gradient. At this point, air and water occupy the voids between soil particles. When the soil becomes saturated, only water is assumed to occupy the voids between the soil particles and the water becomes groundwater (saturated) flow (Mays 2001, p.233). In reality, air also exists in the saturated zone.

Infiltration modelling takes one of three directions: empirical, physical and approximate. Empirical and approximate methods consider the soil to be a semi-infinite medium that saturates from the surface down. Physical methods specify appropriate boundary conditions and use the Richards equation to describe how water flows in soil (Hydrology Handbook 1996, p.103). The Richards equation (or diffusion equation) is:

$$\frac{\partial \theta}{\partial t} = \frac{\partial}{\partial z}\left[D_W(\theta)\frac{d\theta}{dz} \right] + \frac{\partial K(\theta)}{\partial z}$$ (Ward and Trimble 2004, p.73)

Where

θ = soil water content (ratio of water volume to total volume)

t = time (s)

z = distance in the vertical direction (m)

$D_w(\theta)$ = the soil water diffusivity defined as $K(\theta)\partial h/\partial\theta$ (m^2/s)

$K(\theta)$ = hydraulic conductivity expressed as a function of soil water content (m/s)

SWMM provides three infiltration models: Horton, Green & Ampt and NRCS-CN. Horton and NRCS-CN are empirical methods, while Green & Ampt is an approximate method and based on measurable physical properties of the soil (Hydrology Handbook 1996, p.104). Since Green & Ampt is the more widely used and more accurate method of the three (Hsu et al., 2002), it was chosen for this project and this text discusses only this infiltration model further.

3.6.1 Green & Ampt infiltration

Figure 6 (a) shows the theoretical moisture zones during infiltration and Figure 6 (b) shows the Green & Ampt simplification of these zones. In the Green & Ampt version, the wetting front is a sharp boundary that divides soil with an initial moisture content θi from saturated soil. The wetting front has penetrated to depth L at time t. A small water pond of depth h_0 is on the surface. $\Delta\theta$ is the difference between the soil's porosity and the initial moisture content.

The cumulative infiltration over time for vertical column of soil of unit cross-sectional area is:

$$F(t) = L(\eta - \theta i) = L\Delta\theta \quad \text{(Mays 2001, p.239)}$$

Where

L = depth of the wetting front at time t (mm)

η = soil porosity (fraction of volume of voids over total volume)

By applying Darcy's law of groundwater movement, one can arrive at the Green-Ampt equation for cumulative infiltration:

$$F(t) - \psi\Delta\theta \ln\left(1 + \frac{F(t)}{\psi\Delta\theta}\right) = Kt \quad \text{(Mays 2001, p.241)}$$

Where

ψ = wetting front soil suction head (mm)

K = hydraulic conductivity (mm/h)

Values for porosity, the wetting front soil suction head and hydraulic conductivity for different soil textures are available in literature.

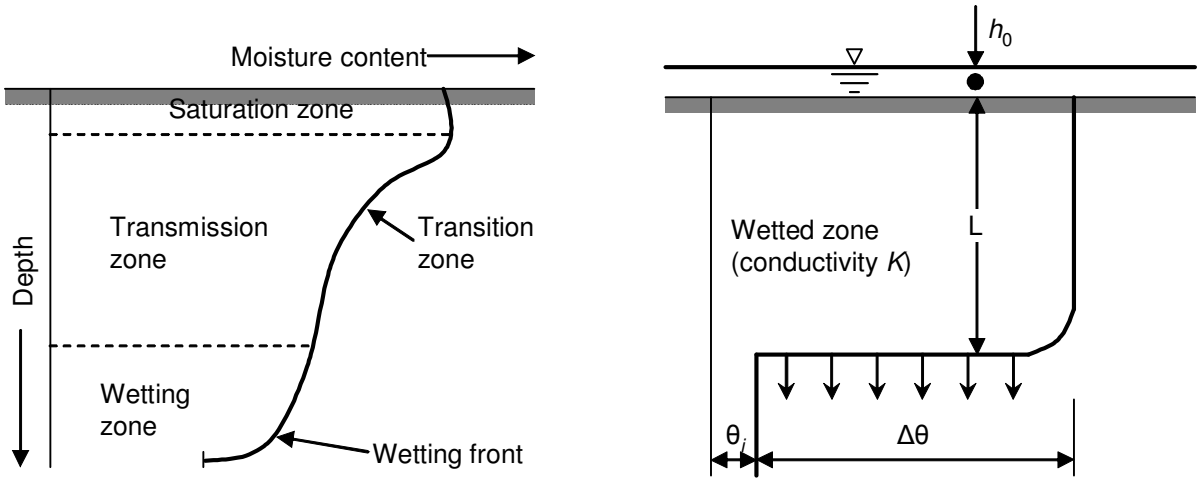

(a) Theoretical *(b) Green & Ampt simplification*

Figure 6: Moisture zones during infiltration (after Mays 2001)

3.7 Groundwater flow

Aquifers store and transport subsurface groundwater and, in its natural state, groundwater usually moves in response to a gradient. Darcy's law expresses water flow through an aquifer and it is the foundation of groundwater hydraulics. It applies to natural groundwater in which the flow is laminar and without turbulence. In this law, the flow rate is proportional to the head loss[14] and inversely proportional to the length of the flow path:

$$Q = -KA\frac{dh}{dL}$$ (Mays 2001, p.148)

Where

Q = flow (m^3/s)

K = hydraulic conductivity (m/s)

A = cross-sectional area (m^2)

h = head loss (m)

L = length of flow path (m)

[14] Head loss is the energy lost due to resistance against the flow of fluids.

3.8 Overland flow

Beven (2001, p.1–14) identifies five mechanisms for overland flow: a) infiltration excess (or Hortonian), b) partial area infiltration excess, c) saturation excess, d) subsurface stormflow and e) perched saturation and throughflow. These types of overland processes may occur in the same catchment in different places or at different times, depending on the antecedent conditions, soil type and rainfall intensity.

Since SWMM assumes Hortonian overland flow, this text discusses further only this type of overland flow. Hortonian flow occurs when sufficient water ponds on the surface to overcome surface tension effects and to fill small depressions. Mathematically, it is modelled as sheet flow that doesn't concentrate in clearly defined channels (Mays 2001, p.274–275). Hortonian overland flow is a one-dimensional flow process with the flow proportional to a power of the storage per unit area:

$Q = \alpha h^m$ (Mays 2001, p.275)

Where

Q = the discharge per unit width (m^3/m^2s)

h = the depth of water per unit area (m/m^2)

α and m = parameters related to the slope, surface roughness, and whether the flow is laminar or turbulent.

3.8.1 Roughness

Overland flow, like channel flow (see paragraph 3.9), includes a measure of the resistance that the surface over which the water flows offers to this flow. Robert Manning used experiments to derive an empirical relation for the resistance coefficient in the Chezy equation[15] to define the Manning's equation for flow in SI units (Mays 2001, p.93):

$$Q = \frac{1.49}{n} A R^{\frac{2}{3}} S_0^{\frac{1}{2}}$$

Where

n = Manning's roughness coefficient ($s/m^{1/3}$)

[15] The Chezy equation relates the velocity of a fluid to its hydraulic radius, the slope of the conveyance medium and a resistance coefficient. It is derived from the three forces that act on a fluid control volume: friction, gravity and hydrostatic pressure (Mays 2001, p.88-89).

A = cross sectional area of the flow control volume[16] (m^2)

R = hydraulic radius (the cross sectional area of the flow control volume divided by the wetted perimeter of the cross section) (m)

S_o = slope of the conveyance surface (m/m)

This project used values for Manning's n for different types of land cover from Mays (2001), p.92 and p.617 and from Kadlec and Wallace (2009), p. 40. Details are in Appendix B on page 104.

Using Manning's equation to express the equation for Hortonian overland flow, one arrives at:

$$Q = \frac{1.49 S^{\frac{1}{2}}}{n} h^{\frac{5}{3}}$$ (Mays 2001, p.276)

Where

$$\alpha = \frac{1.49 S_0^{\frac{1}{2}}}{n}$$

$$m = \frac{5}{3}$$

3.9 Channel flow

Most real channel flows are unsteady, which means that they change over space and with time. The Saint-

Venant equations describe this kind of flow mathematically in one dimension. One of the equations describes channel flow in terms of continuity, based on the law of the conservation of mass. The other equation is stated in terms of momentum and is derived from Newton's second law of motion (Mays 2001, p.293). Kinematic waves govern flow when inertial and pressure forces can be ignored (Mays 2001, p.298). Kinematic wave routing cannot deal with momentum effects because of the terms in the Saint-Venant equations that it ignores. In addition, the numerical solution schemes typically adopted make dynamic wave solutions better suited to nondendritic layouts (James et al. 2008, p.769). Dynamic waves govern flows such as a large flood wave in a wide river (Mays 2001, p.298).

Error! Reference source not found. on page **Error! Bookmark not defined.** lists two forms of the Saint-Venant equations.

[16] A control volume is a given quantity of fluid mass that hydrologists use to simplify hydrological and hydraulic processes and to derive mathematical models of these physical processes (Mays 2001, p.29).

Kinematic waves govern flow when inertial and pressure forces can be ignored (Mays 2001, p.298). Kinematic wave routing cannot deal with momentum effects because of the terms in the Saint-Venant equations that it ignores. In addition, the numerical solution schemes typically adopted make dynamic wave solutions better suited to nondendritic layouts (James et al. 2008, p.769). Dynamic waves govern flows such as a large flood wave in a wide river (Mays 2001, p.298).

Table 6: The Saint-Venant Equations and their application in kinematic and dynamic wave channel routing (after Mays 2001, p.293)

Continuity equations								
$\frac{\partial Q}{\partial x}+\frac{\partial A}{\partial t}=0$								Conservation form
$V\frac{\partial y}{\partial x}+\frac{\partial V}{\partial x}+\frac{\partial y}{\partial t}=0$								Nonconservation form
Momentum equations								
$\frac{1}{A}\frac{\partial Q}{\partial t}$	+ $\frac{1}{A}\frac{\partial}{\partial x}\left(\frac{Q^2}{A}\right)$	+ $g\frac{\partial x}{\partial y}$	− $g(S_0$	− $S_f)$	$=0$			Conservation form
Local acceleration	Convective acceleration	Pressure force	Gravity force	Friction force				
$\frac{\partial V}{\partial t}$	+ $V\frac{\partial V}{\partial x}$	+ $g\frac{\partial x}{\partial y}$	− $g(S_0$	− $S_f)$	$=0$			Nonconservation form
								Kinematic wave
								Dynamic wave

x = longitudinal distance along the channel (m), t = time (s), A = cross-sectional area of flow (m^2), h = water surface elevation (m), S_f = friction slope (m/m), S_o = channel bottom slope (m/m), g = gravitational acceleration (m/s^2), V = flow velocity (m/s), y = flow depth (m).

3.9.1 Roughness

Implementations of the Saint-Venant equations use Manning's equation to account for the friction that the channel bottom and sides exert on the water flow. This project used values for Manning's n for different types of channels from Mays (2001), p.92.

3.9.2 Flow measurements

Discharge equations for flow in open channels and pipes are based on the velocity-area principle:

$Q = VA$ (Herschy 1999, p.15)

Where

Q = discharge (m^3/s)

V = velocity (m/s)

A = wetted area (m^2)

In practice, the above equation is implemented using a stage-discharge curve that relates the water level (the stage) in the channel (or dam) to discharge. Such curves usually take the form:

$Q = C(h+a)^n$ (Hershey 1999, p.21)

Where

Q = discharge (m^3/s)

h = stage (m)

C and n = constants

a = the value of the stage at zero flow

Taking the logarithm transforms the above equation into a straight-line form and so one can derive C, n and a algebraically:

$\log Q = \log C + n \log(h+a)$ (Hershey 1999, p.21)

Thus, by measuring the stage at some point in a river or a dam, one can derive the flow at the same point. Different methods exist for measuring stage; this text describes only the type of instrument used for the flow measurements in this project: pressure transducers (Lloyd 2011, pers. comm., June 17).

A pressure transducer uses the principle that the hydrostatic pressure at a point in a water column is proportional to the height of the water column above this point. The transducer converts changes in water pressure to electric signals that are usually logged remotely (Hershey 1999, p.98–99).

3.10 SWMM

SWMM models various hydrologic processes that produce runoff; they include:

- time-varying rainfall
- evaporation of standing surface water
- rainfall depression storage

- infiltration of rainfall into unsaturated soil layers
- percolation of infiltrated water into groundwater layers
- interflow between groundwater and the drainage system
- nonlinear reservoir routing of overland flow

SWMM divides the study area into a collection of smaller, homogeneous subcatchments, each with its own properties (James et al. 2008, p.2). Each subcatchment is assigned a rain gauge that delivers its rainfall (although more than one subcatchment can use the same rain gauge) and each catchment drains to an outlet node. Conduits (channels) convey water from the subcatchments to the hydraulic transport system (conduits and nodes that connect conduits). Nodes model, for example, the start of channels or the end of channels at confluences of rivers or dams and the catchment outlet. Nodes should be placed such that the conduits that link them are hydraulically homogenous with regard to properties such as slope, roughness and the geometry of the channel. Figure 7 shows a simple model with three subcatchments (S1, S2 and S3) and one rain gauge (the icon at the top between S3 and S1 in Figure 7) assigned to all three. Each subcatchment drains into a junction (J1, J2 and J3). Conduits (C1 to C5) convey the flow to the outlet (Out1). SU1 represents a dam (storage unit).

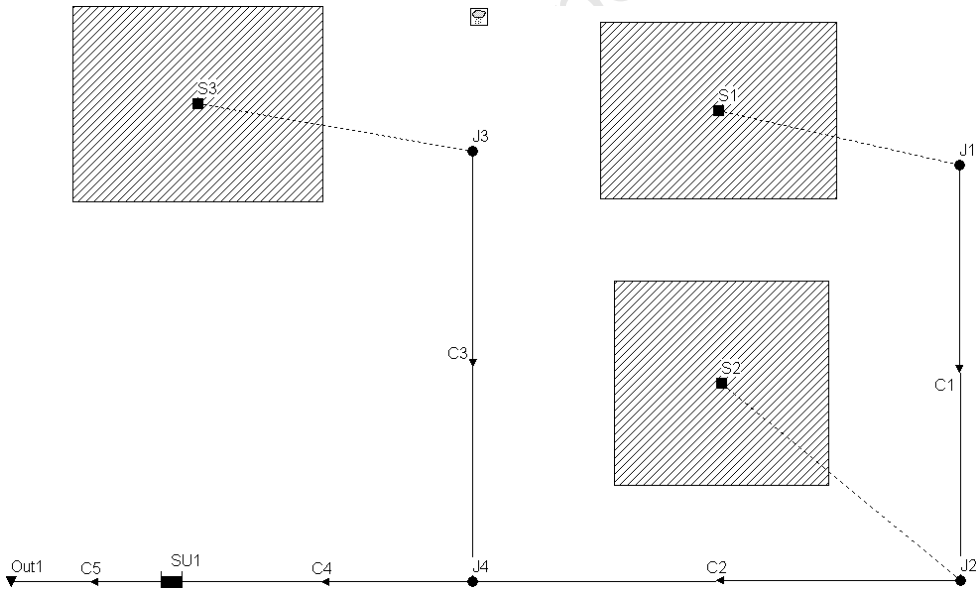

Figure 7: Simple SWMM model as seen in the SWMM user interface

The SWMM software implements its rainfall-runoff model using several modules that manage aspects of the model: rainfall, evapotranspiration, overland flow, infiltration, groundwater and channel flow.

3.10.1 Rainfall

SWMM accepts rainfall time series as depths accumulated at certain time steps. The user can convert rainfall intensities to depths by specifying the duration of the rainfall for intensity measurements. SWMM manages

the distribution of the rainfall across the model's computational time steps using linear interpolation (Computational Hydraulics, 2010).

3.10.2 Interception

SWMM does not model interception from vegetation, but it does model interception from depression storage using a value set for depression storage per subcatchment.

3.10.3 Evapotranspiration

SWMM subtracts evapotranspiration from the amount of rain available for overland flow. To calculate evapotranspiration, it uses evaporation rates, which it accepts as a constant value, as a time series, computed from temperature files or as average values per month. SWMM's results for subcatchments include the total evapotranspiration in mm for the simulation period.

As shown in paragraph 3.10.6 on page 43, SWMM divides wetted soil into an upper (unsaturated) zone and a lower (saturated zone). It calculates the rate of evapotranspiration from these two zones differently. The hierarchy of evapotranspiration from the upper zone is: a) surface evaporation, b) upper zone evapotranspiration, c) lower zone evapotranspiration.

3.10.3.1 Upper zone

SWMM uses the following equations to find the upper zone evapotranspiration rate:

$$ETMAX = VAP(MONTH)$$
$$ETAVLB = ETMAX - EVAPO \quad \text{(James et al. 2008, p.513)}$$
$$ETU = CET \cdot ETMAX$$

Where

$ETMAX$ = maximum total evaporation rate (user input) (mm/day)

$VAP(MONTH)$ = evaporation rate for this month (user input) (mm/day)

$ETAVLB$ = maximum upper zone evapotranspiration rate (mm/day)

$EVAPO$ = portion of ETMAX that surface water evaporation uses (dimensionless)

CET = fraction of evaporation apportioned to upper zone (dimensionless)

SWMM imposes two conditions on these calculations. Firstly, if the moisture content is less than the wilting point[17] of the soil, then evapotranspiration is zero. Secondly, if the infiltration is greater than zero, then the

[17] The point at which plants can no longer extract moisture from the soil.

evapotranspiration is also zero; SWMM assumes that in this case the vapour pressure will be high enough to prevent additional evapotranspiration from the upper zone (James at al. 2008, p.514).

3.10.3.2 Lower zone

This formula represents evapotranspiration from the lower zone over the pervious area of the subcatchment:

$$ETD = \frac{(DET - DWT1) \cdot ETMAX \cdot (1 - CET)}{DET}$$ (James et al. 2008, p.514)

Where

ETD = rate of evapotranspiration from the lower zone (mm/day)

DET = depth over which evapotranspiration can occur (mm)

$DWT1$ = depth of upper zone at beginning of time step (mm)

SWMM imposes two conditions on this calculation. Firstly, if the calculated evapotranspiration rate of the lower zone is greater than the difference between the maximum upper zone evapotranspiration rate and the upper zone evapotranspiration rate, then the evapotranspiration rate of the lower zone becomes the difference between the maximum upper zone evapotranspiration rate and the upper zone evapotranspiration rate. Secondly, if the calculated evapotranspiration rate of the lower zone is less than zero, it is set equal to zero.

3.10.3.3 Dams

SWMM calculates evaporation separately for dams (storage units) using the evaporation rates that the user supplies and the following equation:

$$e_v = 0.5 \cdot A \cdot e_d \cdot t$$ (R. Dickinson, 2011, pers. comm., June 13)

Where

e_v = evaporation loss rate (m^3/s)

A = surface area at the water level in the dam (m^2)

e_d = evaporation rate (mm/day)

t = time step (s)

3.10.4 Overland flow

SWMM treats each subcatchment as a nonlinear reservoir[18] with inflows from precipitation (or designated upstream catchments). Outflows are infiltration, evaporation and surface runoff. Surface runoff occurs only when the depth of water, *d*, on the subcatchment surface exceeds the maximum depression storage, *dp*. Figure 8 on page 40 illustrates this.

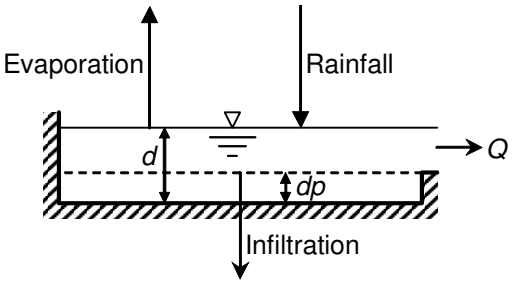

Figure 8: SWMM conceptual runoff view (after James et al. 2008, p.79)

SWMM divides each subcatchment into a pervious area (A2) with depression storage, an impervious area with (A1) and an impervious area without depression storage (A3). See Figure 9. Each area is a nonlinear reservoir that generates runoff.

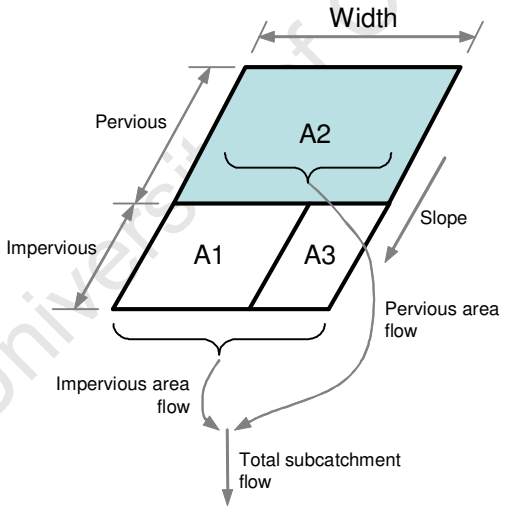

Figure 9: SWMM subcatchment divisions (after James et al. 2008, p.481)

SWMM establishes the nonlinear reservoir by coupling the continuity equation (see Table 6 on page 35) with Manning's equation (see page 33). For a subarea (A1, A2 and A3) the continuity equation can be written as:

[18] The response of nonlinear reservoirs varies with the storage in the reservoir or the flow through the reservoir.

$$\frac{\partial V}{\partial t} - A\frac{\partial d}{\partial t} = A \cdot i^* - Q$$ (James et al. 2008, p.482)

Where

V = $A \cdot d$ = volume of water on subarea (m^3)

D = water depth (m)

t = time (s)

i^* = rainfall excess (mm/h)

Q = outflow rate (m^3/s)

Manning's equation generates the outflow:

$$Q = W \cdot \frac{1.49}{n}\left(d - d_p\right)^{5/3} S^{1/2}$$ (James et al. 2008, p.483)

Where

W = subcatchment width (m)

n = Manning's roughness coefficient ($s/m^{1/3}$)

d_p = depth of storage (m)

S = subcatchment slope (m/m)

Combining these latter two equations into one nonlinear differential equation for a nonlinear reservoir gives an equation that can be solved for the depth, d:

$$\frac{\partial d}{\partial t} = i^* - W \cdot \frac{1.49}{n}\left(d - d_p\right)^{5/3} S^{1/2}$$ (James et al. 2008, p.483)

SWMM solves this equation at each time step using a simple finite difference scheme. Before computing the outflow, SWMM checks if infiltration and evaporation losses exceed rainfall depth plus ponded water. If so, outflow is zero (James et al. 2008, p.484).

3.10.5 Infiltration – Green & Ampt

The Green & Ampt infiltration method is widely used and so its parameters are easily obtained in literature. It was used in this project, so this text explains SWMM's implementation of only this method.

SWMM uses the Mein-Larson formulation for infiltration. It is a two-stage model in which the first step predicts the volume of water that will infiltrate before the soil saturates:

$$F_s = \frac{S \cdot IMD}{\frac{i}{K_s} - 1}$$ (James et al. 2008, p.483)

Where

F_s = cumulative infiltration required to cause surface saturation (m)

S = average capillary suction at the wetting front (m)

IMD = initial moisture deficit (the porosity minus the field capacity[19]) (mm/mm)

i = rainfall intensity (mm/h)

K_s = saturated hydraulic conductivity (mm/h)

After saturation, the Green & Ampt equation predicts infiltration (James et al. 2008, p.466).

$$f_p = K_s\left(1 + \frac{S \cdot IMD}{F}\right)$$ (James et al. 2008, p.483)

Where

f_p = infiltration capacity(m/s)

F = cumulative infiltration during this event (m)

Before saturation, the current rainfall intensity determines the volume of rainfall needed to saturate the surface. If $i > K_s$, SWMM calculates F_s and compares it with the rainfall volume that has already infiltrated during the current event. If F exceeds F_s, the surface saturates and further calculations use the second equation (James at al. 2008, p.467).

When $i \leq K_s$, all rainfall infiltrates and SWMM just updates IMD. After surface saturation, the infiltration capacity depends on infiltration rates in previous time steps. SWMM sums the infiltrated volumes for each time step. When rainfall ceases, or falls below infiltration capacity, ponded water on the surface starts to infiltrate and SWMM adds this to the cumulative infiltration volume (James at al. 2008, p.467).

[19] The field capacity is the minimum moisture content required before water can drain through soil. Values for different soil textures are available in literature.

3.10.5.1 Recovery of infiltration capacity

During time steps when no infiltration takes place due to either rainfall or depression storage, SWMM applies a depletion factor (*DF*) in h^{-1} to the soil moisture:

$$DF = \frac{4 \cdot \sqrt{K_s}}{300}$$ (James et al. 2008, p.468)

Where

K_s = saturated hydraulic conductivity (mm/h)

The depletion volume, *DV,* is:

$$DV = DF \cdot FU_{\max} \cdot \Delta t$$ (James et al. 2008, p.468)

Where

$FU_{max} = L \cdot IMD_{max} \cdot \Delta t$ = saturated moisture content of the upper zone

Then:

$$FU = FU - DF \text{ for } FU \geq 0$$

$$F = F - DV \text{ for } F \geq 0$$ (James et al. 2008, p.469)

Where

FU = current moisture content of upper zone (mm)

F = cumulative infiltration volume of this event (mm)

3.10.6 Groundwater

SWMM models subsurface groundwater areas using aquifer objects. These objects receive infiltration from rainfall and they interchange groundwater with the drainage system, depending on the hydraulic gradient (James at al. 2008, p.70).

SWMM simulates groundwater flow using two zones, an upper (unsaturated) and a lower (saturated) zone (see Figure 10 on page 44). A percolation equation governs flow from the upper to the lower zone. The only loss from the upper zone is evapotranspiration and the inflow to this zone is the calculated infiltration. The lower zone can experience loss via deep percolation, evapotranspiration and groundwater flow. Groundwater flow depends on a user-defined power function of the water table stage and the depth of water in channels (James at al. 2008, p.509).

At each calculation time step, SWMM uses a mass balance equation to calculate the moisture content in the upper zone:

$$TH2 = \frac{[(ENFIL - ETU) \cdot PAREA - PERC] \cdot DELT}{DWT1 + TH}$$ (James et al. 2008, p.512)

Where

TH2 = moisture content in the upper zone at the end of the time step (fraction)

ENFIL = calculated infiltration rate (mm/s)

ETU = rate of evapotranspiration in the upper zone (mm/s)

PAREA = pervious area divided by total area (m^2/m^2)

PERC = calculated percolation rate (mm/s)

DELT = time step value (s)

DWT1 = upper zone depth at beginning of time step (mm)

TH = moisture content in the upper zone at the beginning of the time step (mm/mm)

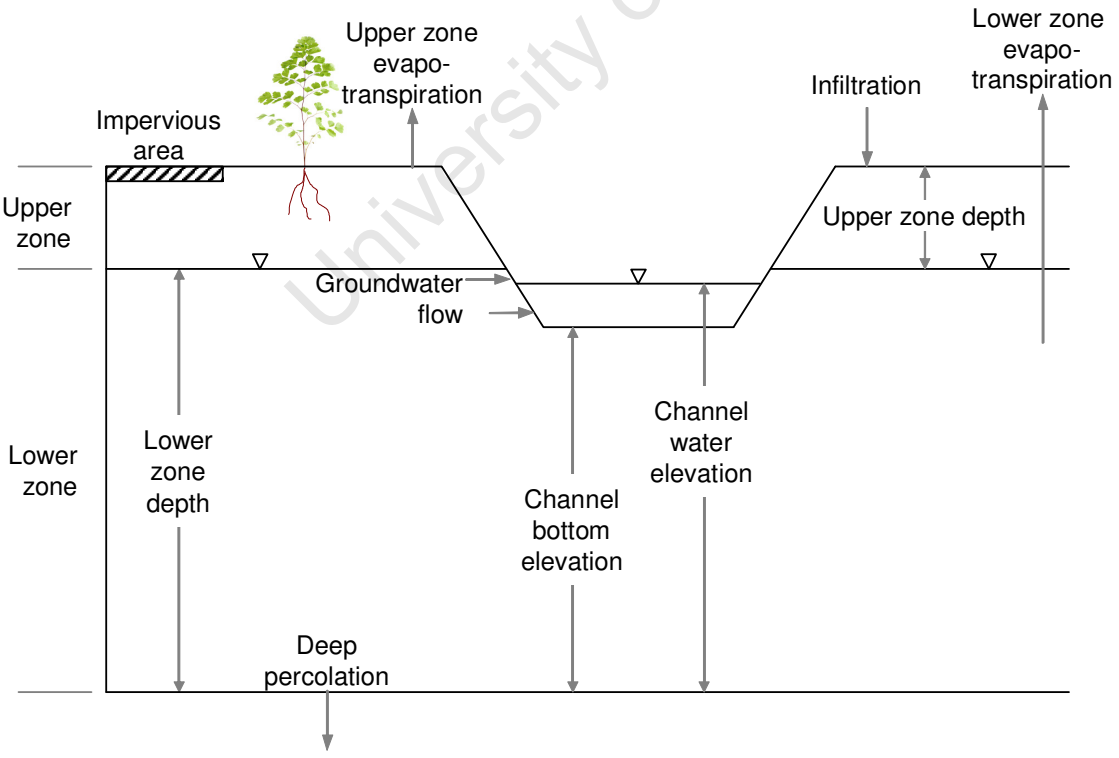

Figure 10: Groundwater flow in SWMM (after James et al. 2008, p.511)

The moisture content in the upper zone is then used to calculate the depth of the lower zone at the end of the time step using one of two equations, depending on whether the water table is rising or falling. For a rising water table:

$$D2 = \frac{\left[PERC - ETD \cdot PAREA - 0.5 \cdot \left(GWFLW + A1 \cdot (D2 - BC)^{B1} + A3 \cdot D2 \cdot TW + DEPPRC + DP \cdot D2/DTOT\right) - TWFLW\right] \cdot DELT + (D2 - D1) \cdot (TH - TH2)}{(PR - TH2 + D1)}$$

(James et al. 2008, p.510)

and for a falling water table:

$$D2 = \frac{\left[PERC - ETD \cdot PAREA - 0.5 \cdot \left(GWFLW + A1 \cdot (D2 - BC)^{B1} + A3 \cdot D2 \cdot TW + DEPPRC + DP \cdot D2/DTOT\right) - TWFLW\right] \cdot DELT + (D2 - D1) \cdot (TH - TH2)}{(PR - TH2 + D1)}$$

(James et al. 2008, p.510)

Where

D2 = depth of the lower zone at the end of the time step (m)

D1 = depth of lower zone at the beginning of the time step (m)

ETD = evapotranspiration rate of the lower zone (m/s)

GWFLW = groundwater flow rate at beginning of time step (m/s)

A1 = groundwater flow coefficient

BC = channel bottom elevation (m)

B1 = groundwater flow exponent

A3 = groundwater flow coefficient

TW = channel water elevation (m)

DEPPRC = deep percolation rate at beginning of time step (m/s)

DP = recession coefficient derived from declines in the water table between events

DTOT = total depth of upper and lower zone (m)

PR = porosity (fraction)

3.10.6.1 Percolation

SWMM uses Darcy's law for unsaturated flow to calculate how much water percolates from the upper zone to the lower zone. It uses a finite difference method to solve the differential equation and takes into account that hydraulic conductivity is a function of moisture content. The equation used is:

$$PERC = HKTH\left[1 + PCO \cdot \frac{(TH - FC)}{0.5 \cdot DWT1}\right]$$ (James et al. 2008, p.518)

Where

HKTH = hydraulic conductivity as a function of moisture content (mm/s)

PCO = ratio between the soil water tension (*PSI*) and moisture content (*TH*) in the region between *TH* and field capacity (*FC*)

DWT1 = upper zone depth at beginning of time step (mm)

3.10.6.2 Deep percolation

Water can exit the system through deep percolation. The water moves vertically beyond the confining layer or it moves sideways to somewhere other than the receiving water. It is very small in most cases.

$$DEPPRC = DP \cdot \frac{D1}{DTOT}$$ (James et al. 2008, p.521)

Where

DEPPRC= deep percolation rate at the beginning of the time step (mm/s)

DP = a recession coefficient derived from interevent water table recession curves

D1= depth of lower zone at the beginning of the time step (mm)

DTOT= total depth of upper and lower zone (mm)

3.10.6.3 Lateral groundwater flow

Some of the groundwater flows laterally from the saturated zone to the receiving water. The flow equation is:

$$GWFLW = A1 \cdot (D1 - BC)^{B1} - A2 \cdot (TW - BC)^{B2} + A3 \cdot D1 \cdot TW$$ (James et al. 2008, p.521)

Where

GWFLW = groundwater flow rate per subcatchment area at the beginning of the time step (m/s)

A1, A2 = coefficient for groundwater and channel water influence flow respectively

D1 = depth of lower zone at the beginning of the time step (m)

B1, B2 = exponents for groundwater and tailwater influence flow respectively

BC = elevation of bottom channel (m)

TW = elevation of water in the channel (m)

The second term in the above equation represents the channel water influence flow rate.

If the depth of the lower zone (*D1*) is less than the bottom channel elevation or the elevation of the water in the channel, the *GWFLW* is set to zero (James at al 2008, p.522).

3.10.7 Channel flow

SWMM can simulate water flow through pipes of various geometries and through natural channels with irregular geometries. It takes outflow hydrographs from the surface runoff module as input and produces discharge hydrographs and velocities for each conduit, and flow depths and water surface elevations at each junction in the model (James et al. 2008, p.650). As explained earlier, SWMM uses a system of links (such as conduits), to convey water flow from node to node in the model. The link-node concept allows SWMM to represent flow control devices, such as weirs and pumps (James at al. 2008, p.651–652). Figure 11 shows the link-node concept with conduits as links.

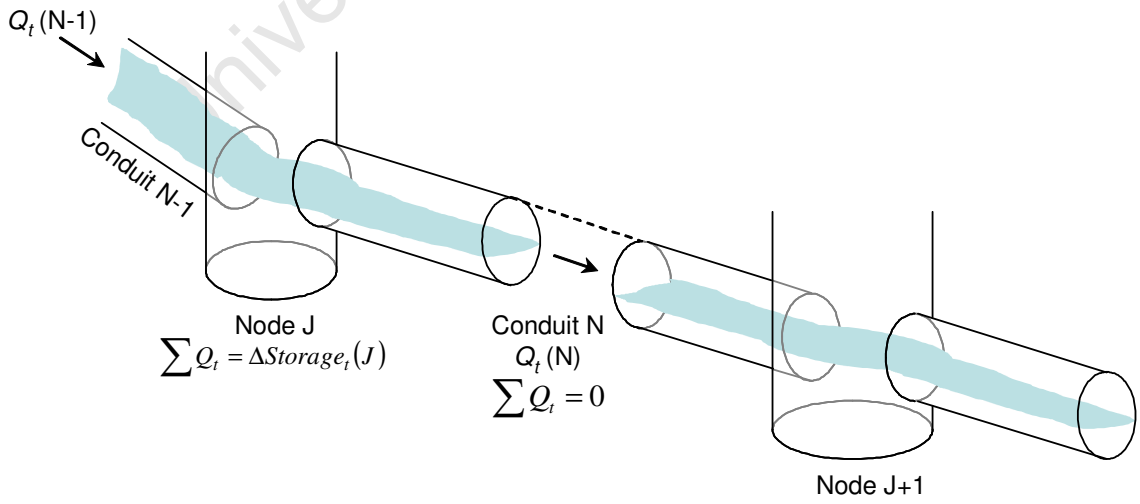

Figure 11: Conceptual view of channel flow in SWMM (after James et al. 2008, p.652)

SWWM solves a combination of the Saint-Venant continuity and momentum equations to find the flow in each conduit at each time step:

$$\frac{\partial Q}{\partial t} + gAS_f - 2V\frac{\partial A}{\partial t} - V^2\frac{\partial A}{\partial x} + gA\frac{\partial H}{\partial x} = 0$$ (James et al. 2008, p.655)

Where

Q = discharge along the conduit (m^3/s)

V = velocity in the conduit (m/s)

A = cross-sectional area of the flow (m^2)

H = hydraulic head (invert elevation plus water depth (m)

S_f = friction slope (m/m)

Manning's equation gives the friction slope:

$$S_f = \frac{k}{gAR^{\frac{4}{3}}}Q|V|$$ (James et al. 2008, p.655)

Where

k = gn^2 (m/s^2)

n = Manning's roughness coefficient ($s/m^{1/3}$)

g = gravitational acceleration (m/s^2)

R = hydraulic radius (m)

At nodes, SWMM uses the following equation to relate Q and H:

$$\frac{\partial H}{\partial t} = \sum \frac{Q_t}{A_{s_t}}$$ (James et al. 2008, p.656)

Where

A_s = surface area of node (m^2)

SWMM solves the latter two equations sequentially to find the discharge in each link and the head (water level) at each node over a computational time step. It uses the modified Euler method to integrate these two equations.

3.10.7.1 Transmission losses during dry periods

Water loss from channels will be used in Section 7.4.2 to validate the rainfall-runoff model used in this project and so this section discusses the processes that extract water from natural channels during dry periods. The processes that may do this are: (i) direct evaporation from standing or flowing water in a channel; (ii) evaporation and transpiration losses from seepage areas where groundwater or channel bank soil water is draining into the channel; (iii) groundwater recharge from streamflow where the phreatic surface lies below the channel (river channels often follow lines of structural weakness and surface fracturing, offering an ideal opportunity for infiltration into the channel bed); (iv) bed losses, where unconsolidated alluvial material underlies the river channel (these losses can be substantial during low flows); and (v) losses to relatively dry soils forming the banks of streams (riparian vegetation may enhance this process through evapotranspiration) (Smakhtin, 2001). These losses are collectively called transmission losses. Figure 12 on page 49 shows a cross section of a river bed at low flow with the processes that cause transmission losses. The process numbers in the figure correspond to the numbers used in this paragraph.

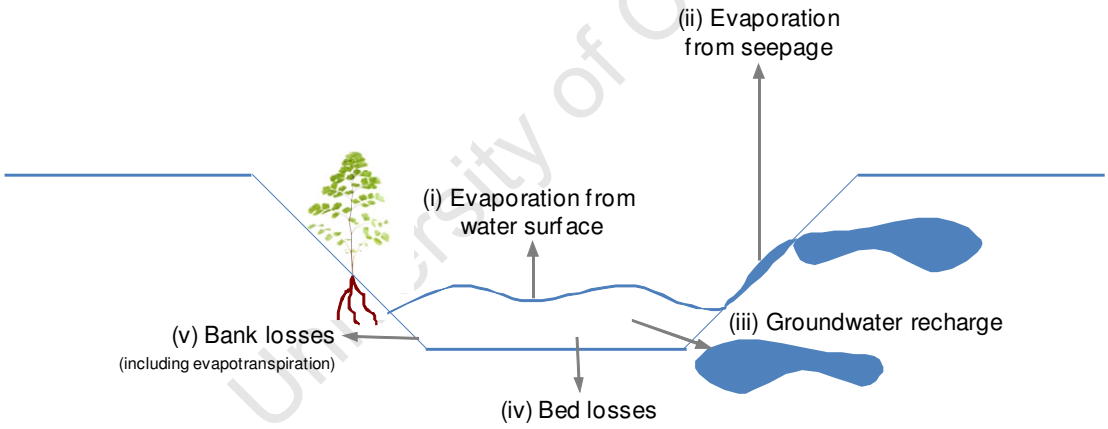

Figure 12: Cross section of river channel showing transmission losses

3.11 A SWMM model in summary

The preceding sections explained how SWMM implements runoff and channel flow theory. Figure 13 on page 51 illustrates in summary how the different parts of SWMM interact to produce and outflow hydrograph. The left-hand side of the figure shows a schematic of the physical entities that translate to SWMM objects and the right-hand side of the figure shows more detail about the SWMM components.

At each calculation time step and for each subcatchment in the model, the RUNOFF module subtracts evaporation and infiltration from the rainfall input to calculate the rainfall excess (effective rainfall). In these

calculations, SWMM uses the provided evaporation data and the soil properties. SWMM then uses the sub-catchment properties, such as area, flow length, slope and hydrological roughness to calculate the surface runoff for each catchment. This runoff hydrograph is routed to an inlet node in the link-node network. The link-node network also receives exfiltration from aquifers at specified nodes. The EXTRAN module then routes the input hydrographs to the catchment outlet using the properties of the link-node network. At the end of each calculation time step SWMM stores the state of each object to use as starting values during the next calculation time step.

3.12 Evaluating rainfall-runoff model performance

> *It is not enough merely to know when a model may be said to be useful – it's important to know how reliable it is.*
>
> *William James*

Rainfall-runoff models require measures of how the model is performing for two reasons: to calibrate the model and to determine if the model is good enough for its purpose. To measure model performance, one needs an objective function – a parameter that has measured values with which one can compare the calculated values. In hydrology engineers often use functions such as peak flow, time of peak flow, peak volume, and total flow volume as objective function. The choice depends on the purpose of the model. A variety of functions that hydrologists use to evaluate their models are listed in James (2005, pp.194–202) and the ones available in the software used in this project are listed in Table 7 on page 50. In all formulas OOF_i refers to 'observed objective function measurement i' and COF_i refers to 'calculated objective function measurement i'. The observed and calculated time series consist of n observations that are compared with one another. Dimensionless error measures allow for meaningful comparison of different models that use data sets differing in magnitude and in number of records (Green and Stephenson, 1986).

Table 7: Functions for evaluating models

Name	Formula	Comments
Simple least squares	$\sum_{i=1}^{n}(OOF_i - COF_i)^2$	Tends to favour large errors and large flows. Most common (Green and Stephenson, 1986).
First dimensionless form of simple least squares	$\sum_{i=1}^{n}\left(\frac{OOF_i - COF_i}{OOF_i}\right)^2$	Tends to be independent of long records and to favour large flows.
Mean absolute error	$\frac{\sum_{i=1}^{n}\lvert OOF_i - COF_i\rvert}{n}$	Suited to optimisation (Green and Stephenson, 1986).
Root mean square error	$\sum_{i=1}^{n}\left[\frac{(OOF_i - COF_i)^2}{n}\right]^{\frac{1}{2}}$	-

Name	Formula	Comments
Root mean square error dimensionless	$\frac{\sum_{i=1}^{n}\left[\frac{(OOF_i - COF_i)^2}{n}\right]^{\frac{1}{2}}}{\overline{OOF}}$	-
Standard error of estimate	$\sum_{i=1}^{n}\frac{(OOF_i - COF_i)^2}{n-2}$	A measure of the variability of the estimate. Dimensional and independent of the number of points (Green and Stephenson, 1986).
N-S correlation	$1-\frac{\sum_{i=1}^{n}(OOF_i - COF_i)^2}{\sum_{i=1}^{n}(OOF_i - \overline{OOF})^2}$	Ranges from –∞ to 1. One is a perfect match and a model with an N-S correlation of 0 has the same predictive power as the mean of the observed values. Has gained wide acceptance and is a good choice for a dimensionless measure of fit (Green and Stephenson, 1986).

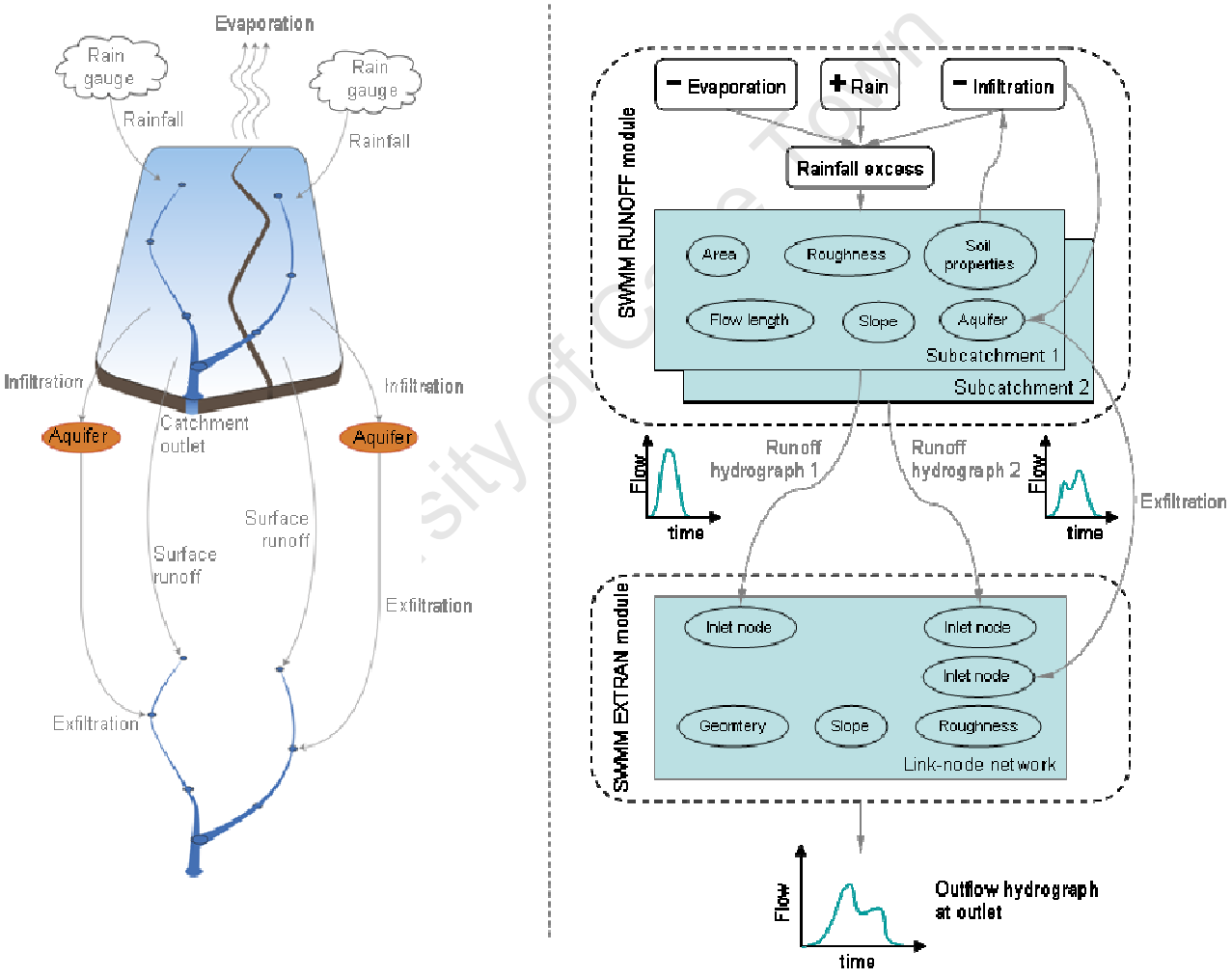

Figure 13: How SWMM model objects interact

3.12.1 Event modelling and continuous modelling

Many studies reported in literature calibrate a model against one data set and then evaluate the model against another, separate dataset. This is called event modelling. Other studies use continuous modelling in which the model is calibrated against the entire, continuous dataset. Event modelling was especially useful before computer models became ubiquitous, but modern computers can better handle the immense number of calculations and volumes of data necessary for continuous modelling. By omitting some information from the calibration process, one foregoes the opportunity to calibrate the model against all the information available and it may result in an inferior model (James 2005, pp.80–81). However, continuous models cannot take into account significant hydrologic or hydraulic modifications to the study area.

3.13 Inundation modelling

Inundation modelling refers to finding the extents of a river and visualising these on a map. This requires the shape of the land surface in and around the river, as well as the shape of the water surface at different river stages.

Whiteaker et al. (2006) used the following procedure to create a flood inundation polygon:

1. Create a water surface raster.
    a. Extract the water surface elevations at various points along the river.
    b. Assign water surface elevations to river cross sections.
    c. Create a Triangulated Irregular Network (TIN) of the water surface elevations using cross sections as soft break lines.
    d. Clip the TIN to the convex hull of river cross sections.
    e. Convert the TIN to a raster.
2. Generate river extents.
    a. Subtract the land surface elevation raster from the water surface raster created in the previous step. The result is a raster that represents the depth of the river.
    b. Convert raster cells with positive depth to polygons and dissolve the polygon into one inundation polygon.

Chen et al. (2009) coded their own inundation model and used a raster-based approach. In each iteration the algorithm:

1. Assesses and updates each cell's wet or dry status.
2. Increments the water depth in each wet cell.

3. Searches the cells surrounding wet cells for dry cells with elevations lower than the wet cell's water level and sets these dry cells' water levels equal to the wet cell's water level.

3.13.1 Validating inundation models

To validate an inundation model one ideally needs the extent of the inundation and the depth of the inundation. Researchers use field data and remotely sensed images (Baldassare et al., 2009, Horrit and Bates, 2002 and Matgen et al., 2007) to find inundation extents. Radar images are especially useful because they can penetrate the cloud cover that is typically present during the rain storms that cause floods. For inundation depths researchers need field data or stage instruments. Residents also report flood extents and depths to central authorities, especially in cities. Another source of information about flood extents are photographs published in news media and on the web.

4. Model selection

4.1 Model requirements

The original aim of this project was to create a real-time flood warning system that models rainfall-runoff and that shows the resulting inundation extents. Furthermore, the project aims to use free and open source software in the scientific workflow. To fulfil these aims, the ideal rainfall-runoff model had to satisfy the following requirements:

Requirement	Reason for requirement
1. Provide a free and, preferably, open source software implementation of the model.	Purpose of the study.
2. Take as input data available for free from the Internet, especially for dynamic data such as rainfall.	Purpose of the study.
3. Model overland flow and channel flow.	Simpler than having to couple two separate models.
4. Model input flow from outside the catchment.	Study area includes a tunnel outlet that transfers water from the Katse dam into the catchment.
5. Model events or model continuously.	Satisfy different operational requirements.
6. Make the model results available in an external file so that another program can read it.	A control program must be able to access the results and use it in other parts of the monitoring system.
7. Use a sub daily computational and reporting time step.	The study area has a response time of at most 13 hours and a real-time flood system needs to make its information available as soon as possible.
8. Produce results that are spread out over the catchment. In other words, it must be a distributed model and the modeller must be able to determine the level of discretization.	Enable inundation modelling.
9. Have a 'hotstart' capability to process new data that comes in, starting with the results of the previous model run.	Reduces the time it takes the model to run and so makes the results available as soon as possible.

4.2 Models reviewed

The initial investigation for this project discovered a number of models to consider. Table 8 lists the rainfall-runoff models that the investigation found but that this researcher did not use, and the reasons for not using them:

Table 8: Discarded rainfall-runoff models

Model name	Type	Source	Reason for discarding model
ACRU	Rainfall-runoff	Kime, D (2010) pers. comm. April 12.	Daily time step model. Proprietary software.
ARNO	Rainfall-runoff	Literature review	Software unavailable.

Model name	Type	Source	Reason for discarding model
Data-based mechanistic	Rainfall-runoff	Literature review	Lumped model Proprietary software
GBHM	Rainfall-runoff	Literature review	Software unavailable.
GeoSFM	Rainfall-runoff	Literature review	Proprietary software (ArcGIS plugin).
GRASS GIS r.sim.water model	Overland flow	Internet search	No channel flow component. Not suited to large catchments (Mitasova, H, 2010, pers. comm. June 14).
HEC-HMS with HEC-RAS	Overland flow Channel flow and inundation	Literature review	Two models are not coupled. HEC-RAS prone to instabilities during supercritical flow[20] (Brooker, C. 2011, pers. comm. March 1).
IHACRES	Rainfall-runoff	Literature review	Lumped model that gives flow results at the outlet of the catchment only. Does not model inflows.
Input Storage Output (ISO)	Rainfall-runoff	Literature review	Lumped model that gives flow results at the outlet of the catchment only. Only applicable to small catchments (< 20 ha).
ISIS	Channel flow	Internet search	Channel flow only.
Jflow	Rainfall-runoff	Literature review	Proprietary software.
KINEROS	Rainfall-runoff	Literature review	Event-based model. Models small detention ponds only, not large dams.
LISEM	Rainfall-runoff	Internet search	Software unstable and no support available.
Nonpoint-Source Pollution and Erosion Comparison Tool	Rainfall-runoff and water quality	Literature review	Runs in ArcGIS, which is proprietary software (Thomas et al., 2010, p.iv).
Open-book watershed model	Rainfall-runoff	Literature review	Software unavailable.
Runoff, Infiltration and Non-point Source Pollution Estimation	Rainfall-runoff and water quality	Literature review	Runs in ArcGIS, which is proprietary software (Thomas et al., 2010, p.v).
SHE	Rainfall-runoff	Literature review	Requires extensive climate data that were not available.
SLURP	Rainfall-runoff	Literature review	Proprietary software.
Soil and Water Assessment Tool (SWAT)	Rainfall-runoff	Internet search	Daily time step only
SPATSIM	Rainfall-runoff	Literature review	Uses ESRI Map Objects, which requires a licence. Daily and monthly time steps only.
Terrestrial hydrologic model	Rainfall-runoff	Literature review	Software unavailable.
TOPKAPI	Rainfall-runoff	Suggested by developer (Sinclair, S, 2010, pers. comm. March 5).	Software did not work with sample data. Minimal support available. Documentation does not explain how input data should be prepared.

[20] Supercritical flow occurs when the water's flow velocity is faster than its wave velocity. It typically happens when water accelerates over steep channel sections or over control structures, such as weirs. This kind of flow is rapid and unstable.

Model name	Type	Source	Reason for discarding model
Topmodel	Rainfall-runoff	Literature review	Only demonstration software available for free.
USDA-NRCS-CN	Rainfall-runoff	Literature review	Lumped model that gives flow results at the outlet of the catchment only. Cannot model inflows.
Xinanjiang	Rainfall-runoff	Literature review	Only valid for humid catchments.

4.3 Motivation for using SWMM

The US EPA first started developing SWMM in 1971. Modellers use it mostly in urban settings, but it is also suitable for non-urban applications such as mapping floodplains in natural channel systems. SWMM 5 (the latest version) is an approved model for national flood insurance studies in the US (Storm Water Management Model (SWMM), 2011). As demonstrated in Section 2.1.1 of this document, researchers often use SWMM to model an area before and after development to assess the impact of the development.

SWMM is free and open source software available from the US EPA web site[21]. Several companies have integrated SWMM with data processing and visualisation functions, which they then sell as proprietary software. Computational Hydraulics International (CHI) is one such company and it lists 1 908 clients of their PCSWMM package around the world; 90 are in South Africa. The South African clients include consulting engineers, municipalities, the CSIR and DWA[22]. Innovyze is another such company and it has 1 314 clients who use its InfoSWMM package around the world, including two in South Africa[23]. For support, SWMM has an active email list[24] and extensive user and developer documentation on the web and in printed format, including the 852-page *User's guide to SWMM 5*. Support is important because of this researcher's lack of previous experience in hydrological modelling. Support would also be essential if this model was to be used operationally.

Modelling natural channels in SWMM usually involves detailed cross sections of the rivers at regular intervals; this implies high-resolution elevation data. Such data were not available for this study, but engineers expressed the opinion that SWMM would do as good a job as any of the other popular models, such as the HEC family of models, given the coarse data available for defining and running the model (James, R (2010), pers. comm. October 22 and Townsend, D (2010), pers. comm. September 27).

SWMM is widely used, recognised and supported and it satisfies most of the criteria listed in Section 4.1. In the absence of a high-resolution DEM, the rivers could be modelled as trapezoidal channels with configurable widths, depths and bank slopes. The only other model found during the discovery phase of the project that comes close to satisfying as many criteria would be a coupled HEC-HMS/HEC-RAS model and HEC-

[21] http://www.epa.gov/nrmrl/wswrd/wq/models/swmm/. Retrieved 24 June 2011.
[22] http://www.chiwater.com/Company/ClientList.asp. Retrieved 24 June 2011.
[23] http://www.innovyze.com/about/clients/?clients=cities. Retrieved 24 June 2011.
[24] http://www.epa.gov/nrmrl/wswrd/wq/models/swmm/#Contact. Retrieved 24 June 2011.

RAS also requires detailed river transects. Therefore, this researcher chose SWMM as the model for use in this project.

5. Data collection

This chapter describes that data collected for this project and the reasons for using the chosen data. It first discusses selecting a source of SBRE. Then it lists the data procured from the internet and from other sources.

5.1 Selecting a rainfall data source

This researcher investigated a number of satellite-based rainfall estimates for use in this project. These SBRE generally use the same sensor platforms (see Section 3.3.3.3 on page 26), but they use different algorithms to calculate their precipitation estimates (Tian and Peters-Lidard, 2010). Table 9 lists the SBRE considered for this project. Others are available, but their resolutions (spatial or temporal) are coarser and so they are not listed here.

Table 9: Satellite based rainfall estimates considered for use in this project

Name	Spatial resolution	Temporal resolution	Date range available
CMORPH	0.25°× 0.25°	3 h	2002 to present
Naval Research Laboratory (NRL) Blended	0.25°× 0.25°	3 h	2003 to present
PERSIANN	0.25°× 0.25°	3 h	2000 to present
TRMM 3B42	0.25°× 0.25°	3 h	1998 to present

Raymond and Sapiano (2010) aggregated the CMORPH, NRL-Blended, PERSIANN and TRMM 3B42 satellite-based rainfall estimates to 2.5° monthly means to compare them to the Global Precipitation Climatology Project[25] values. They concluded that no single dataset outperforms the others. However, researchers more frequently study the TRMM data products. A multi-database online search (using the University of Cape Town Library's search and discovery tool on 27 July 2011) gives 1 751 peer reviewed articles for 'TRMM', compared to 65 for 'CMORPH', 49 for 'PERSIANN' and 27 for 'NRL-Blended'. Therefore, this researcher chose the TRMM 3B42 product to use as rainfall input to the hydrological model.

5.2 Data from the Internet

Table 10 lists the data downloaded from the Internet for this project, along with the purpose of each dataset in the reason for using it.

[25] The Global Precipitation Climatology Project has since 1979 merged data from over 6,000 rain gauge stations, and satellite geostationary and low-orbit infrared, passive microwave, and sounding observations to estimate monthly rainfall on a 2.5-degree global grid (http://www.gewex.org/gpcp.html, retrieved 27 July, 2011).

Table 10: Internet data sources used in this project

Name	Format	Source	Comments	Purpose and reason for using	Processing
DWA Rivers	GIS vector	DWA web site (http://www.dwaf.gov.za/iwqs/gis_data/river/All.zip)	1:500 000 rivers for the whole country.	Most accurate source of river data available on the Internet. Used as a starting point for constructing conduits in the SWMM model.	Clip to study area
DWA quaternary catchments	GIS vector	DWA web site (http://www.dwaf.gov.za/iwqs/gis_data/river/hca_4.ZIP)	Quaternary catchments for the whole country	Delineate the boundaries of the study area. More accurate than delineating the watershed from the SRTM 90 m DEM.	Single out study area.
DWA dams	GIS vector	DWA web site (http://www.dwaf.gov.za/iwqs/gis_data/river/dams500g.zip)	Major dams in SA.	Most accurate source of dam locations available on the Internet. Used as a starting point for constructing storage units in the SWMM model.	Clip to study area
DWA flow data	HTML	DWA hydrology web site (http://www.dwa.gov.za/hydrology/CGI-BIN/HIS/CGIHis.exe/Station)	Flow data for flow meters C8H036 (Katse inflow) and C8R004 (Saulspoort dam) in the study area, measuring flow and water level.	Required to evaluate the SWMM model.	Python script to download, parse, combine and convert to text. Import to SWMM.
DWA evaporation data	HTML	DWA hydrology web site (http://www.dwa.gov.za/hydrology/CGI-BIN/HIS/CGIHis.exe/Station)	S-Pan evaporation data at Bethlehem (meter number C8E003).	Required for SWMM overland flow modelling.	Python script to download, parse, combine and convert to text. Import to SWMM.
SRTM 90 m DEM	GIS raster	Global Land Cover Facility at the University of Maryland FTP site (ftp://ftp.glcf.umiacs.umd.edu/glcf/SRTM/Degree_Tiles/s029/SRTM_f03_s029e028/SRTM_f03_s029e028.tif.gz)	90 m pixel size.	This DEM was used because the other DEM available at the start of the project (the CD:NGI 25 m DEM) contained errors. Finest resolution DEM available on the Internet.	Clip to border of study area and to study area extents.
MODIS land cover (NASA, 2008)	HDF raster	USGS FTP site ftp://e4ftl01.cr.usgs.gov/MOTA/MCD12Q1.005/2008.01.01/MCD12Q1.A2008001.h20v11.005.2009338162324.hdf)	500 m pixel size.	Only GIS layer available with complete land cover for the whole catchment. Used with CD:NGI land cover layers to determine Manning's *n* for overland flow using literature values.	Use MODIS Reprojection Tool software to convert to GIS raster format and clip to study area.
Harmonised world soil database (HWSD)	GIS raster and Microsoft Access database	HWSD web site (http://www.iiasa.ac.at/Research/LUC/External-World-soil-database/HTML/)	0.0083° (approximately 865 m) pixel size	Soil texture used to derive soils' hydraulic conductivity, suction head and initial deficit for SWMM model. Best Internet source of soil data.	Clipped raster to study area and converted to polygons with soil texture attributes.

Name	Format	Source	Comments	Purpose and reason for using	Processing
TRMM 3B42 Rainfall (v.6)	NetCDF	NASA Mirador (http://mirador.gsfc.nasa.gov/cgi-bin/mirador/presentNavigation.pl?tree=project&dataset=3B42:%203-Hour%200.25%20x%200.25%20degree%20merged%20TRMM%20and%20other%20satellite%20estimates&project=TRMM&dataGroup=Gridded&version=006&CGISESSID=40c3240ad14aaf40248f0c4032486b1c)	3 hourly rainfall intensity values in 0.25° square grids (~26 km^2 when projected).	Used as rainfall input to SWMM model. Section 5.1 on page 58 explains reasons for choosing this dataset.	Python script to convert to extract values for study area and save as text files. Import to SWMM.

5.3 Data from other sources

Table 11 lists the data obtained from other sources for this project, along with the purpose of each dataset in the reason for using it.

Table 11: Other data sources used in this project

Name	Format	Source	Comments	Purpose and reason for using	Processing
Saulspoort dam survey	Text	DWA Pretoria	Horizontal slices of the major dam in the study area, showing area and volume vs. depth.	SWMM requires a storage curve or a discharge function to model dams. This is a large dam and it has a significant influence on the hydrology of the catchment area, so it needed to be modelled as accurately as possible.	Create storage curve (table of depth and surface area) for dam in SWMM.
Aerial photos	GIS raster	CD:NGI office, Mowbray	-	Used as background to check river channels and dam locations.	None.
CD:NGI 25 m DEM	Text	CD:NGI office in Mowbray	Upon investigation it was found that this DEM has a discrepancy of 10 m in the area of two flight overlaps and was therefore discarded.	Not used.	Import into GRASS and mosaic.
CD:NGI 20 m contour lines	GIS vector	CD:NGI office, Mowbray	-	Best topographic data available at the start of the project. Used to check and correct problems with SRTM DEM and to find areas of homogenous slope when creating conduits for the SWMM model.	Clip to study area
CD:NGI land use	GIS vector	CD:NGI office, Mowbray	-	Used with MODIS image to determine Manning's *n* for overland flow using literature values. Better resolution of land cover than MODIS image, but limited coverage.	Clip to study area

Name	Format	Source	Comments	Purpose and reason for using	Processing
CD:NGI inland water	GIS vector	CD:NGI office, Mowbray	-	Used to find locations and areas of smaller farm dams that were not on the DWA dam layer, but were visible on the aerial photographs.	None.
Rainfall	Text	SAWS	-	Hourly rainfall depth at Bethlehem Weather Office. Used to determine flood events and to compare with TRMM data.	None.
20 m DEM	GIS raster	DWA	Derived from the 1:50 000 CD:NGI contour lines with error correction by ComputaMaps. Became available only later in the project.	Used to investigate inundation modelling because SRTM DEM was too coarse.	Clip to study area.

6. Data processing and model construction

This section describes how data were processed for use in this project. It describes how ground-based rainfall data were used to determine the study period and how the TRMM data cells overlay the study area. It also explains the methods used to compare the TRMM 3B42 SBRE with the one ground-based rain gauge available near the study area. How SWMM objects were used to construct the model follows next and it concludes with remarks about removing continuity errors from the SWMM model and calibrating it.

6.1 Determining flood events

One can find a major rainfall event that may lead to a flood by comparing events to long-term averages and to percentiles. In this project, the BWO gauge rainfall was examined from 1 March 1993 to 31 March 2010 because its values are probably more reliable than the TRMM data and it is close enough to measure rainfall that would occur over the study area during a major flood event (see Figure 14 on page 63). Sorting the data revealed the largest measurements. Events before 1998 were discarded because the TRMM data is only available from 1998. Events after 2007 were discarded because a hydroelectric turbine was installed at the Saulspoort dam during 2008 and most of its flow is diverted through the turbine. The flow measurements through the turbine are not publicly available.

The flow at Saulspoort dam was also examined during the identified events to finally determine the simulation period. For this study, the 99th percentile was used as a cut-off point to determine flood events.

6.2 TRMM rainfall

6.2.1 Extraction

The TRMM rainfall grid cells that cover this project's study area were determined and their array indices used to extract the corresponding rainfall values for the study area over the study period. This researcher wrote a python script to read the NetCDF files downloaded from the Internet and to convert them to plain text files.

Figure 14 on page 63 shows how the three TRMM grid cells overlay the study area. The number in each cell identifies the cell and its rainfall values later in this document. The crosses are at the centroid of each cell and were used to assign rain gauges (using the TRMM rainfall time series) to subcatchments in the SWMM model. The map also shows the BWO with the only usable ground-based rain gauge in the vicinity of the study area[26]. The satellite rainfall estimates were compared to the rainfall measurements at this weather office.

[26] DWA has a rain gauge at the Katse tunnel inlet higher up in the catchment, but its measurements are available as daily values only and the measurements are unreliable (Oosthuizen, J, 2010, pers. comm. November 18).

6.2.2 Comparison with gauge measurements

Ideally this kind of comparison uses multiple ground-based gauges (point values) located at different places inside the TRMM grid cell (an area value). One can then convert the multiple point values to an area value using various interpolation methods. For this study only one point source was available – the SAWS rain gauge at the BWO. Its values are available as rainfall depth in millimetres every hour, while the TRMM SBRE are given as rainfall intensities in mm/h at three hour intervals. To compare these two values one has to convert between the two units. The following two sections describe the comparisons carried out for this study.

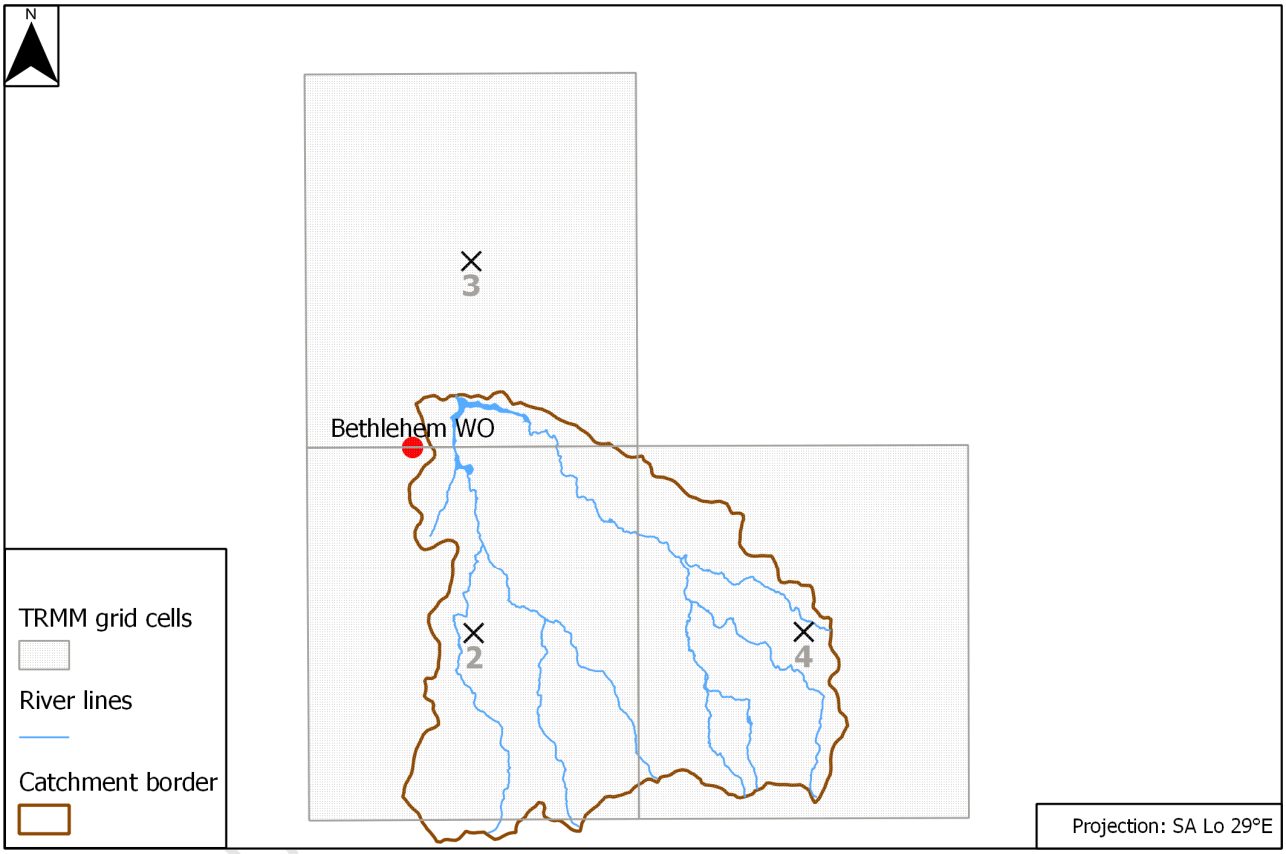

Figure 14: TRMM grid cells in study area

Only one TRMM cell was used in this comparison – TRMM2 (refer to Figure 14). The centroids of the TRMM2 and TRMM3 cells are equal distances away from the BWO, but the TRMM2 cell covers a larger part of the study area. The comparison covers 1 November 2003 to 31 October 2005.

6.2.2.1 Three-hourly comparison

To convert instantaneous rainfall to cumulative rainfall, Fulton et al. (1998) suggest taking the mean of the current instantaneous TRMM reading and the previous instantaneous TRMM reading and multiplying it by the time elapsed between the two readings. The BWO readings were accumulated over three hours for com-

parison with the TRMM data. The statistics calculated were the Pearson correlation coefficient, probability of detection, false alarm rate, critical success index and bias.

6.2.2.2 Monthly comparison

When using instantaneous rainfall values in SWMM, the modeller needs to specify the time interval during which the measurement is valid. For short time intervals between measurements, such as 15 minutes, one can reasonably assume that the measurement is valid for the whole interval. With coarse time resolutions however, other values may be better since rainfall events may not last the full length of the time interval. This section describes the method used to determine the best interval to use in the SWMM model constructed for this study.

The TRMM instantaneous rainfall values were converted to cumulative rainfall values to simulate storms that last one hour, two hours, two and a half hours and three hours. These results were accumulated monthly over two years to eliminate the problem of when exactly in the rainfall event the TRMM values were measured. The comparison covers 1 November 2003 to 31 October 2005.

Table 12 shows the accumulated rainfall for two years' data. The aim is to get a TRMM2 storm duration that closest approximates the BWO values. From the table it is clear that a two or two and a half hour storm would be best.

Table 12: Rain gauge and TRMM2 yearly accumulated rainfall totals

Year	Nov. 2003 to Oct 2004	Nov. 2004 to Oct. 2005
TRMM2 1h storm total rainfall	225.83	294.54
TRMM2 2h storm total rainfall	451.66	589.08
TRMM2 2.5h storm total rainfall	564.58	736.35
TRMM2 3h storm total rainfall	677.49	883.62
BWO total rainfall	**488.8**	**719.2**

Table 13 on page 64 shows the accumulated rainfall values by month and it is clear that the 2.5 hour storm best approximates the rain gauge values over the two-year period, especially during the wet summer months – November to April (shown in italics in Table 13). Therefore, the rain gauges in SWMM were set to use 2.5 hours as their time interval. Figure 15 on page 66 shows the data in Table 13 graphically.

Table 13: TRMM2 monthly accumulated rainfall as percentage of rain gauge rainfall

Month	TRMM2 2 h storm (% of rain gauge)	TRMM2 2.5 h storm (% of rain gauge)	Month	TRMM2 2 h storm (% of rain gauge)	TRMM2 2.5 h storm (% of rain gauge)
2003/11	*70%*	*88%*	*2004/11*	*96%*	*120%*
2003/12	*65%*	*81%*	*2004/12*	*76%*	*96%*

Month	TRMM2 2 h storm (% of rain gauge)	TRMM2 2.5 h storm (% of rain gauge)	Month	TRMM2 2 h storm (% of rain gauge)	TRMM2 2.5 h storm (% of rain gauge)
2004/01	*129%*	*161%*	*2005/01*	*77%*	*96%*
2004/02	*92%*	*115%*	*2005/02*	*70%*	*87%*
2004/03	*123%*	*154%*	*2005/03*	*118%*	*148%*
2004/04	*84%*	*105%*	*2005/04*	*75%*	*94%*
2004/05	20%	25%	2005/05	211%	264%
2004/06	54%	67%	2005/06	100%	100%
2004/07	0%	0%	2005/07	110%	110%
2004/08	40%	50%	2005/08	180%	225%
2004/09	524%	655%	2005/09	223%	279%
2004/10	92%	115%	2005/10	67%	84%
Whole year	92%	116%	Whole year	82%	102%

6.3 SWMM model construction

This section describes how physical entities were translated to SWMM objects and how parameters for the SWMM objects were determined. Although not ideal, SWMM's default object properties were used in some cases because the data to determine the values were simply not available. For example, channel roughness is usually determined by matching photographs of oblique river views with similar images in literature. Such views of the rivers in this catchment were not available. Also, limited information was available about aquifer properties, except for those that can be derived from the soil type.

6.3.1 Evaporation

DWA has a meter (C8E003) at Bethlehem that measures evaporation from an S-class pan. The pan factors for each month of the year are in Table 14 and Figure 16 on page 66 graphs the daily evaporation values before and after the pan factor correction. These evaporation values were loaded into SWMM's climatology editor.

Table 14: Symons pan factors (Haarhoff & Cassa 2009, p.108)

Month	Jan	Feb	Mar	Apr	May	Jun	Jul	Aug	Sep	Oct	Nov	Dec
Pan factor	0.84	0.88	0.88	0.88	0.87	0.85	0.83	0.81	0.81	0.81	0.82	0.83

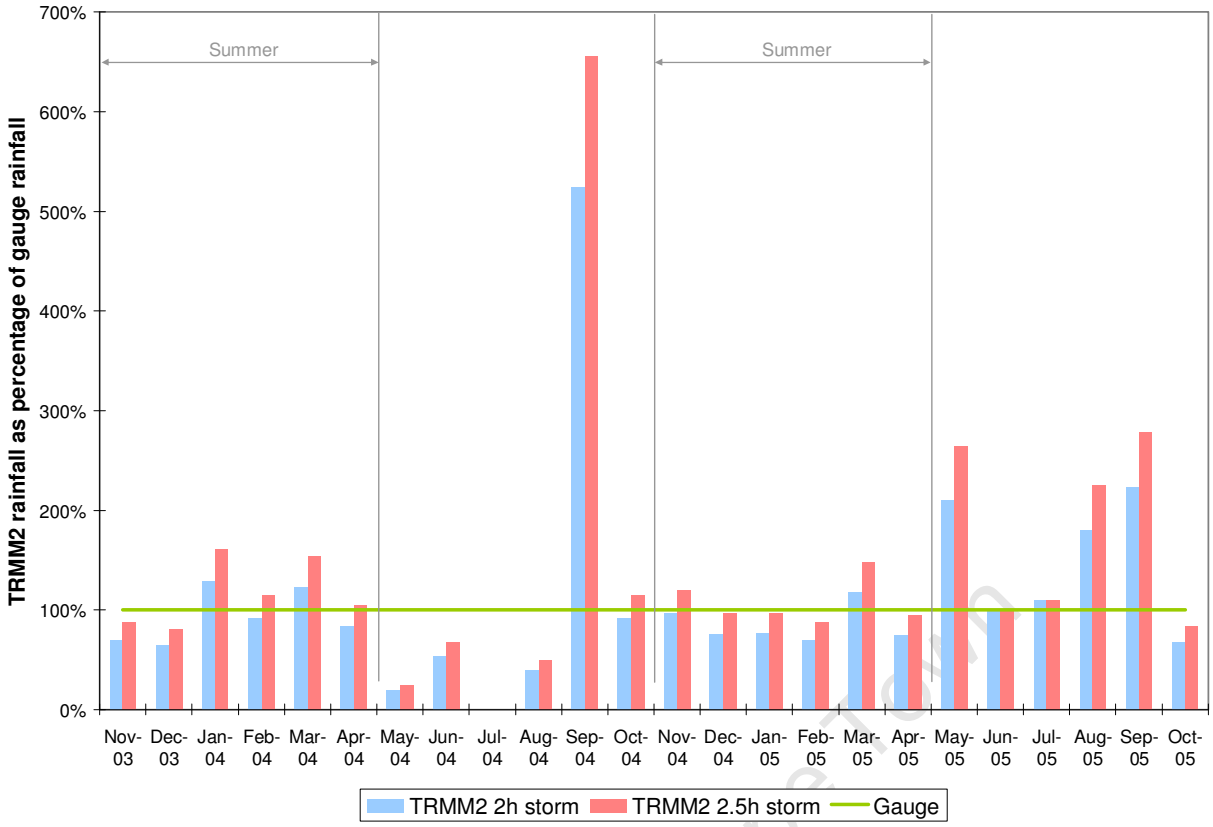

Figure 15: TRMM2 monthly accumulated rainfall as percentage of rain gauge rainfall

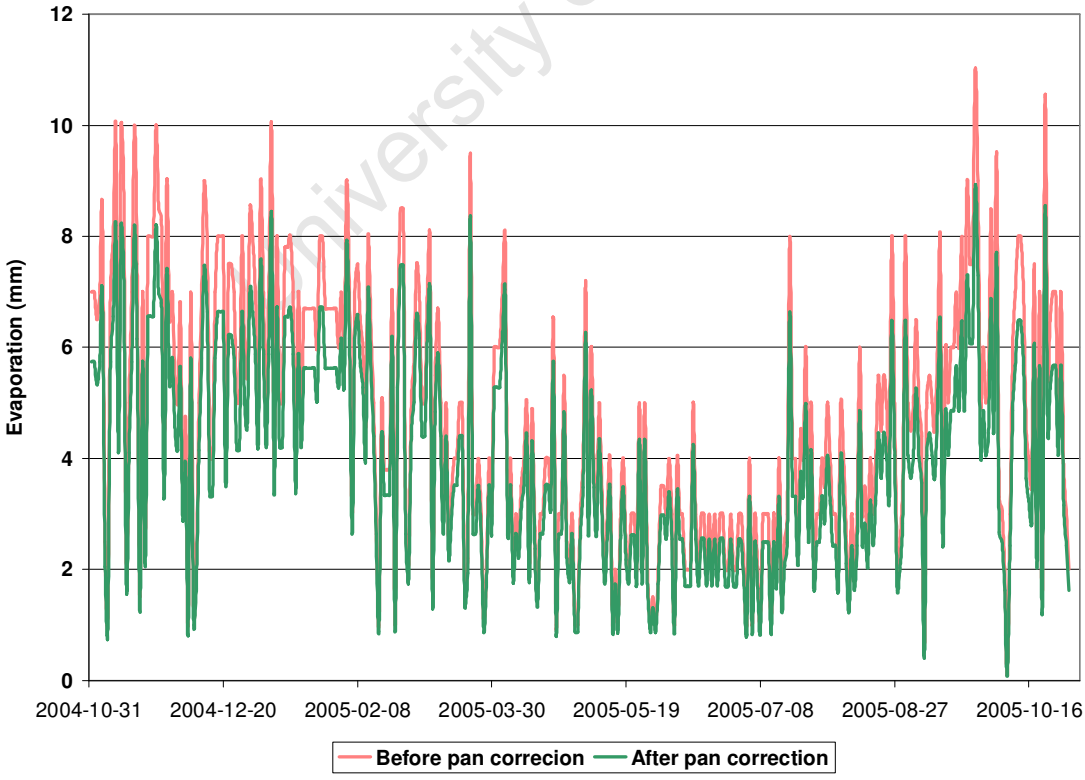

Figure 16: Daily evaporation (DWA gauge C8E003)

6.3.2 Subcatchments

GRASS GIS's r.watershed command was used to start delineating the study area into subcatchments from the SRTM DEM. The threshold parameter that determines the minimum size of the watershed was used to divide the study area into eight subcatchments – the coloured areas in Figure 17 (a). A smaller threshold was used to divide the catchments further (Figure 17 (b)) until a combination of the two delineations could be used to create subcatchments that had only one river reach. In some cases at the confluences of rivers the SRTM DEM was too coarse to delineate boundaries properly. In these places the CD:NGI 20 m contour layer was used to adjust the subcatchment boundaries. The steep sections in the southern and south eastern parts of the study area were then manually digitised using the DEM and 20 m contour layers to create sub-catchments that were more homogenous with regard to slope. The final subcatchment boundaries are shown in black in Figure 17 (a) and (b).

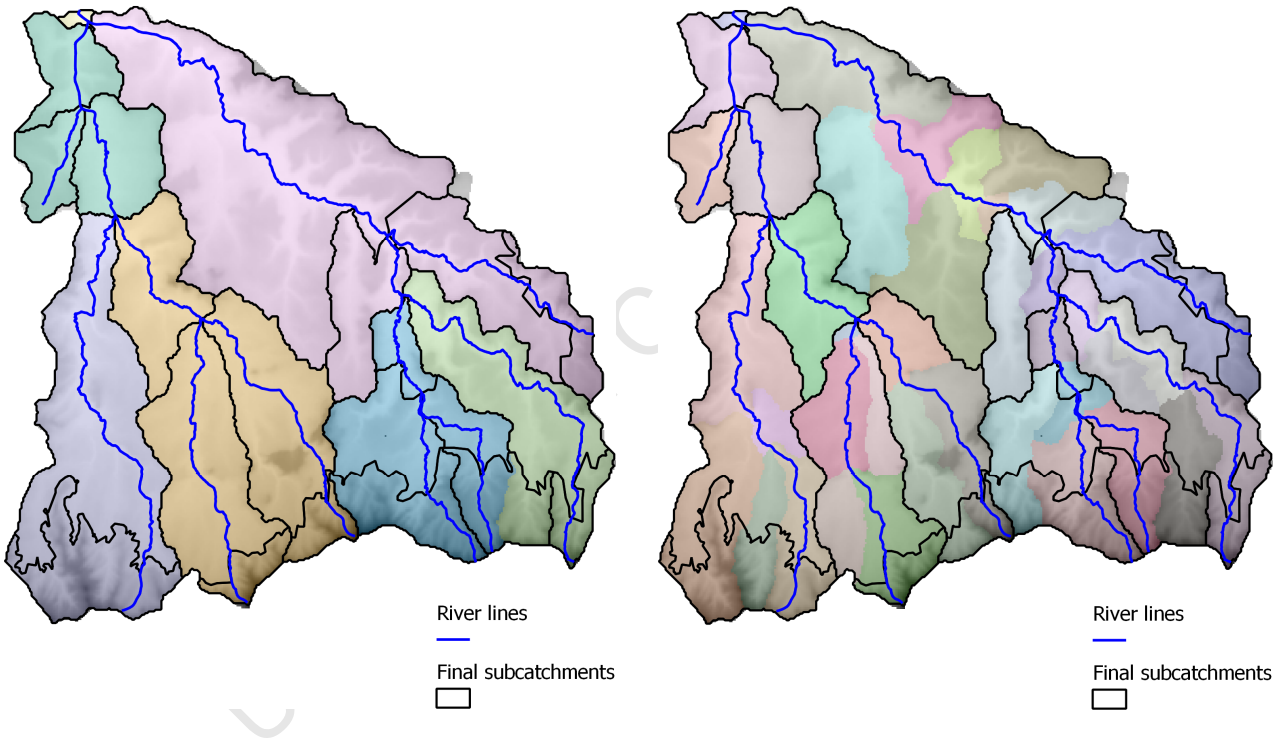

(a) Minimum catchment size = 8 000 pixels *(b) Minimum catchment size = 1 000 pixels*

Figure 17: Subcatchment delineation

Table 15 shows the main object properties for a subcatchment in a SWMM model and how they were calculated. All subcatchments were set to flow into upstream junctions, except for the two small catchments near the outlet that flow directly into the Saulspoort dam object in the model.

Table 15: Derivation of subcatchment properties

Property	Derivation
Area	Calculated in GIS as square metres and divided by 10 000 to get the size in hectares.
Average slope	Zonal statistics of slope map (in percentage) derived from SRTM 90m DEM.

Property	Derivation
Width	Maximum Euclidean distance between subcatchment boundaries and rivers. Multiply this value by 2.
Soil infiltration parameters	From HWSD, which stores up to six soil types per mapping unit with their textures and percentage share of the soil composition. Details are in Appendix A. Used PCSWMM's area weighting function to assign values to subcatchments.
Manning's *n* for overland flow	From MODIS 2008 image overlaid with CD:NGI land use layers and literature. Used 2008 image because it was closest in time to the CD:NGI data. See Appendix B for details. Used PCSWMM's area weighting function to assign values to subcatchments.

6.3.2.1 Aquifers

To model groundwater flow, the model contains an aquifer for each subcatchment. Field capacity and conductivity were taken from the soil type of the subcatchment connected to the aquifer. Since no further information was available for these objects, SWMM's default property values were used. Table 16 lists aquifer properties and their values. The aquifer receiving node in the subcatchment is the same as the one used for runoff.

Table 16: Aquifer properties

Property	Value	Property	Value
Porosity	0.50	Upper evaporation fraction	0.350
Wilting point	0.15	Lower evaporation depth	14.000
Field capacity	From subcatchment	Lower groundwater loss rate	0.002
Conductivity	From subcatchment	Bottom elevation	0.000
Conductivity slope	10.00	Water table elevation	1.000
Tension slope	15.00	Unsaturated zone moisture	0.300

6.3.3 Conduits

The conduits in the SWMM model come from the DWA rivers layer. Rivers were split into conduits every 5 km (to keep hydraulic characteristics approximately the same for each conduit) and at the boundaries of subcatchments. However, this was done before adding the storage units, which shortened some conduits. In the steep southern parts of the study area the 20 m contours layer was used to split rivers into sections that had approximately the same slope. The available DEM was too coarse to find river profiles, so a trapezoidal shape was used to model the cross sections of rivers. Since only the width of a river is measurable from GIS layers (aerial photos, for example) the conduits' depth and bank slopes were estimates. All conduits started with a width close to the average for the catchment. The width and depth of some conduits changed during the process of removing the continuity errors from the model (see Section 6.5 on page 71). During calibration the model was found insensitive to bank slopes. Table 17 on page 69 shows the main properties for a conduit in a SWMM model and their derivation or estimates for their initial values.

Table 17: Conduit properties

Property	Derivation / initial value
Length	Calculated in GIS.
Roughness	0.05 – average for natural channels (see Appendix B).
Cross section shape	Trapezoidal.
Geometry	Width: 10 m Depth: 5 m Slope: 1:2

Because SWMM models a dam as a single point, the conduits that flowed into the dam were straightened from the point where they entered the dam and these parts of the conduits were not considered when calculating their lengths.

6.3.4 Junctions

SWMM places junctions at the beginning and end of each conduit because a conduit must have an inlet and outlet node. Table 18 lists the main properties for a junction in a SWMM model and their derivation or estimates for initial values in this project.

Table 18: Junction properties

Property	Derivation / initial value
Invert elevation	SRTM 90 m DEM. Some elevations were incorrect and made water flow upwards. Elevations for these junctions were corrected using the 20m contours layer.
Rim elevations	5 m above the invert elevation to begin with. This makes the initial junction depths the same as the initial conduit depths.

6.3.5 Storage units

SWMM's storage unit objects modelled the natural marshes and artificial dams in the study area.

6.3.5.1 Saulspoort

The Saulspoort dam is the major dam at the outlet of the catchment. DWA compiled a detailed survey of the dam in 2004 and made the report available for this project. The report contains a table for the surface area of the dam at different water levels. SWMM can use such a table to model the dam's water storage and outflow, based on the inflow to the dam and losses from evaporation. Storage units are nodes in the SWMM model and so it calculates the water level in each storage unit at each time step.

A transverse weir object modelled the dam wall. Weirs are links in SWMM and so it calculates flow and depth in the weir at each time step. The combination of the two objects allowed comparison of the gauged flow and level against computed levels.

Weirs require a discharge coefficient in SWMM and Chris Brooker provided a starting value – 1.9 (Brooker, C, 2010, pers. comm., November 1) from personal experience. During calibration the model was found insensitive to bank the weir discharge coefficient.

6.3.5.2 Smaller dams

The CD:NGI inland water polygon layer provided the locations of smaller dams and marshes that interrupt water flow in conduits (rivers). Since detailed surveys of these water bodies were not available, their surface areas were calculated in GIS. As a starting value, the maximum depths of all dams were estimated to be 5 m. Some of these dams' depths changed during the process of removing continuity errors (see Section 6.5 on page 71).

6.4 Final model

From the previous paragraphs it is clear that the SWMM model for this catchment contains many estimates rather than measured values for object parameters because of a lack of more detailed data.

Figure 18 shows the final SWMM model as it appears in the PCSWMM user interface. For rainfall input, the lighter green subcatchments use the TRMM4 cell, the darker green subcatchments use the TRMM2 cell and the blue-grey subcatchments use the TRMM3 cell. Table 19 on page 71 shows the complete model inventory.

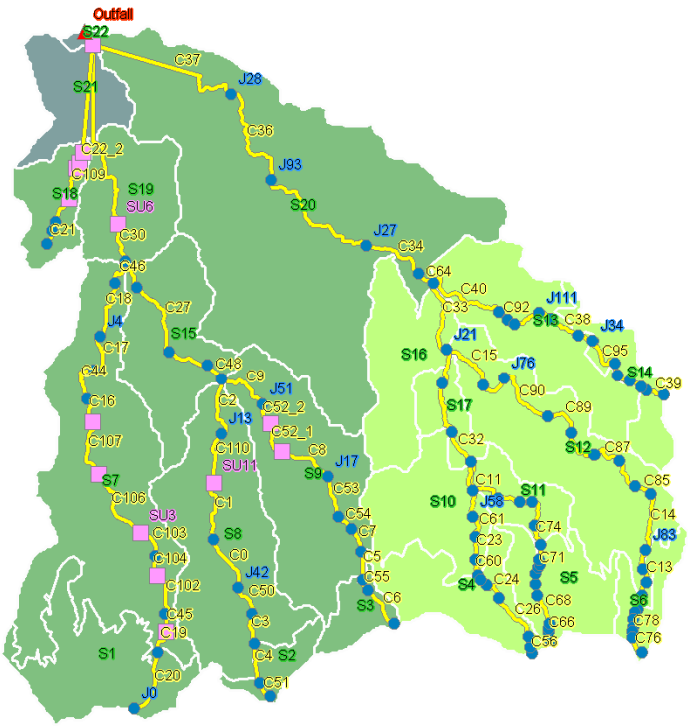

Figure 18: Final SWMM model

Table 19: Model inventory

SWMM object	Number of objects in final model	SWMM object	Number of objects in final model
Subcatchments	22	Junctions	93
Aquifers	22	Storage units	13
Rain gauges	3	Weirs	1
Conduits	111	Outlets	1

SWMM allows several simulation options and Table 20 shows the ones used in this project and the reasons for using them.

Table 20: Simulation options

Option	Selection	Reason for choice
Infiltration	Green & Ampt	More widely used and more accurate method of the options available in SWMM (Hsu et al., 2002).
Routing method	Dynamic wave	Solves the complete one-dimensional Saint Venant flow equations and therefore produces the most theoretically accurate results (Computational Hydraulics International, 2010)
Inertial terms	Dampen: reduces the inertial terms in the Saint Venant momentum equation as flow comes closer to being critical and ignores them when flow is supercritical.	Default.
Define supercritical flow by	Water surface slope > conduit slope and Froude no. > 1	Recommended choice (Computational Hydraulics International, 2010)
Variable time step	Yes. Uses variable time step at each routing time period and selects an adjustment (or safety) factor to apply to this time step. The variable time step satisfies the Courant condition[27] within each conduit. Adjustment factor = 75%	Helps to prevent supercritical flow by shortening the calculation time step when necessary (Computational Hydraulics International, 2010)
Routing calculation time step	300 s	Short enough to prevent flow routing continuity errors.
Runoff calculation time step	15 min	Making this value longer does not affect the results, but it does make the output hydrographs less smooth.
Reporting time step	15 min	Making this value longer does not affect the results, but it does make the output hydrographs less smooth.

6.5 Continuity errors

When first running a SWMM model the modeller needs to bring continuity errors in the model to a 'reasonable' level of at most 10% (James et al. 2008, p.189). Continuity errors represent the difference between ini-

[27] In the Courant condition the time step is limited to the time that a dynamic wave takes to propagate the length of a conduit (James et al. 2008, p.659).

tial storage plus inflow, and final storage plus outflow. They therefore represent water 'lost' from or 'gained' in the system, so violating the mass continuity condition. SWMM reports continuity errors for runoff and channel routing separately. It also reports the conduits and junctions with the largest continuity errors.

The most common reasons for continuity errors are computational steps that are too long or conduits that are too short. This model had relatively long conduits and a short routing time step, so continuity errors were reduced by adjusting the widths and depths of problematic conduits and by adjusting the depths of problematic junctions and storage units.

6.6 Model calibration

Once the model has acceptable continuity errors, it's ready for calibration. PCSWMM provides a 'tuning' tool to adjust parameter values and to see how they influence the model's performance. The modeller can choose which parameters to make available for adjustment and can adjust them separately or together. This modeller usually adjusted parameters for objects of the same type together, using the Nash-Sutcliffe R^2 (named 'R^2' in the list of error measures in Figure 19) as a measure of the model's accuracy during calibration. In other words, the N-S correlation was the objective function during calibration. Figure 19 shows the 'tuning' screen in PCSWMM with conduit roughness the adjustable parameter.

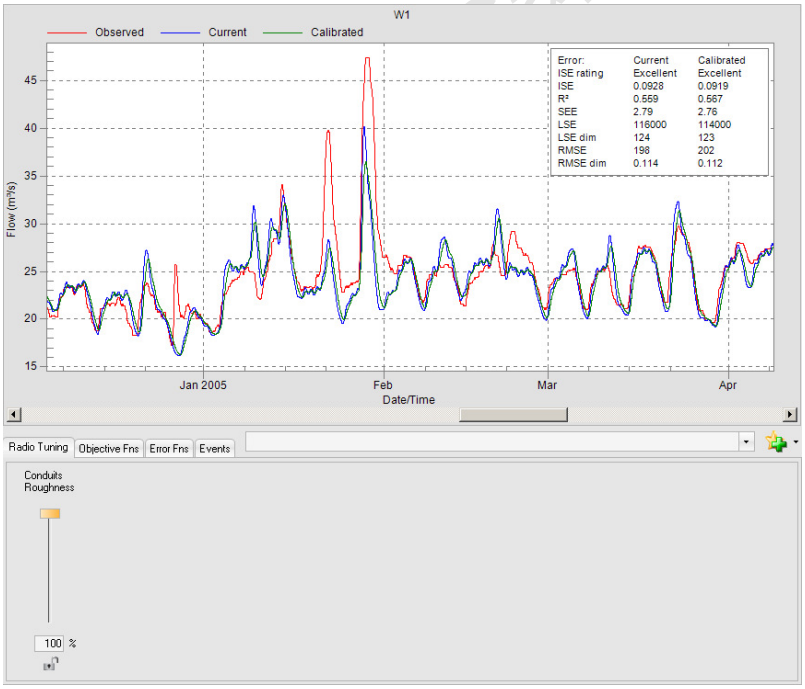

Figure 19: Model calibration in PCSWMM

7. Results and analysis

This section presents the results of the work done for this project. It shows the period selected for modelling, how the TRMM rainfall compares to the BWO rainfall and the results of the SWMM model during the selected study period. Then it discusses some additional tests on the SWMM model and the TRMM data.

7.1 Flood events and simulation periods

Figure 20 shows the major rainfall events found for the gauge values measured at the Bethlehem Weather Office. To show all the events at a visible scale on one graph, the horizontal axis shows the event duration in hours rather than showing dates. Only the amplitudes of the events are considered here for selecting the study period, not the event duration. 'Tails' on either side of event peaks simply show that the time series starts a few hours before the event or ends a few hours after the event. Figure 21 on page 74 shows the major flow events at Saulspoort dam. Its horizontal axis also shows the event duration rather than the date of the storm so that all events can be shown at visible scale on one graph. Examining the major rainfall events together with the major flow events, only two events remain that are above the norm that defines a flood in this project (the 99th percentile) with regard to rainfall *and* flow – October 2001 and January 2005. The latter event was selected for the simulation because it is closer to the date of the MODIS image used to find the Manning's *n* values in the SWMM model and to the dates of the available aerial photos of the study area.

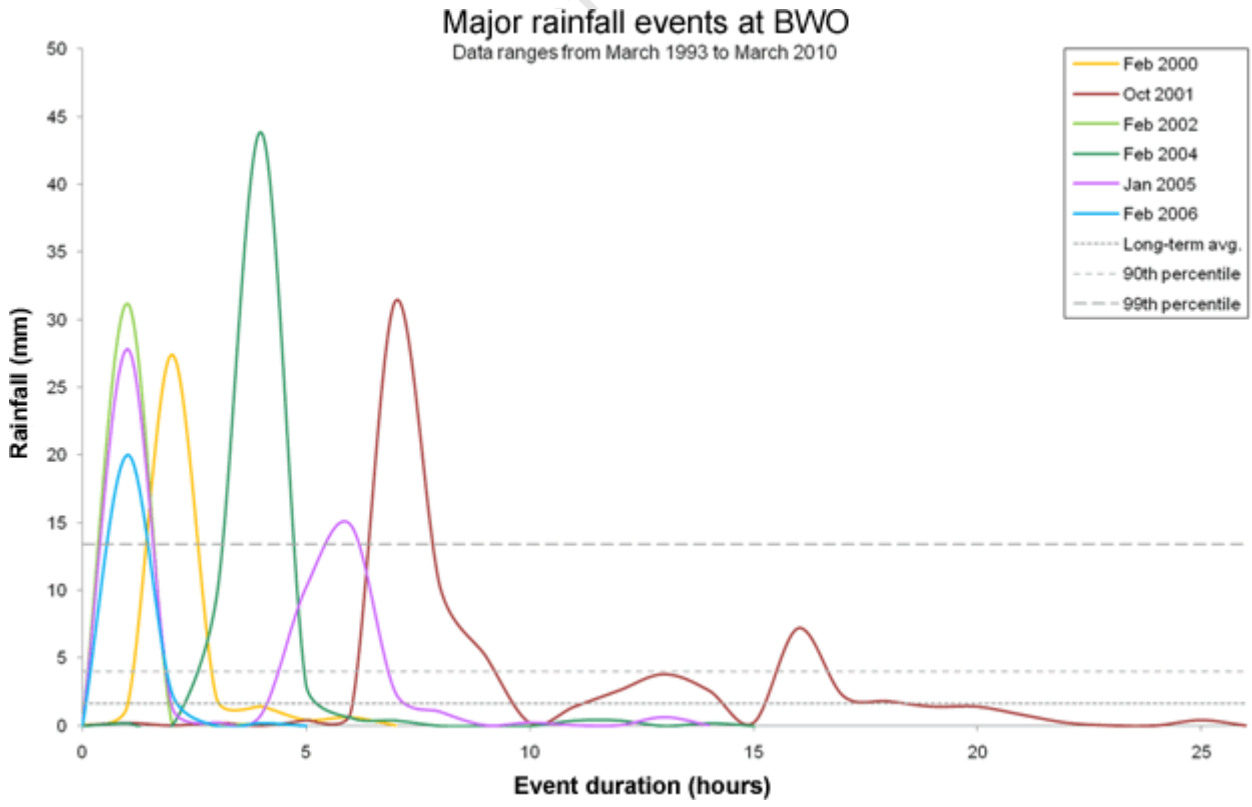

Figure 20: Major rainfall events at BWO

Because the study area is in a summer rainfall area, the model was constructed from the start of the summer during which the major rainfall event occurred until the start of the next summer: 1 November 2004 to 31 October 2005. The evaluation period is the year after: 1 November 2005 to 31 October 2006.

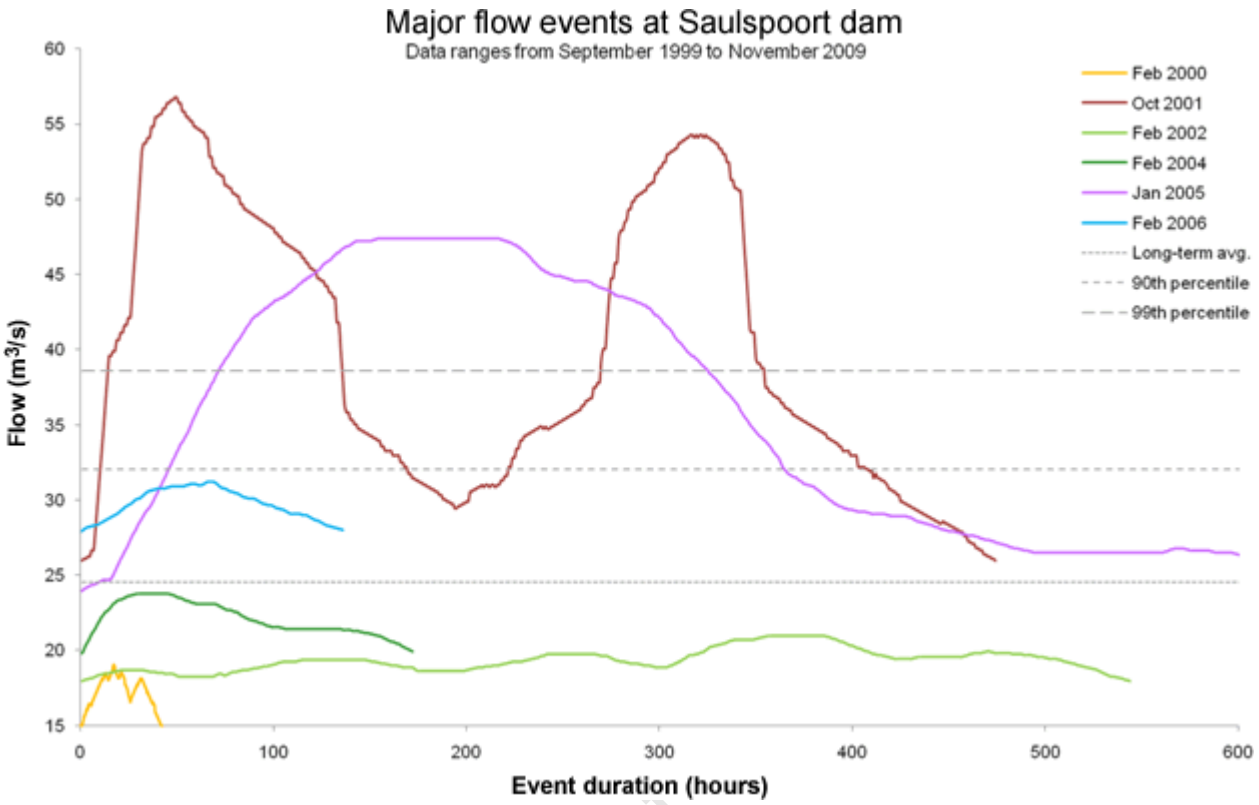

Figure 21: Major flow events at Saulspoort dam

7.2 TRMM rainfall compared with gauge measurements

Figure 22 on page 75 shows the two hyetographs of the gauge measurements. These two graphs coincide relatively well except for a spike in the BWO rainfall in February 2004 that the TRMM SBRE did not detect. Conversely, the TRMM displays a spike in January 2005 that the BWO measurements do not replicate. The scale of the graph makes it difficult to see details of the two time series, so a scattergram was also drawn (Figure 23 on page 76). The scattergram shows more clearly the disparity between the two datasets – most of the points lie off the ideal 45° line where the two datasets would coincide perfectly. Particularly noticeable is that many points lie on either the horizontal axis or the vertical axis. This indicates that each dataset often detects rainfall events that the other doesn't detect at all. The statistics of the comparison are in Table 21 on page 75. These statistics are difficult to interpret because no other studies were found that compared a single gauge measurement to a single SBRE grid cell. However, the positive bias is in line with the finding of Huffman et al. (2007). The small POD and large FAR confirm the interpretation of the scattergram above. The low Pearson correlation coefficient and the distributed scattergram may indicate that comparing a point value to an aerial value is not really useful though. A study by Sorooshian et al. (2000) supports this assertion; they found that gauge measurements and SBRE correlate better as the number of gauges in an SBRE

cell increases. This comparison can therefore not indicate whether the TRMM 3B42 data is a good source of rainfall estimates for this project or not.

Table 21: BWO rain gauge and TRMM2 three-hourly comparison statistics

Statistic	Value
Pearson correlation coefficient	0.23
Probability of detection	0.55
False alarm rate	0.65
Critical success index	0.27
Bias	29%

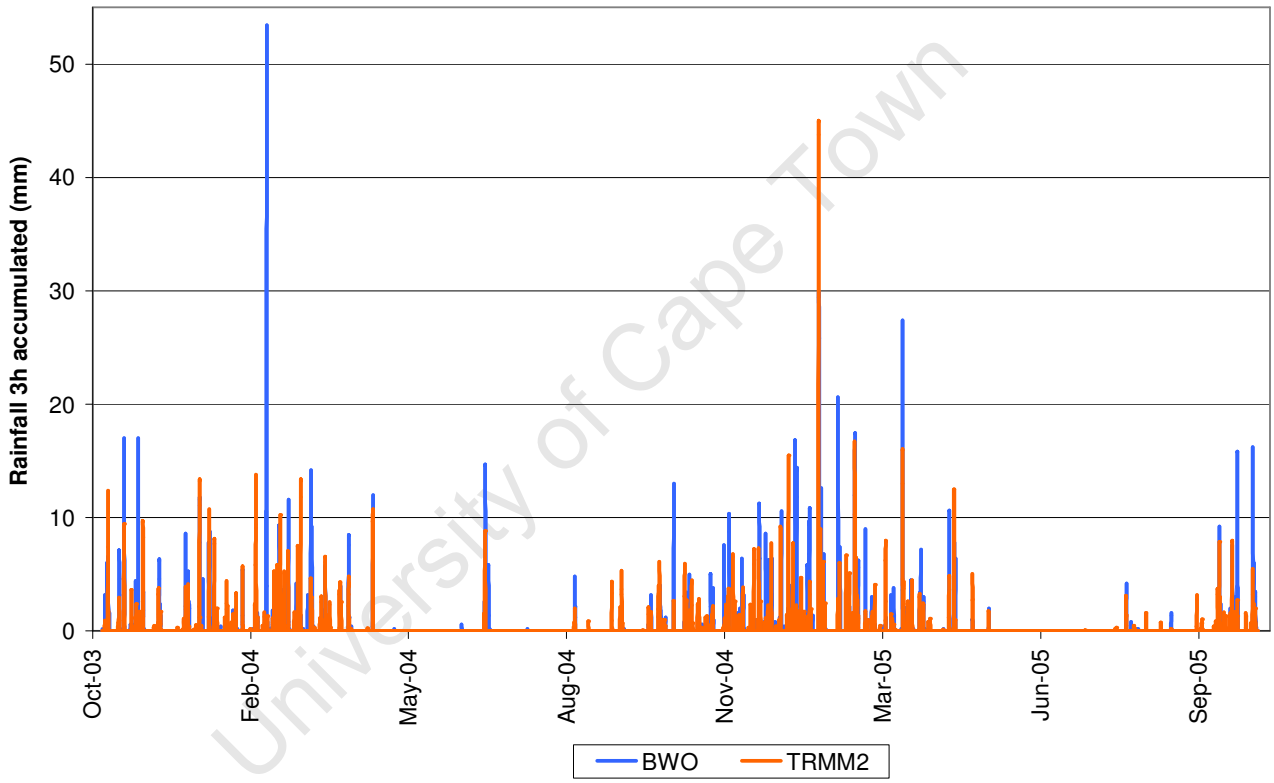

Figure 22: Hyetograph for BWO rain gauge and TRMM2

7.3 SWMM model

7.3.1 Calibration

The model was found to be sensitive to the following parameters:

- Subcatchments
  - Suction head (adjusted –21%)
  - Conductivity (adjusted +174%)

- ♦ Initial deficit (adjusted –57%)

- Channels
  - ♦ Roughness (adjusted between +120% and +300%)

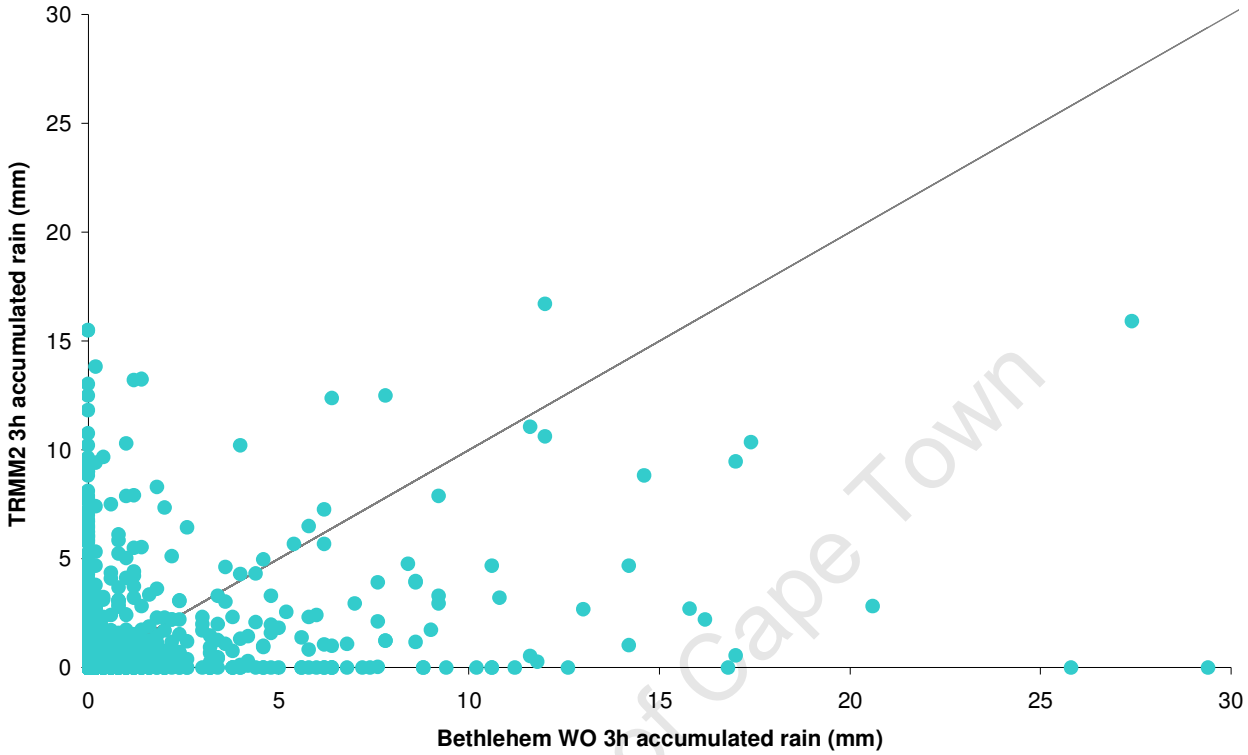

Figure 23: Scattergram for BWO rain gauge vs. TRMM2

These are large adjustments, but soil infiltration characteristics are highly variable in space and can vary greatly within metres. The channel roughness value was set to one value for all channels to start with and so adjustments are justified. The following paragraphs discuss these adjustments in more detail, including their physical viability.

Soil infiltration characteristics can vary greatly within a soil texture class. For example, the suction head for sandy clay loam can vary between 44.2 mm and 1080.0 mm, but 218.5 mm is the recommended value (Mays 2001, p.241). Engineers therefore routinely use these characteristics to calibrate hydrological models. The final suction head values after calibration in this model ranged from 139.63 mm to 428.21 mm. These values can range between 9.70 mm and 1565.0 mm (Mays, 2001, p.241) and so the calibrated values are still reasonable. Literature values for conductivity range from 0.3 mm/h to 117.8 mm/h (Mays 2001, p.241). The calibrated values for the model ranged from 5.47 mm/h to 21.52 mm/h and so they are reasonable. Literature values for initial deficit range from 0.097 to 0.375 (James et al., 2008, p.764). The calibrated values for the model range from 0.07 to 0.10 and are therefore outside of reasonable physical values.

Literature values for Manning's *n* for natural channels range from 0.025 to 0.150 (Mays 2001, p.92). The calibrated values for the model range from 0.11 to 0.20 and are therefore outside reasonable physical values. Figure 24 on page 78 shows the calibrated model values compared to literature values. The values were reset to the limits of the literature values and results from both these calibrated models are presented in Section 7.3.2.

In addition to the above parameters that were adjusted using PCSWMM's calibrating tool, the percent imperviousness of all subcatchments were set to 5% to start with and then brought down to 4.1% as part of the calibration process. This was done because the calculated flow was consistently lower than the observed flow. Some impervious areas do exist in the study area in the form of roads and paved areas around homesteads. Setting baseline flows at the seven starting junctions of streams high up in the mountains further improved underestimation of the calculated flow. Seeps from persistently wet areas or reduced evapotranspiration because of shading could be the sources of such flows. The depths of some junctions and channels were increased to avoid surcharging and to reduce continuity errors. In the light of the coarseness of the model, these adjustments to the imperviousness and geometries of objects in the model are justified.

7.3.2 Results

This section presents the results of the uncalibrated model, the calibrated model with parameters outside of literature values (calibrated model 1) and the calibrated model with parameters adjusted back to the valid range (calibrated model 2). Results are also shown for the evaluation period for both calibrated models.

Figure 25 on page 79 shows the calculated flow at the Saulspoort dam during the calibration period from 1 November 2004 to 31 October 2005 for calibrated model 2 (W1 in Figure 25). Its description is 'W1' because the weir object 'W1' represents this flow in the model. 'W1 (obs)' is the flow that meter C8R004 measured during the same period. (PCSWMM requires this naming convention to calibrate the model.) At the top of the figure is the TRMM2 rainfall for the same period. Overall this hydrograph compares favourably with those in the studies discussed in Section 2.

Table 22 on page 79 shows the error statistics for the model before and after calibration, and for the evaluation period. Figure 26 on page 80 shows the N-S correlation for the five cases. It is clear that calibration greatly improved the results, especially during the wet summer months. Calibrated model 2 performed only slightly worse than calibrated model 1. In general, the model performed better during winter (dry season) than during summer (wet season). Specifically, the performance of the model during the three flow peaks in late January 2005 (called 'three biggest storms' in Table 22 and shown in Figure 27 on page 81) is not accurate enough for a real-time flood monitoring system. The large peak flow error, even after calibration, confirms this fact.

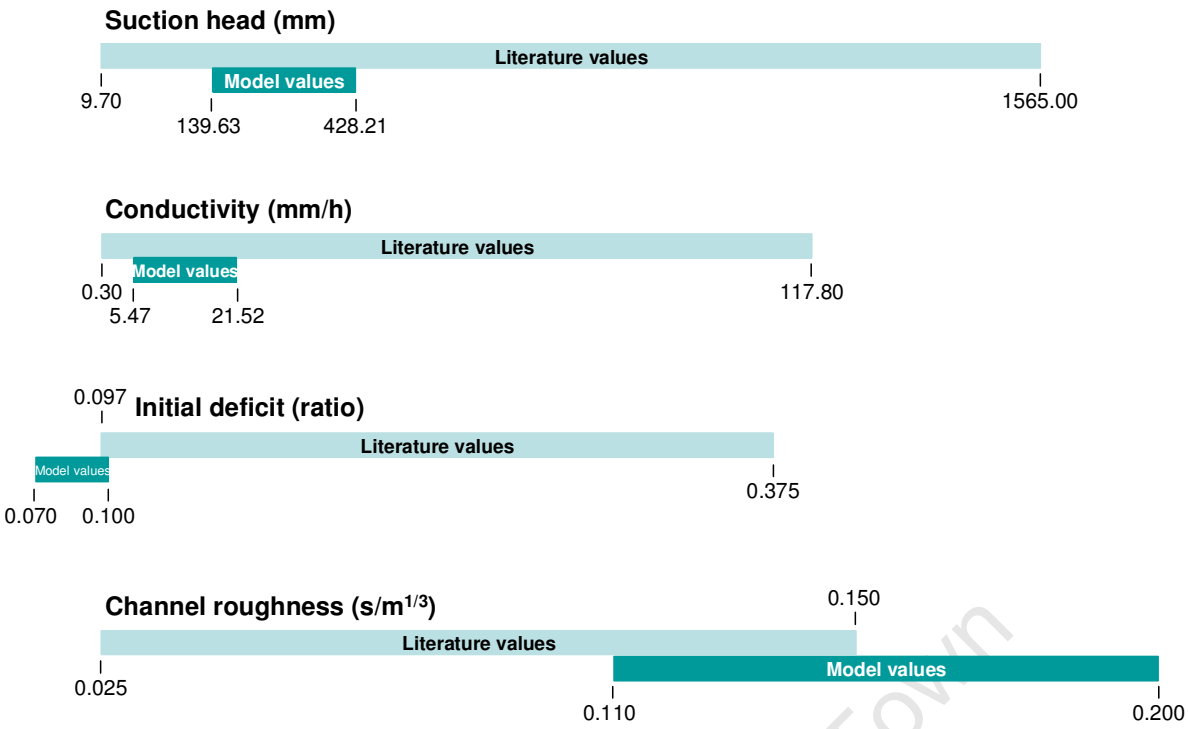

Figure 24: Calibrated parameters compared to literature values

The results are worse for the evaluation period (see Figure 28 on page 81 for the hydrograph) than the calibration period, as is usually the case, and overall the model's performance has now fallen below the standard set for this project: an N-S correlation coefficient of 0.80.

The model's inadequate performance in wet periods and relatively good performance during dry periods indicate that the model is simulating channel flow well but overland flow less well. This can be ascribed to several possible factors:

a) coarse time and spatial resolution of the TRMM rainfall estimates

b) errors in the TRMM rainfall estimates

c) errors in the model

d) errors in the way SWMM models overland flow and runoff

The TRMM rainfall estimates do of course have errors. In the absence of knowledge about the size of these errors, they cannot be factored into the model. The lack of several ground-based rainfall measurements inside the TRMM coverage prevents this researcher from obtaining such an error estimate.

All models contain errors. The SWMM model is coarse because of its available input data and the node-link (hydraulic) part of the model is the coarsest because the least information was available about the rivers in the catchment. Yet this part of the model performed best, so it is possible that the two sources of error mentioned above contribute more to the inadequate performance of the model during wet periods.

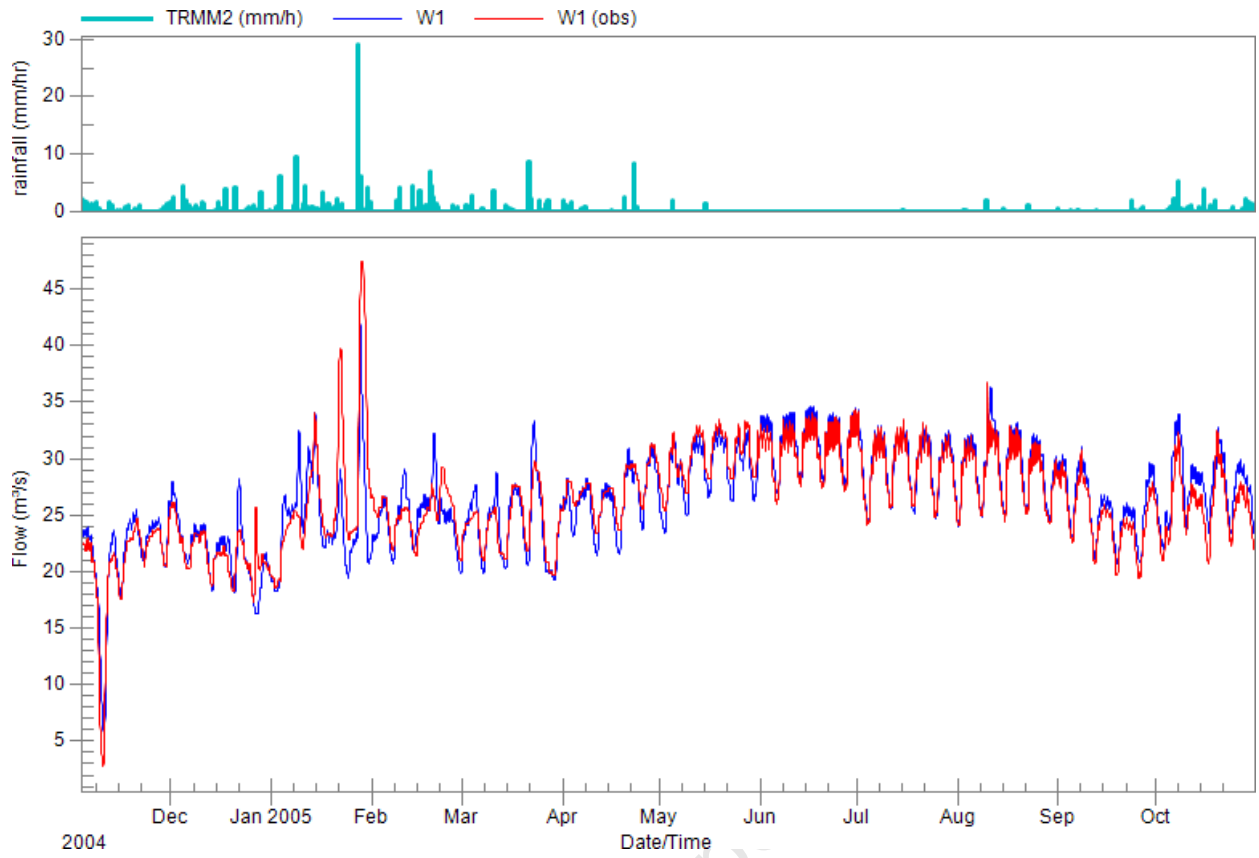

Figure 25: Calculated and observed flow at Saulspoort dam (calibrated model 2)

Table 22: Model error statistics

Error statistic	Model				
	Uncalibrated	Calibrated 1	Calibrated 2	Calibrated 1 (evaluation)	Calibrated 2 (evaluation)
	Nov 04 – Oct 05	Nov 04 – Oct 05	Nov 04 – Oct 05	Nov 05 – Oct 06	Nov 05 – Oct 06
Runoff continuity error (%)	0.00	-0.02	-0.02	-0.01	-0.01
Channel flow continuity error (%)	-0.75	-0.02	-0.02	-0.02	-0.03
Peak flow error (%)	-28.08	-14.83	-11.39	-33.67	-33.07
Mean flow error (%)	-8.77	0.42	0.61	2.61	2.39
Total flow error (%)	-9.04	1.05	0.59	0.55	2.39
MAE (m3/s)	7.01	1.28	1.21	2.17	2.11
RMSE (m^3/s)	552.12	267.98	255.04	451.14	441.00
N-S R^2 overall	0.43	0.80	0.80	0.57	0.58
N-S R^2 summer	0.18	0.70	0.68	0.51	0.51
N-S R^2 three biggest storms	-0.52	0.35	0.31	N.A.	N.A.
N-S R^2 winter	0.44	0.84	0.87	0.71	0.73

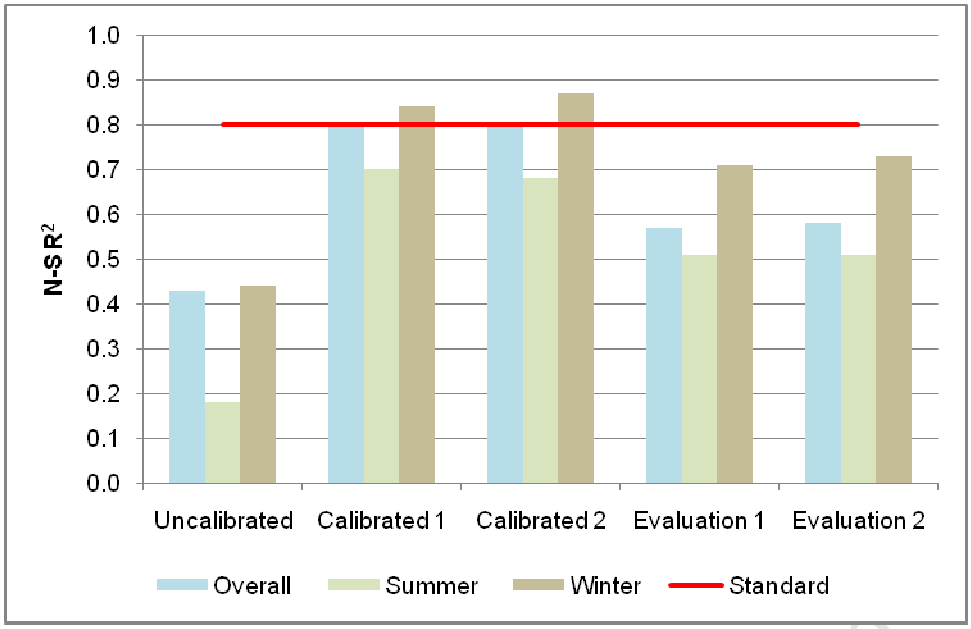

Figure 26: N-S R^2 for uncalibrated and calibrated models

Errors in the way that SWMM models overland flow and runoff seem unlikely given SWMM's long and successful record of use in rural and urban studies as was shown in Sections 2.1.1 and 2.1.2. Even if this was a factor, it would probably be small compared to the other three factors and it could be reduced during calibration.

Further work was done to test the hypothesis that the TRMM 3B42 SBRE is the largest source of error that affects the model results and the following section discusses this work.

7.4 Additional testing of the model and TRMM data

This section describes additional tests performed to establish the source of the SWMM model's inadequate performance. The SWMM model is examined to see if it follows physical principles and the TRMM rainfall is examined to see if it results in a reasonable runoff coefficient for the study area.

7.4.1 Does the model follow physical principles?

7.4.1.1 Flow velocity in channels with different geometries

A hydrological model that observes physical principles supports the assertion that the model is sound. For example, water flows faster in a steeper than a flatter channel because of increased gravitational force. Furthermore, water flows faster in a narrower than a wider channel because of the velocity-area principle, which states that flow in an open channel is the product of the area and the velocity (see section 3.9.2 on page 35). These principles were tested for two conduits in the SWMM model (C51 and C4) at the source of the perennial Kroonspruit. Figure 29 on page 83 shows the location of these two conduits in the study area.

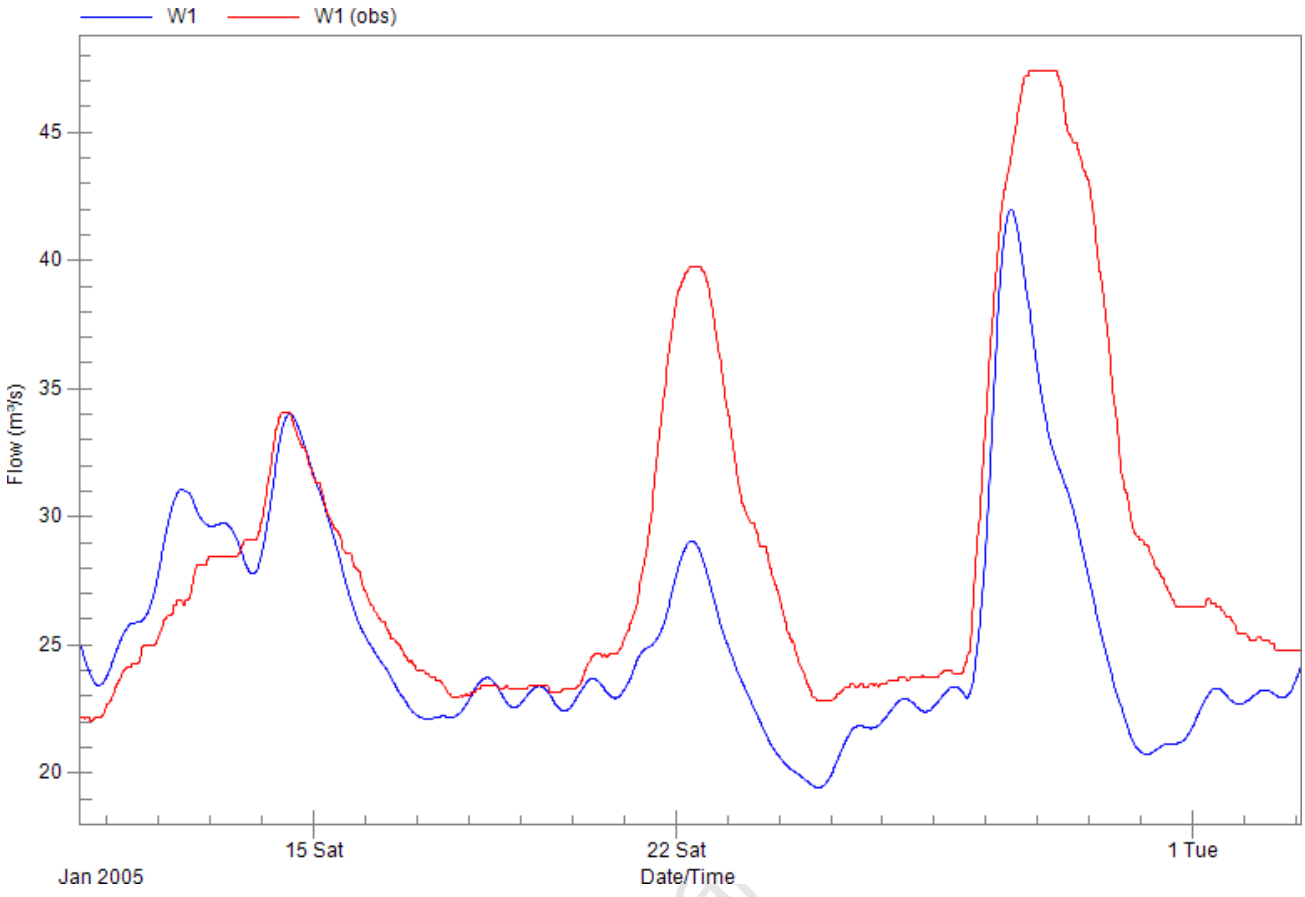

Figure 27: Calculated and observed flow during peak flows, January 2005 (model 2)

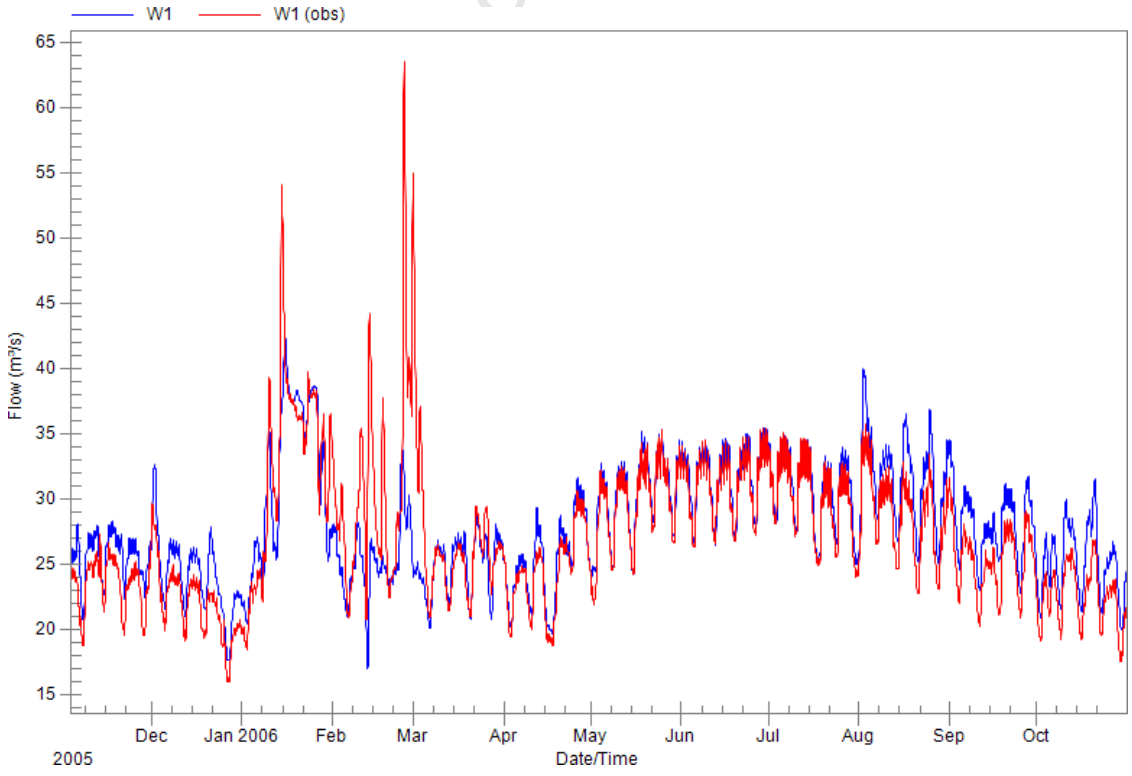

Figure 28: Calculated and observed flow at Saulspoort dam during the validation period (model 2)

From the spacing of the contour lines on the map in Figure 29 it is clear that the upstream channel (C51) has a much steeper slope than the downstream channel (C4). In fact, the slope of C51 is 30% and the slope of C4 is 6%, according to the STRM 90 m DEM. The aerial photograph in the background shows further that the Kroonspruit is narrower at C51 than at C4, where it starts to widen in the plain. (This map also shows that the DWA river lines do not coincide exactly with the actual river channels – in this part of the study area the offset is on average around 50 m, which is still smaller than the pixel size of the SRTM 90 m DEM.)

Figure 30 on page 83 shows the TRMM2 rainfall and the SWMM model's calculated water flow rate and velocity through C51 and C4 during a rain storm on 27 January 2005. It is clear that the velocity in C51 was always higher than the velocity in C4, even when the flow rate in C51 dropped below that of C4 at around 6 pm. So, the model does follow the physical principles stated above: water flows faster in steeper and narrower channels.

Figure 32 on page 86 illustrates the flow rate through C51 and C4 at different points during the storm on January 27, 2005. The widths of the conduit lines in the maps at the bottom of the figure are directly proportional to the water flow rate in these two conduits. At point 1 (3:00 pm) the flow rates in the two conduits are still approximately equal.

At point 2 (3:15 pm) flow has increased much faster in C51 than in C4 because the steeper surroundings convey the surface runoff faster to the river and, once in the river, the water flows faster.

At point 4 (5:45 pm), the water from the upper part of the catchment is 'emptying' into the lower part of the catchment and the flow is now higher in C4 than in C51. The flow velocity is still slightly higher in C51, though (see Figure 30 on page 83).

At point 5 (6:15 pm), the effect of the rain is abating and the flow rates are returning to the base flow rates.

In conclusion, the model follows physical principles. The absolute shapes and amplitudes of the runoff hydrographs may not be correct (if they were, the overall model performance would be better), but their relative shapes and amplitudes are as expected.

7.4.1.2 Runoff correlations

Runoff depends on many interconnected factors, but subcatchments with a larger slope will generate more runoff resulting in a positive correlation between runoff and slope. Conversely, larger amounts of precipitation will infiltrate in subcatchments with greater saturated hydraulic conductivity resulting in a negative correlation between runoff and saturated hydraulic conductivity.

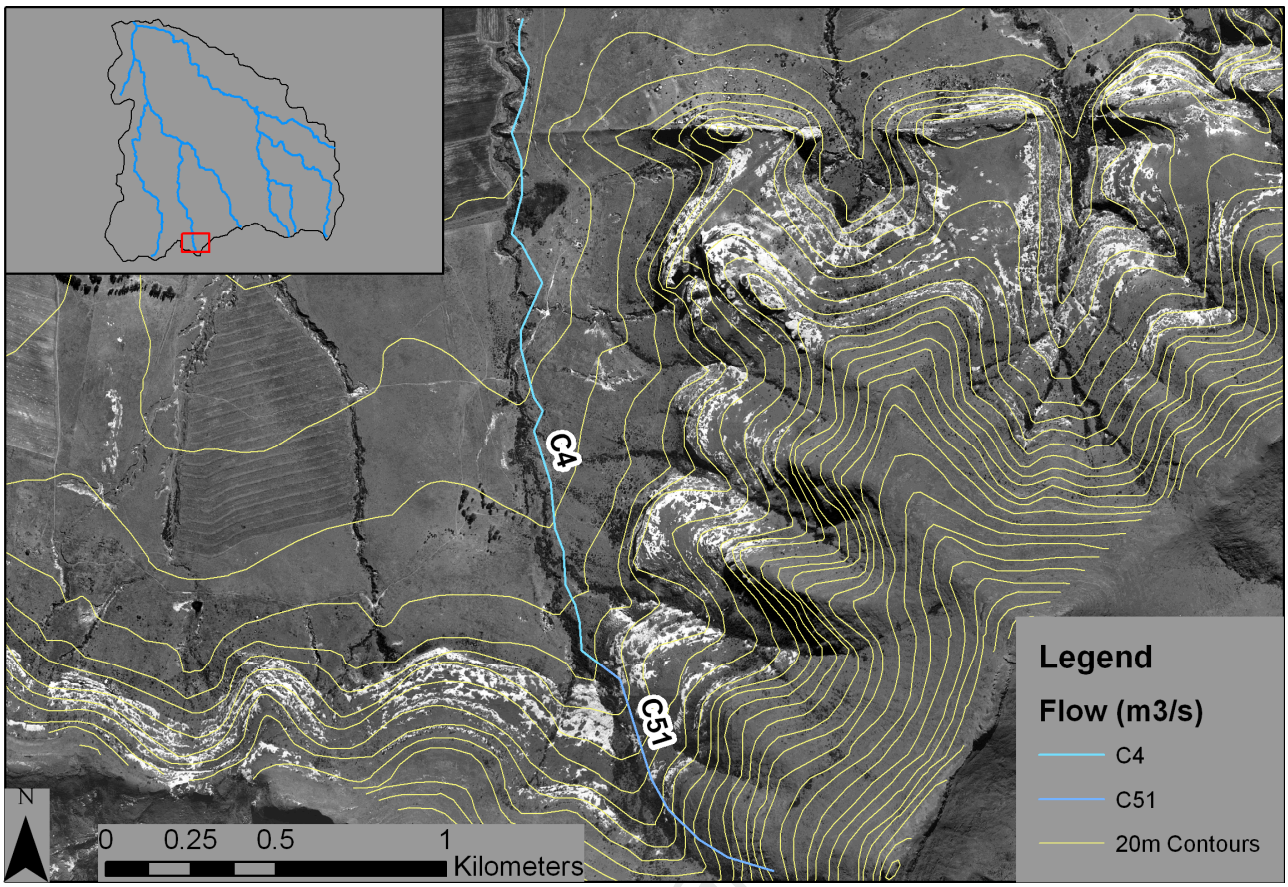

Figure 29: Conduits C51 and C4 at the source of the Kroonspruit

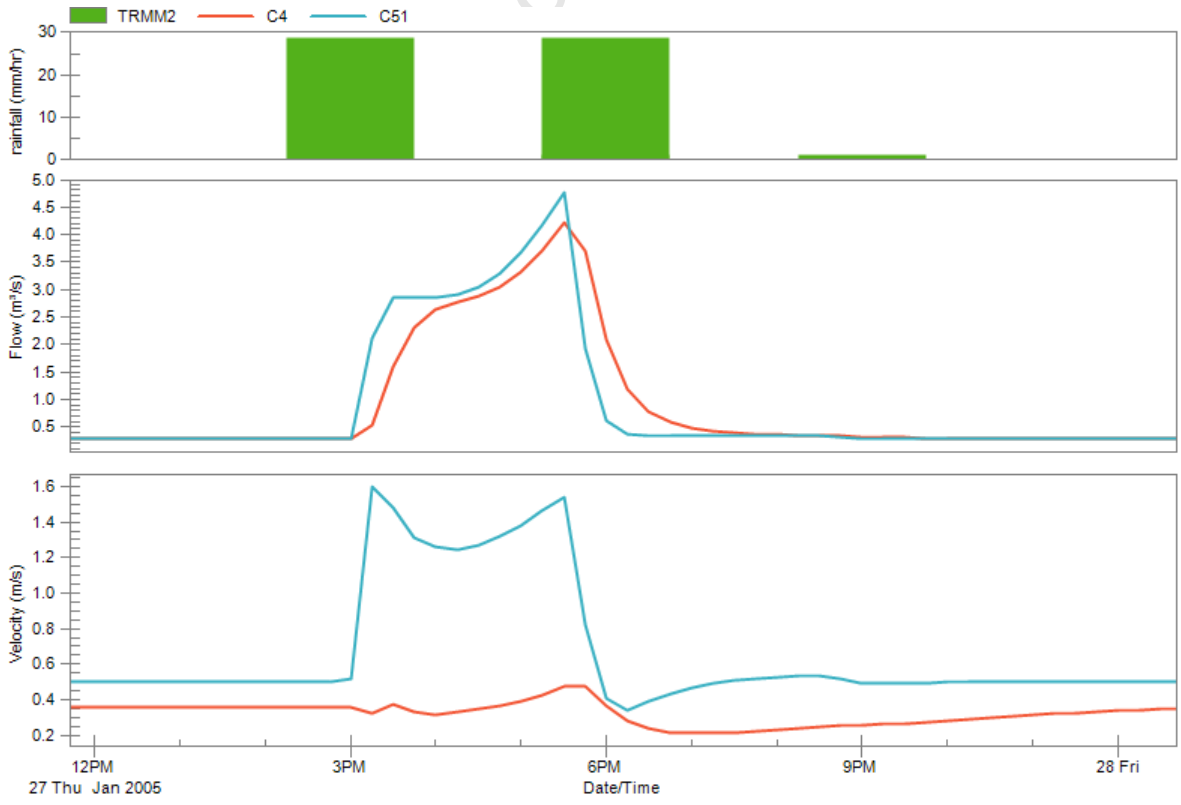

Figure 30: Flow and velocity in conduits C51 and C4 during rain storm on 27 January 2005

The SWMM calibrated model 2 (with parameters adjusted to literature values) was recalibrated with the total flow volume as objective function (rather than the N-S correlation) until the total flow volume during the wet season was within 0.31% of the measured flow volume. This calibration adjusted the impervious areas in the subcatchments from 4.1% to 5.0%. This recalibrated model was used to test the correlation between slope and runoff and between hydraulic conductivity and runoff. To account for the effect of the size of the subcatchment on the runoff, the correlations were calculated between the runoff per unit area and the other two variables.

Linear regression between the total volume of runoff per unit area (m) during the peak runoff in 2005 (a period of three days) and the average slope of a subcatchment (%) resulted in a positive coefficient for the slope of the regression line (1.1) and an R^2 value of 0.25. Linear regression between the runoff per unit area (m) during the same period and the saturated hydraulic conductivity (mm/h) resulted in a negative coefficient for the slope of the regression line (–2.5) and an R^2 value of 0.50. See Figure 31 on page 85 for the graphs.

Once again, the SWMM model behaves broadly as expected with regard to physical principles.

7.4.2 Runoff coefficient

To further examine the TRMM 3B42 data for its use as input to a hydrological model at the scale of this project, an additional investigation was carried out to estimate the volume of surface runoff using only measured quantities and no modelled quantities. To do this, one has to calculate the loss of water in the catchment in the absence of rain, that is, during a dry period. The processes that remove water from streams during dry periods are collectively called transmission losses (see Section 3.10.7.1). From the loss of water in the absence of rain, one can estimate how much water entered the catchment as surface runoff from rain during a wet period. The runoff coefficient can then be determined by dividing the calculated surface runoff by the rain that the TRMM 3B42 product estimated during the same period. This runoff coefficient should be close to values available in literature for this catchment: between 0.033 and 0.063 (Midgley et al., 1994).

7.4.2.1 Calculating volume of surface runoff

During the dry season only one source of water comes from outside the catchment – the Katse inflow – and DWA meter C8H036 measures this inflow. At the same time, DWA meter C8R004 measures the outflow from the catchment at the Saulspoort dam. Three rivers feed into this dam and in general its outflow is higher than the Katse inflow. The water remaining in the system after accounting for the Katse inflow during the dry season is called the 'dry residual' in this text and can be calculated as follows:

dry residual (m^3/s) = catchment outflow (m^3/s) – Katse inflow (m3/s)

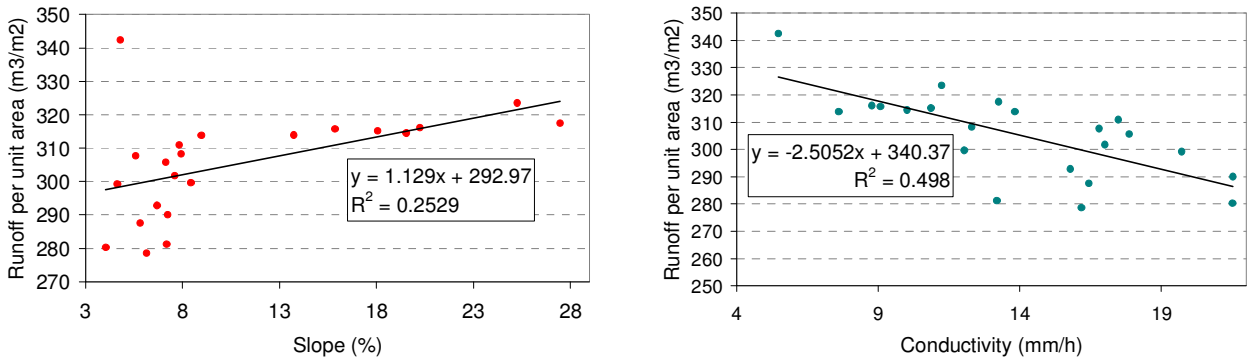

(a) Linear regression between runof per unit area and slope

(b) Linear regression between runoff per unit area and conductivity

Figure 31: Linear regression for the 22 subcatchments in the model

Before calculating the dry residual, the lag between the Katse inflow and the catchment outflow was determined from peaks and troughs in the two hydrographs. Because the Katse inflow is a very 'noisy'[28] dataset with many peaks and troughs in short periods, this lagged Katse inflow was smoothed using a moving average until a time over which to apply the moving average was found that best coincides with the shape of the outflow hydrograph. A one-day moving average was used. Figure 33 on page 87 shows the catchment outflow (red graph), the lagged and smoothed Katse inflow (green graph) and the dry residual (blue graph). A mean value for the residual was determined for July 2005. However, zero or small values in the time series can reduce the mean, so the mean was calculated using different minimum flow values or cut-off values for inclusion in the mean calculation. The results that follow later in the section show that such a cut-off value to calculate the mean dry residual flow does not affect the result of this test.

This test assumes that the average dry residual can be used in wet periods because on a wet summer's day the cloud cover and lower temperature should result in evaporation close to that of a sunny but cold day in the dry winter period.

During a wet period, the estimated surface runoff as a result of rain in the catchment is:

estimated surface runoff from rain (m^3)
= *catchment outflow (m^3) during wet period*
– *Katse inflow (m^3)*
– *mean dry residual (m^3/s)*
× *duration of wet period (s)*

[28] The term noisy refers here to the large and frequent variations in the data, not the accuracy of the data.

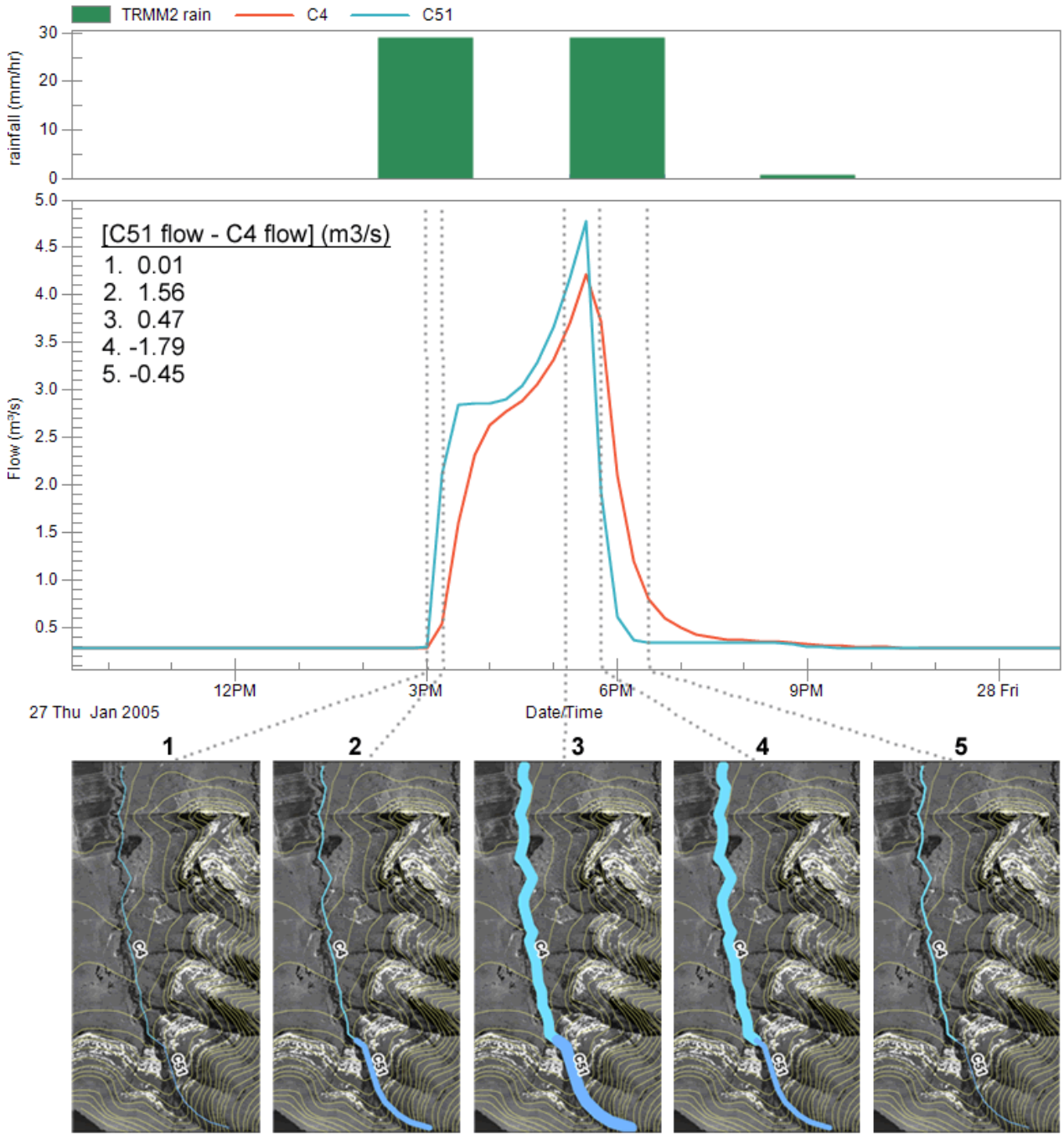

Figure 32: Visualising flow rates through conduits C51 and C4 during rain storm on 27 January 2005

The biggest storm event during 2005 was chosen to determine the surface runoff: 27 January to 3 February (7 days). Figure 34 on page 88 shows the catchment outflow, as well as the rainfall in the three TRMM grid cells that cover the study area for the peak of the selected storm event. In this figure, the rainfall axis is inverted, so its magnitude increases from zero at the top of the scale downward.

During the storm event, the volume of catchment outflow (as measured by meter C8R004) was 19,710,000 m^3 and the lagged, smoothed volume of Katse inflow (as measured by meter C8H036) was 11,730,000 m^3.

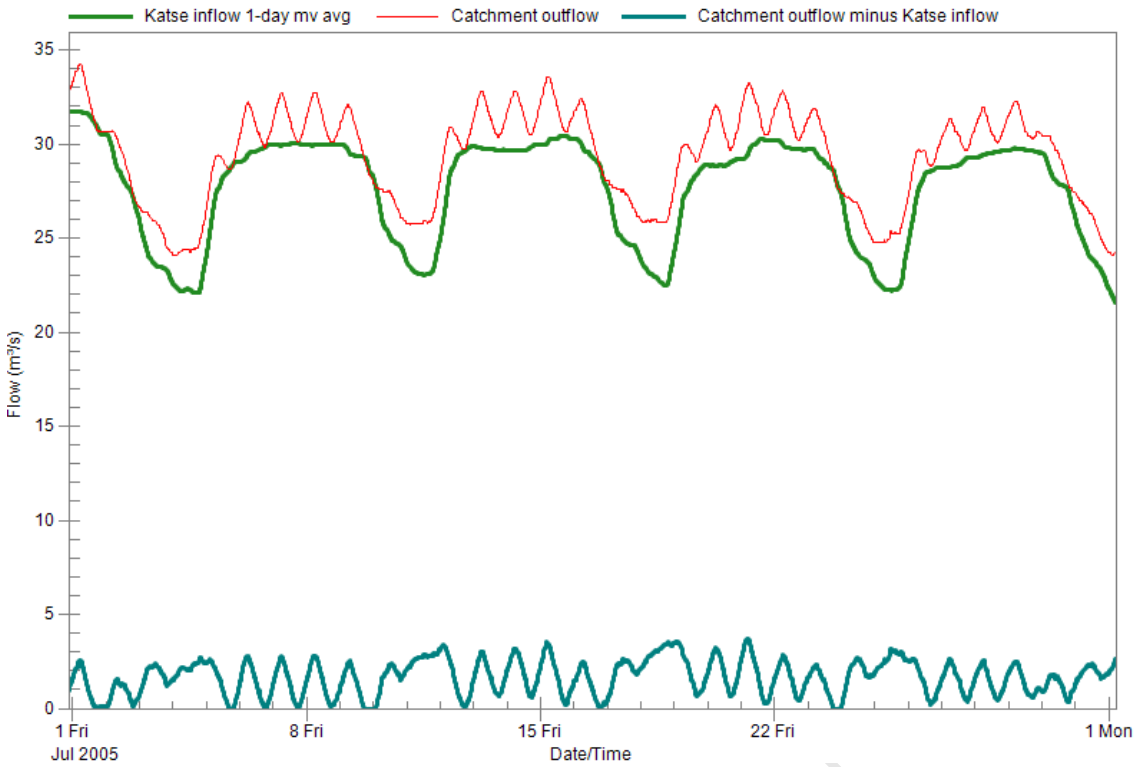

Figure 33: Catchment outflow minus smoothed Katse inflow

Therefore,

estimated surface runoff from rain (m^3)
= 19,710,000 m^3 – 11,730,000 m^3 – mean dry residual (m^3/s) × period of wet period (s)

Table 23 lists the calculated surface runoff volume as a result of rain (from the equation above) for different cut-off values in the calculation of the mean dry residual flow rate, the resulting mean dry residual flow rates, the volumes of the mean dry residual flow during the storm event and the resulting volumes of surface runoff as a result of rain. The last column in Table 23 will be used in the next section to calculate runoff co-efficients.

Table 23: Calculated surface runoff volumes as a result of rain

Cut-off flow rate in mean dry residual flow rate calculation (m^3/s)	Mean dry residual flow rate (m^3/s)	Volume of mean dry residual flow during storm event (m^3)	Estimated surface runoff volume from rain (m^3)
0.00	1.679	1,012,558	6,967,442
0.50	1.717	1,035,475	6,944,525
1.00	1.820	1,097,591	6,882,409

Next, the volume of TRMM estimated rain will be calculated to determine the resulting runoff coefficients.

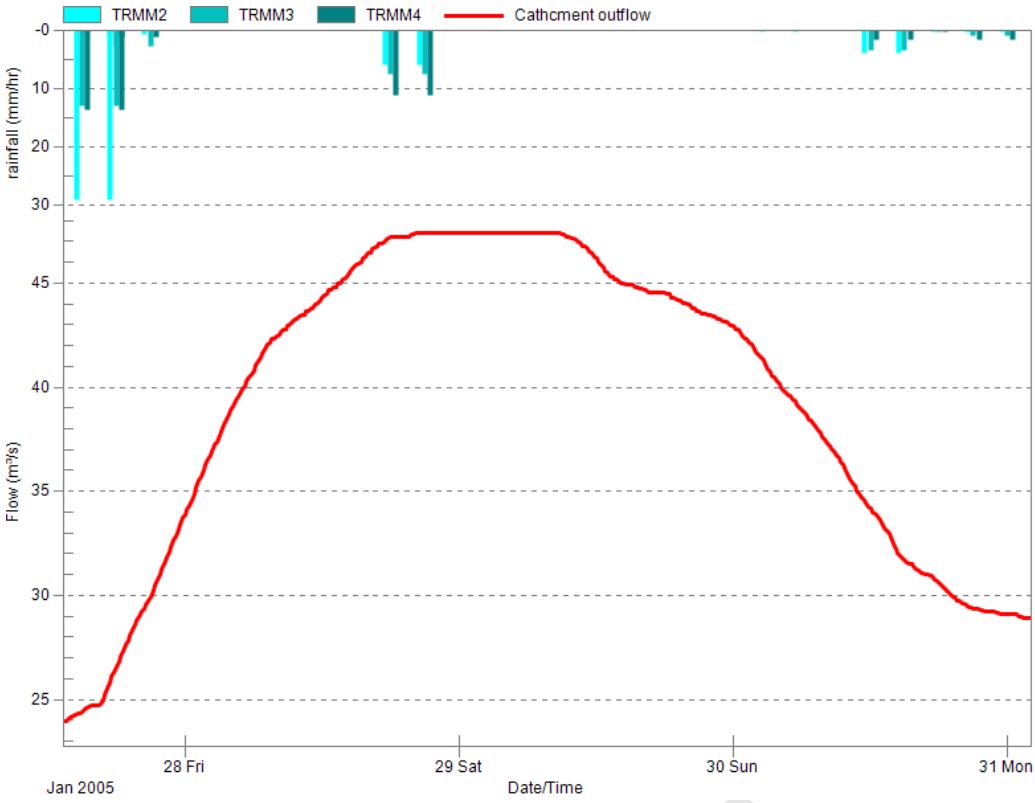

Figure 34: Hydrograph and rainfall during the height of the storm event during 2005

7.4.2.2 Calculating volume of TRMM rainfall estimate

The steps followed to calculate the volume of rain that the 3B42 estimated fell during the selected storm event were:

1. Convert the instantaneous rainfall estimates (mm/h) in the three TRMM cells that overlap the study area to rainfall depths (mm) using the mean of the current instantaneous TRMM reading and the previous instantaneous TRMM reading and multiplying this mean by the time elapsed between the two readings. Fulton et al. (1998) suggest this method for converting instantaneous rainfall to rainfall depth.
2. Sum the rainfall depths for the storm period in each TRMM grid cell.
3. Find the area of the intersection between the TRMM grid cell and the study area in m^2.
4. Convert the rainfall to volume by multiplying the rainfall depth in each TRMM grid cell by the intersection area.
5. Sum the resulting three volumes (from the three TRMM grid cells) to get the total volume of rain that fell during the storm period.

Following the above steps, the volume of rain that fell during the storm period is 83,613,891 m^3. From this value and the calculated volume of surface runoff determined in the previous section, one can now calculate the runoff coefficient. Table 24 shows the result for the different values of calculated surface runoff (the last

column in Table 23) and the runoff coefficient is greater than 0.08 in all cases. This is much larger than the available runoff coefficient from literature for this catchment: 0.033 to 0.063 (Midgley et al., 1994).

Table 24: Runoff coefficient required to balance TRMM rainfall volumes

Estimated surface runoff volume from rain (m^3) (from Table 23)	TRMM rain volume (m^3)	Required runoff coefficient to balance TRMM rain volumes
6,967,442	83,613,891	0.083
6,944,525	83,613,891	0.083
6,882,409	83,613,891	0.082

The SWMM calibrated model 2 (with parameters adjusted to literature values) has a runoff coefficient of 0.033 (values for individual subcatchments ranged from 0.031 to 0.040), which is very close to within the literature range. The recalibrated model with the total flow volume closely approximating the measured flow volume (see Section 7.4.1.2 on page 82) has a runoff coefficient of 0.040 (values for individual subcatchments range from 0.038 to 0.047), which is within the literature range.

Figure 35 compares the ranges of the modelled and calculated runoff coefficients to the known range for this catchment from literature. In the figure, 'SWMM model 2' refers to the SWMM calibrated model 2 with infiltration and roughness parameters adjusted to literature values and 'SWMM 2 recal.' refers to the latter recalibrated with the total flow volume closely approximating the measured flow volume.

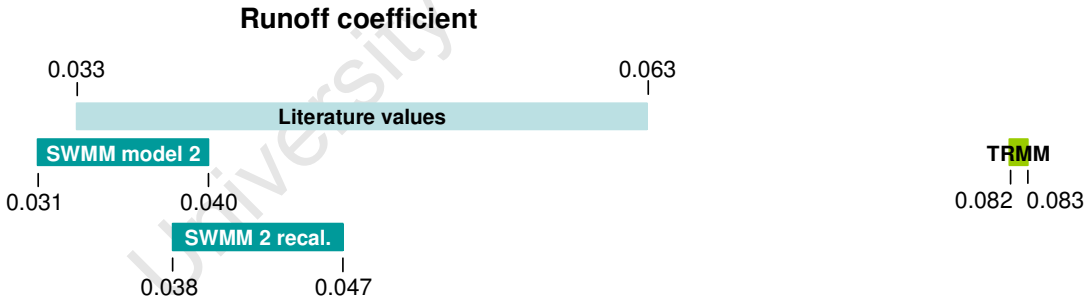

Figure 35: Comparing runoff coefficients

From Figure 35 it is clear that the TRMM rainfall estimates require a runoff coefficient outside of the known range for the study area to account for the surface runoff, while the SWMM models come close to, or are inside of the range.

7.5 Concluding remarks

Section 7 details the chosen modelling periods, how the TRMM rainfall estimates compares with gauge rainfall measurements and the results of the SWMM model runs. The SWMM model did not perform well

enough during the wet season for a flood monitoring system and so Section 7.4 presents the results of an additional investigation to test the model and the TRMM SBRE. From this investigation one can conclude that the SWMM model follows physical principles and that the TRMM SBRE rainfall volumes result in a runoff coefficient far removed from the known and accepted range for the study area.

8. Discussion

The purpose of this project was to determine if it is possible to use only free data available on the Internet as input to a hydrological model and to use the model into a real-time flood monitoring system. This chapter discusses the extent to which the study achieved this purpose and recommends avenues for research that arise from these results.

8.1 Hypotheses

8.1.1 Hypothesis 1

The first hypothesis that this study tested was to see if sufficient hydrological data for the study area are available on the Internet to satisfy a free and open source hydrological model. The results of this study indicate that this hypothesis should be accepted. The chosen hydrological model, SWMM, is free and open source and free data available from the Internet could satisfy all its input requirements, albeit for a coarse model. These input requirements are: catchment boundaries, river lines, DEM (for slope and elevation data), soil texture, land use, rainfall, evaporation rates and flow data. SWMM models of natural channels conventionally use river profiles, which require very detailed topographic data of the channels at closely spaced intervals. These profiles could not be derived from the available data sources, but the profiles were successfully approximated with a trapezoidal geometry. This assertion is supported by the fact that the model performed best during dry periods when only channel flow influences the model.

An important dataset for the model – the Saulspoort dam hydrological survey – was not available on the Internet, but it was available for free from DWA. In the absence of such a survey one could use an estimated storage table or a storage function. This researcher felt that it was important not to ignore available information.

8.1.2 Hypothesis 2

The second hypothesis that this study tested was to see if the hydrological model can predict the flow in the study area with an N-S correlation of 0.8 or better between observed and calculated flow. The results of this study indicate that this hypothesis should be rejected because, even if one adopts a continuous modelling strategy (use just the calibrated model), the required N-S correlation could not be achieved during the summer months when floods are most likely to occur.

The further work done on testing the SWMM model and the TRMM 3B42 data suggests that the model follows physical principles and that it can be calibrated with the total flow volume as objective function to very close to the measured flow volume without much adjustment. In other words, the parameters of the model are still close to physically realistic. So, the model can accurately calculate the total volume of flow in a wet

period, but it cannot accurately represent the shape of the hydrograph for the same period. The N-S correlation measures how well the shape of the calculated hydrograph matches that of the measured hydrograph and this statistic is below the standard set for this project during the wet season.

Furthermore, the SWMM model performs above the set standard during the dry season when it models only channel flow; no rain is present to generate overland flow. However, this part of the model contains the least accurate data and the most estimates of SWMM model object properties. These factors suggest that the inadequate performance of the model stems from the rainfall data, be it the resolution (spatial and temporal) or the accuracy of the TRMM 3B42 data.

Because the SWMM model could not adequately model the shape of the measured output hydrograph, a real-time flood monitoring system could not be implemented using the combination of input data and model at the time and spatial scales studied in this project.

8.2 Conclusion

The amount of data available on the Internet to use as input for hydrological models is impressive. Rainfall estimates and DEMs derived from sensors mounted on satellites have created new possibilities for applying these data to real-world problems, such as disaster risk management. However, at the moment the spatial and temporal scales of these data, as well as their accuracy, probably limit such applications to larger study areas. Larger catchments have longer response times and therefore modelling at longer time steps might still be useful in such cases.

Hydrological modelling is a specialist field and much of the time available for this project was spent to process the background information needed to select and build a model. A model that requires less physical data may be more suited to study areas with limited available information, but overall SWMM met most of the requirements set initially for this project. Without inundation modelling, it is difficult to visualise the results of a hydrological model, but the predicted flow values in comparison to a statistical measure of past flows could still be useful. Without the requirement for distributed results, the selection of models become larger, but even so, none of the models evaluated for this project are possibilities without some modifications. For example, one could use the USDA-NRCS-CN method, but would have to separately route the Katse inflow to the catchment outlet and combine this hydrograph with the routed surface runoff. The data-based mechanistic (DBM) approach, which uses a general linear transfer function to relate rainfall to discharge, seems like a good approach in the absence of detailed physical data about a catchment. In this approach, the data determines the mathematical form of the model instead of using the physical processes involved in transporting and storing water to determine the mathematical form of the model. However, the only implementation of this method known to this researcher is the Matlab Captain Toolbox. Neither Matlab nor Captain Toolbox is free, and thus do not satisfy the objectives of this study.

The current DEMs available on the Internet are inadequate to model flood inundation for all but the largest South African rivers. However, the CSIR is creating a 5 m digital terrain model for the whole country, but at the time of this study they had not completed the terrain model for this project's study area and progress with the 5 m terrain model depends on the CD:NGI's progress with 0.5 m ground pixel resolution aerial photography and resulting 5 m contour data (Breytenbach, A, 2010, pers. comm., 4 October). A terrain model at such fine spatial resolution would open up many possibilities for hydrological modelling at smaller scales, provided that its relative elevations are accurate to within 0.5 m.

8.3 Recommendations

Smaller municipalities with limited resources would typically need to model smaller catchments, and so research at the scale investigated here is useful. To improve the performance of a SWMM model applied to this size catchment would require better data, of which the most important are the rainfall and the DEM.

Rainfall data at better spatial and temporal resolutions will improve the model's performance in wet periods. SBRE have the advantage that the flood cannot wash away the sensor. A study that produces a fine spatial and temporal scale error model for the SBRE that cover South Africa can help to adjust the estimates to more accurate values. This would require extensive ground-based data at good spatial and temporal resolutions. Such a measurement network could be moved from area to area to avoid the costs of covering the whole country at once.

Another source of better rainfall data is radar rainfall data from the SAWS. However, a modelling project that uses radar rainfall data would require careful planning because the SAWS's radar rainfall retrieval and storage system is not set up to easily access historical data. The radar data will therefore have to be retrieved in real time and stored to later construct and calibrate the model. Once the model is calibrated, hotstart files will enable real-time modelling and flood warnings.

An alternative to radar rainfall data is for local councils to invest in a rain gauge network, such as most of the metropolitan areas already have. If councils cannot practically maintain such a network over time, it may be used in the shorter term to calibrate the SBRE that covers the area. SBRE can then be used in place of the gauge data. Local municipalities who often experience flooding may find that the early warning of a real-time flood monitoring system has a positive return on investment if such a system enables them to prevent flood damage by removing people and assets from areas that are about to be flooded.

The CSIR is creating a 5 m DEM for the whole country and DEM at such fine spatial resolution would improve the SWMM model's performance and application. If the DEM accurately captures river valleys and profiles, the profiles could be used to model the rivers in the SWMM model, rather than the trapezoids that are currently used. A DEM with accurate river valleys will enable flood inundation modelling. Future re-

search could investigate the accuracy of the 5 m DEM to evaluate its use for river profiling and inundation modelling.

Ideally, a model used for real-time flood forecasting should correct itself with every new set of information, as the Lambert ISO model does. Unfortunately the assumptions of this model limit its use to very small catchments and future research may focus on adapting the Lambert ISO model to eliminate the assumptions that limit it to small catchments. Statistical rainfall-runoff models may also prove a productive avenue to explore, since they require no information about the physical properties of the catchment. Critics of statistical models think that these models bypass the need to understand the physical process involved, but a flood warning system that can accurately predict flow from past statistics could be useful for under resourced authorities who have to manage the effects of disasters.

References

Alertnet (2011), *Pakistan floods 2010 -Worst floods in living memory*. Retrieved 04 November 2011 from http://www.trust.org/alertnet/crisis-centre/crisis/pakistan-floods-2010

Artan, G, Hussein, G, Smith, J, Asante, K, Bandaragoda, C and Verdin, J (2007) 'Adequacy of satellite derived rainfall data for stream flow modeling' *Natural Hazards* vol. 43 no. 2 pp.167–185. Retrieved 17 February, 2010 from http://www.springerlink.com/content/w1t23705v821j142/fulltext.pdf

Asante, K, Macuacua, R, Artan, G, Lietzow, R and Verdin, J (2007) 'Developing a Flood Monitoring System From Remotely Sensed Data for the Limpopo Basin' *IEEE Transactions On Geoscience And Remote Sensing* vol. 45 no. 6 pp.1709–1714. Retrieved February 10, 2010 from http://ieeexplore.ieee.org/stamp/stamp.jsp?tp=&arnumber=4215028&isnumber=4215027

Ba, A (2008) *An Overview of Satellite-Based Rainfall Techniques,* Sixth NOAA-CREST Symposium, Mayagüez, Puerto Rico, February 20-22, 2008. Retrieved June 14 from http://ece.uprm.edu/noaa-crest/Symposium_08/presentations/page3/files/BA_CREST_SYMPOSIUM.pps

Baldassarre, G, Schumann, G and Bates, P (2009) 'Near real time satellite imagery to support and verify timely flood modeling' *Hydrological Processes* vol. 23 no. 5 pp.799–803. Retrieved 27 January, 2010 from http://www3.interscience.wiley.com/cgi-bin/fulltext/121634418/PDFSTART

Barco, J, Wong, K and Stenstrom, M (2008) 'Automatic Calibration of the U.S. EPA SWMM Model for a Large Urban Catchment' *Journal of Hydraulic Engineering* vol. 134 no. 4 pp.466–474. Retrieved 25 May 2011 from http://web.ebscohost.com.ezproxy.uct.ac.za/ehost/pdfviewer/pdfviewer?sid=f05212a0-cb6b-4217-9bf5-c3bfe5d8a444%40sessionmgr113&vid=2&hid=111

Beven, K (2001), *Rainfall-Runoff Modelling The Primer*, John Wiley & Sons, England.

Chen, J and Adams B (2007) 'Development of analytical models for estimation of urban stormwater runoff', *Journal of Hydrology* vol. 336 no.3–4 pp.458– 469. Downloaded 25 May 2011 from http://www.sciencedirect.com.ezproxy.uct.ac.za/science?_ob=MImg&_imagekey=B6V6C-4MWXR1X-2-1&_cdi=5811&_user=635696&_pii=S0022169407000479&_origin=&_coverDate=04%2F07%2F2007&_sk=996639996&view=c&wchp=dGLbVzb-zSkWA&md5=161ddb5887792e7bc156c0e27dd68555&ie=/sdarticle.pdf

Chen, J, Hill, A and Urbano, L (2009) 'A GIS-based model for urban flood inundation' *Journal of Hydrology* vol. 373 no. 1–2 pp.184–192. Retrieved 5 March 2010 from http://www.sciencedirect.com.ezproxy.uct.ac.za/science?_ob=MImg&_imagekey=B6V6C-4W6XYM0-6-C&_cdi=5811&_user=635696&_pii=S0022169409002546&_origin=gateway&_coverDate=06%2F30%2F2009&_sk=996269998&view=c&wchp=dGLzVzz-zSkzS&md5=ec9ac772394296b80e1da88e02f0aac9&ie=/sdarticle.pdf.

Chung, E-S, Hong, W-P, Lee, K and Burian, S (2011), 'Integrated Use of a Continuous Simulation Model and Multi-Attribute Decision-Making for Ranking Urban Watershed Management Alternatives', *Water Resources Management* vol. 25 no. 2 pp.641–659. Retrieved 7 March, 2011 from http://www.springerlink.com/content/k254445233817250/fulltext.pdf

City of Austen (1997), *Barton Creek Watershed Model Study*, City of Austin Watershed Protection and Development Review Department, Environmental Resources Management Division, Austen, Texas. Retrieved 28 February 2011 from http://www.ci.austin.tx.us/watershed/publications/files/BCWMS.pdf.

Computational Hydraulics International (2010), *PCSWMM Professional v.4.2.914 Help Files*, Computational Hydraulics International, Guelph, Ontario.

Davies, E (2011) *Brisbane faces floods clear-up of "post-war proportions"*. Reuters. Retrieved 12 July 2011 from
http://www.reuters.com/article/2011/01/12/us-australia-floods-idUSTRE6BU09620110112

Department of Science and Technology (2010), *South African Risk and Vulnerability Atlas*. Pretoria. Retrieved 18 February 2011 from
http://www.rvatlas.org/download/sarva_atlas.pdf

El-Sharif, A (1998), *A study of the flooding problem in Truro, NS*, M.Eng. Thesis, Dalhousie University - Daltech, Halifax, Nova Scotia. Retrieved March 7, 2011 from
http://www.collectionscanada.gc.ca/obj/s4/f2/dsk2/ftp03/MQ39648.pdf

ESRI (Environmental Systems Resource Institute) (2009), ArcMap 9.3. ESRI, Redlands, California.

FAO/IIASA/ISRIC/ISS-CAS/JRC, 2009. Harmonized World Soil Database (version 1.1). FAO, Rome, Italy and IIASA, Laxenburg, Austria.

Fulton, R, Breidenbach, J, Seo, D-J And Miller, D (1998), 'The WSR-88D Rainfall Algorithm', *Weather and Forecasting*, vol. 13 no. 2 pp.377-395. Retrieved January 27, 2011 from
http://search.ebscohost.com/login.aspx?direct=true&db=aph&AN=1011996&site=ehost-live

Graham, E, Whiteley, H and Thomson, N (1997) 'Development and Initial Refinement of a Water Balance Model as a Planning Tool for Stormwater Management Application', in James, William (ed.), *Advances in Modeling the Management of Stormwater Impact* Volume 5, Computational Hydraulics International, Guelph, Ontario pp.263–275.

GRASS Development Team, 2008. Geographic Resources Analysis Support System (GRASS) Software. Open Source Geospatial Foundation Project. http://grass.osgeo.org

Green, I and Stephenson, D (1986) 'Criteria for comparison of single event models', *Hydrological Sciences Journal* vol. 31 no. 3 pp.395-411. Downloaded May 25, 2011 from
http://iahs.info/hsj/310/hysj_31_03_0395.pdf

Greer, G (2011) *Australian floods: Why were we so surprised?*. Guardian UK. Retrieved 12 July 2011 from
http://www.guardian.co.uk/environment/2011/jan/15/australian-floods-queensland-germaine-greer

Haarhoff, J and Cassa, A (2009), *Introduction to Flood Hydrology*, Juta, Cape Town.

Herschy, R (1999) 'Flow Measurement' in Hershey, R, (ed), *Hydrometry: Principles and Practices*, Wiley, England,pp.15–78.

Hong, Y, Adler, F, Hossain, F, Curtis, S and Huffman, G (2007) 'A first approach to global runoff simulation using satellite rainfall estimation' *Water Resources Research*, vol. 37 W08502 8 pp. Retrieved 17 February, 2010 from
http://trmm.gsfc.nasa.gov/publications_dir/2007_WRR_TRMM_Global_Runoff.pdf

Horritt, M and Bates, P (2002) 'Evaluation of 1D and 2D numerical models for predicting river flood inundation' *Journal of Hydrology* vol. 268 no. 1–4 pp.87–99. Retrieved 27 January 2010 from
http://www.sciencedirect.com/science?_ob=ArticleURL&_udi=B6V6C-469C5R8-7&_user=635696&_origUdi=B6V6C-44CW075-H&_fmt=high&_coverDate=11%2F01%2F2002&_rdoc=1&_orig=article&_acct=C000033878&_version=1&_urlVersion=0&_userid=635696&md5=c221bc0c21f6220f89a7db2dacf29748

Hossain, F and Anagnostou, E (2004) 'Assessment of current passive-microwave- and infrared-based satellite rainfall remote sensing for flood prediction' *Journal of Geophysical Research* vol. 109 D07102 14 pp. Retrieved 10 February, 2010 from
http://iweb.tntech.edu/fhossain/papers/JGR_Floods.pdf.

Hossain, F, Anagnostou, E and Bagtzoglou, A (2006) 'On Latin Hypercube sampling for efficient uncertainty estimation of satellite rainfall observations in flood prediction' *Computers & Geosciences* vol. 32 no. 6 pp.776–792. Retrieved 27 January 2010 from
http://www.sciencedirect.com/science?_ob=MImg&_imagekey=B6V7D-4HNSJKD-1-Y&_cdi=5840&_user=635696&_pii=S0098300405002311&_orig=search&_coverDate=07%2F31%2F2006&_sk=999679993&view=c&wchp=dGLzVzz-zSkzS&md5=366cffa4c192908723ebb285afab3360&ie=/sdarticle.pdf

Huffman, G (1997) 'Estimates of Root-Mean-Square Random Error for Finite Samples of Estimated Precipitation' *Journal of Applied Meteorology* vol. 36 no. 9 pp.1191–1201. Retrieved 27 July 2011 from
http://journals.ametsoc.org/doi/pdf/10.1175/1520-0450%281997%29036%3C1191%3AEORMSR%3E2.0.CO%3B2

Huffman, G, Adler, R, Bolvin, D, Gu, G, Nelkin, E, Bowman, K, Hong, Y, Stocker, E and Wolff, D (2007) 'The TRMM Multisatellite Precipitation Analysis (TMPA): Quasi-Global, Multiyear, Combined-Sensor Precipitation Estimates at Fine Scales' *Journal of Hydrometeorology* vol. 8 no. 1 pp.38–88. Retrieved 14 June 2011 from
http://journals.ametsoc.org/doi/pdf/10.1175/JHM560.1

Hughes, D (2006) 'Comparison of satellite rainfall data with observations from gauging station networks', *Journal of Hydrology* vol. 327 no. 3–4 pp.399–410. Retrieved 22 February, 2010 from
http://www.sciencedirect.com/science?_ob=MImg&_imagekey=B6V6C-4J91NPN-1-R&_cdi=5811&_user=635696&_pii=S0022169405006256&_orig=search&_coverDate=08%2F20%2F2006&_sk=996729996&view=c&wchp=dGLzVzz-zSkzS&md5=74acdf273794153679bfe89c9e0f2628&ie=/sdarticle.pdf

Hsu, S, Ni; C-F and Hung, P-F (2002) 'Assessment of Three Infiltration Formulas based on Model Fitting on Richards Equation', *Journal of Hydrological Engineering* vol. 7 no 5 pp.373–379. Retrieved 24 August 2011 from
http://140.134.131.73/marko/publications%5CAssessment%20of%20Three%20Infiltration%20Formulas%20based%20on%20Model%28Journal%20of%20Hydrologic%20Engineering%29.pdf

Hydrology Handbook (1996), American Society of Civil Engineers – Task Committee on Hydrology Handbook, New York.

James, W (2005), *Rules for Responsible Modeling*, Computational Hydraulics International, Guelph, Ontario.

James, W, Rossman, L, Huber, W, Dickinson, R, James, WRC, Roesner, L and Aldrich, J (2008), *User's guide to SWMM*, Computational Hydraulics International, Guelph, Ontario.

Jang, S, Cho, M, Yoon, J, Yoon, Y, Kime, S, Kim, G, Kim, L, and Aksoy, H (2007), 'Using SWMM as a tool for hydrologic impact assessment', *Desalination*, vol. 212 no. 1-3 pp.344–356. Retrieved 7 March 2011 from
http://www.sciencedirect.com/science?_ob=MImg&_imagekey=B6TFX-4NX9C8D-16-1&_cdi=5238&_user=635696&_pii=S0011916407002834&_origin=gateway&_coverDate=06%2F25%2F2007&_sk=997879998&view=c&wchp=dGLbVlz-zSkzk&md5=9cc29f44fee2d6dd092b89ff303f1791&ie=/sdarticle.pdf

Jia, Y, Zhao, H, Niu, C, Jiang, Y, Gan, H, Xing, Z, Zhao, X and Zhao, Z (2009) 'A WebGIS-based system for rainfall-runoff prediction and real-time water resources assessment for Beijing' *Computers & Geosciences* vol. 35 no. 7 pp.1517–1528. Retrieved 27 January 2010 from
http://www.sciencedirect.com/science?_ob=MImg&_imagekey=B6V7D-4VHSDH6-2-T&_cdi=5840&_user=635696&_pii=S0098300409000302&_orig=search&_coverDate=07%2F31%2F2009&_sk=999649992&view=c&wchp=dGLzVzz-zSkWz&md5=9b4b82144a96f253625ebb8e244c9d0f&ie=/sdarticle.pdf

Jun, S, Park, J-h, Lee, W, Park, C, Lee, S, Lee, K and Jeong, G-C (2010), 'The changes in potential usable water resources by increasing the amount of groundwater use: the case of Gapcheon watershed in Korea', *Geosciences Journal* vol. 14 no. 1 pp.33−39. Retrieved 7 March 2011 from
http://www.springerlink.com/content/y4535025n3u1013v/fulltext.pdf

Kadlec, R, and Wallace, S (2009), *Treatment Wetlands*, CRC Press , Boca Raton, Florida, USA.

Knebl, M, Yanga, Z-L, Hutchison, K, and Maidment D (2005), 'Regional scale flood modeling using NEXRAD rainfall, GIS, and HEC-HMS/RAS: a case study for the San Antonio River Basin Summer 2002 storm event', *Journal of Environmental Management* vol. 75 no. 4 pp.325–336. Retrieved June 20, 2011 from
http://www.sciencedirect.com.ezproxy.uct.ac.za/science?_ob=MImg&_imagekey=B6WJ7-4FV3614-1-C&_cdi=6871&_user=635696&_pii=S0301479705000228&_origin=browse&_coverDate=06%2F30%2F2005&_sk=999249995&view=c&wchp=dGLzVzz-zSkWl&md5=8296128a66b2e99731c33e89e1aa154f&ie=/sdarticle.pdf

Lacroix, M, Kite, G and Droogers, P (2000). *Using Datasets from the Internet for Hydrological Modeling: An Example from the Küçük Menderes Basin, Turkey*. Research Report 40. Colombo, Sri Lanka: International Water Management Institute. Retrieved January 27, 2010 from
http://www.iwmi.cgiar.org/Publications/IWMI_Research_Reports/PDF/Pub040/Report40.pdf

Levizzani, V, Amorati, R, and Meneguzzo, F (2002), *A Review of Satellite-based Rainfall Estimation Methods*. Retrieved June 14, 2011 from
http://www.geomin.unibo.it/hydro/music/reports/d6.1_satellite%20rainfall%20overview.pdf

Li, L, Hong, Y, Wang, J, Adler, R, Policelli, F, Habib, S Irwn, D, Korme, T and Okello, L (2008), 'Evaluation of the real-time TRMM-based multi-satellite precipitation analysis for an operational flood prediction system in Nzoia Basin, Lake Victoria, Africa' *Natural Hazards* vol. 50 no. 1 pp 109–123. Retrieved 18 April, 2011 from
http://hydro.ou.edu/PUB/LiLi_SERVIR_AFrica_Nzoia.pdf

Li, Z-J and Zhang, K (2008), 'Comparison of Three GIS-Based Hydrological Models', *Journal of Hydrologic Engineering* vol. 13 iss. 5 pp.364–370. Retrieved March 13, 2010 from
http://scitation.aip.org/getpdf/servlet/GetPDFServlet?filetype=pdf&id=JHYEFF000013000005000364000001&idtype=cvips&prog=normal

Lynch, S, (2004), *Development of a raster database of annual, monthly and daily rainfall for southern Africa*, report number 1156/1/04, Water Research Commission, Pretoria. Retrieved 12 July, 2011 from
http://www.wrc.org.za/Knowledge%20Hub%20Documents/Research%20Reports/1156-1-04.pdf

Makwananzi, N and Pegram, G, (2004), *A Flood Nowcasting System For The Ethekwini Metro Volume 2: Modelling Flood Inundation In The Mlazi River Under Uncertainty*, report no. 1217/2/04, Water Research Commission, Pretoria.

Matgen, P, Schumann, G, Henry, J-B, Hoffmann, L and Pfister, L (2007) 'Integration of SAR-derived river inundation areas, high-precision topographic data and a river flow model toward near real-time flood management' *International Journal of Applied Earth Observation and Geoinformation* vol. 9 no. 3 pp.247–263. Retrieved 27 January, 2010 from

http://www.sciencedirect.com/science?_ob=ArticleURL&_udi=B6X2F-4M7CDS5-1&_user=635696&_origUdi=B6V6C-4VGF41K-4&_fmt=high&_coverDate=08%2F31%2F2007&_rdoc=1&_orig=article&_acct=C000033878&_version=1&_urlVersion=0&_userid=635696&md5=59588ab00c890396eb0b84a99811bf4c

Mays, L (2001), *Water Resources Engineering*, John Wiley & Sons, New York.

McIntyre, N and Al-Qurashi, A (2009), 'Performance of ten rainfall–runoff models applied to an arid catchment in Oman' *Environmental Modelling & Software* vol. 24 no. 6 pp.726–738. Retrieved 27 January 2010 from

http://www.sciencedirect.com/science?_ob=MImg&_imagekey=B6VHC-4V462FC-3-1&_cdi=6063&_user=635696&_pii=S1364815208001977&_orig=search&_coverDate=06%2F30%2F2009&_sk=999759993&view=c&wchp=dGLzVtz-zSkzS&md5=c22f97f1b9293c3fe0ac914680f46972&ie=/sdarticle.pdf

Melesse, A, Graham, W and Jordan, J (2003), 'Spatially Distributed Watershed Mapping And Modeling: GIS-Based Storm Runoff Response And Hydroraph Analysis: Part 2', *Journal of Spatial Hydrology* vol. 3 no. 2 pp.1–28. Retrieved 10 February, 2010 from

http://www.spatialhydrology.com/journal/paper/microclimate/microclimate_2.pdf

Midgley, D, Pitman, W and Middleton, B (1994), *Surface Water Resources of South Africa 1990. Volume II, Drainage Region C, Vaal,. Book of Maps*, report number 298/2.2/94, Water Research Commission, Pretoria.

NASA (2008), MCD12Q1 Land cover type, MCD12Q1.A2008001.h20v11.005.2009338162324.hdf, Collection 3, USGS, Reston, VA, USA, 2008-01-01 to 2008-12-31.

National Geographic, n.d., *Floods*. Retrieved 12 July 2011 from

http://environment.nationalgeographic.com/environment/natural-disasters/floods-profile

Neteler, M and Mitasova, H (2008), *Open Source GIS: a GRASS GIS Approach*, Springer, New York.

Nye, T, Dickinson, R, Thompson, M, Schmidt, M, Martin, V and Peralta, G (2005) 'Continuous Surface Runoff, Groundwater, and Water Quality Modeling of the C100 Basin, Miami-Dade County, Florida', in James, W, Irvine, K, McBean, E and Pitt, R (eds.), *Effective Modeling of Urban Water Systems* Volume 13, Computational Hydraulics International, Guelph, Ontario pp.101–116.

Pegram, G and Sinclair, S (2002), *A Linear Catchment Model for Real Time Flood Forecasting*, report number 1005/1/02, Water Research Commission, Pretoria.

Pomeroy, C, Postel, N, O'Neill, P and Roesner, L (2008), 'Development of Storm-Water Management Design Criteria to Maintain Geomorphic Stability in Kansas City Metropolitan Area Streams' JOURNAL OF IRRIGATION AND DRAINAGE ENGINEERING vol. 134 iss. 5 pp.562–566. Retrieved March 7, 2011 from

http://web.ebscohost.com/ehost/pdfviewer/pdfviewer?hid=15&sid=338381d7-c243-48a4-92e9-e9b69aa796c8%40sessionmgr14&vid=2

Quantum GIS Development Team, 2011. Quantum GIS Geographic Information System. Open Source Geospatial Foundation Project. http://qgis.osgeo.org

Raymond, M and Sapiano, P (2010) 'An evaluation of high resolution precipitation products at low resolution', *International Journal of Climatology* vol. 30 iss. 9 pp.1416–1422. Retrieved July 27, 2011 from
http://onlinelibrary.wiley.com.ezproxy.uct.ac.za/doi/10.1002/joc.1961/pdf

Rodriguez, E, Morris, C, Belz, J, Chapin, E, Martin, J, Daffer, W, and Hensley, S (2005), *An assessment of the SRTM topographic products*, Technical Report JPL D-31639, Jet Propulsion Laboratory, Pasadena, California, 143 pp. Retrieved 12 July, 2011 from
http://www2.jpl.nasa.gov/srtm/SRTM_D31639.pdf

Schmidt, M, Cunningham, B and Mack, B (1997) 'The Feasibility of Using Continuous SWMM for Water Resources Conservation Planning', in James, William (ed.), *Advances in Modeling the Management of Stormwater Impact* Volume 5, Computational Hydraulics International, Guelph, Ontario pp.101–116.

Schultz, G (1996), 'Remote sensing applications to hydrology: runoff' *Hydrological Sciences* vol. 41 no. 4 pp.453–475. Retrieved 2 February, 2010 from
https://www.itia.ntua.gr/hsj/41/hysj_41_04_0453.pdf

Shaban, A, Robinson, C and El-Baz, F (2009) 'Using MODIS images and TRMM data to correlate rainfall peaks and water discharges from the Lebanese coastal rivers', *Journal of Water Resource and Protection* vol. 1 no. 4 pp.227–236. Retrieved 6 May, 2010 from
http://find.galegroup.com/gtx/retrieve.do?contentSet=IAC-Documents&qrySerId=Locale%28en%2CUS%2C%29%3AFQE%3D%28JN%2CNone%2C50%29%22Journal+of+Water+Resource+and+Protection+%28Jwarp%29%22%3AAnd%3ALQE%3D%28DA%2CNone%2C8%2920091001%24&inPS=true&tabID=T002&prodId=AONE&searchId=R1&retrieveFormat=PDF&currentPosition=1&userGroupName=unict&resultListType=RESULT_LIST&sort=DateDescend&docId=A211175874&noOfPages=10

Shamsi, U and Schneider, A (1993) 'GIS Based Hydraulic Model Pictures the Interceptor Future', in James, William (ed.), *New Techniques for Modelling the Management of Stormwater Quality Impacts*, Computational Hydraulics International, Guelph, Ontario pp.415–442.

Sinclair, S (2007), *Spatio-temporal Rainfall Estimation and Nowcasting for Flash Flood Forecasting*, Phd Thesis, University of Kwa-Zulu Natal.

Sinclair, S and Pegram, G (2004), *A Flood Nowcasting System For The Ethekwini Metro Volume 1: Umgeni Nowcasting Using Radar – An integrated Pilot Study*, report number 1217/1/04, Water Research Commission, Pretoria.

Silberbauer, M. J. (2006) *The construction of a hydrologically-correct, annotated 1:500 000 spatial dataset of the rivers of South Africa and contiguous basins - (N/000/00/REH/0701)*. Technical report, Resource Quality Services, Department of Water Affairs and Forestry, Pretoria, South Africa. Retrieved 1 February 2011 from
http://www.dwa.gov.za/iwqs/gis_data/river/River_Report_01.pdf.

Silberstein, R (2006) 'Hydrological models are so good, do we still need data?' *Environmental Modelling and Software* vol. 21 no. 9 pp.1340–1352. Retrieved 27 January 2010 from
http://www.sciencedirect.com/science?_ob=MImg&_imagekey=B6VHC-4H87GPN-2-1&_cdi=6063&_user=635696&_pii=S1364815205001428&_orig=search&_coverDate=09%2F30%2F2006&_sk=999789990&view=c&wchp=dGLzVzz-zSkWz&md5=07493724296aa2d9a0dad12fbfac878a&ie=/sdarticle.pdf

Smakhtin, V, (2001) 'Low flow hydrology: a review' *Journal of Hydrology* vol. 240 no. 3–4 pp.147-186. Retrieved 7 November 2011 from
http://www.sciencedirect.com.ezproxy.uct.ac.za/science/article/pii/S0022169400003401

Smith, D (2011) *South Africa flood death toll rises as government declares 33 disaster zones*. Guardian UK. Retrieved 12 July 2011 from
http://www.guardian.co.uk/world/2011/jan/24/south-africa-flood-death-toll

Solanki, H and Suau, S (1996) 'Reconciliation of Hydrologic Models to Coastal Flatland Watersheds', in James, William (ed.), *Advances in Modeling the Management of Stormwater Impacts*, Computational Hydraulics International, Guelph, Ontario pp.49–63.

Sorooshian, S, Hsu, K-L, Gai, X, Gupta, H, Imam, B and Braithwaite, D (2000), 'Evaluation of PERSIANN System Satellite-Based Estimates of Tropical Rainfall', *Bulletin of the American Meteorological Society* vol. 81 no. 9 pp.2035–2046. Retrieved 24 March, 2010 from
http://web.ebscohost.com/ehost/pdf?vid=1&hid=13&sid=6f666b70-7d89-4b8a-93d1-c4bab9fa5e8d%40sessionmgr14

Storm Water Management Model (SWMM) (2011). Retrieved 24 June 2011 from
http://www.epa.gov/nrmrl/wswrd/wq/models/swmm/

Thomas, A, Chingombe, W, Ayuk, J and Scheepers, T (2010), *A Comprehensive Investigation of the Kuils-Eerste River Catchments Water Pollution and Development of a Catchment Sustainability Plan*, report number 1692/1/10, Water Research Commission, Pretoria.

Tian, Y and Peters-Lidard, C (2010), 'A global map of uncertainties in satellite-based precipitation Measurements' *Geophysical Research Letters*, vol. 37, L24407, 6 pp. Retrieved 27 July 2011 from
http://www.agu.org.ezproxy.uct.ac.za/journals/gl/gl1024/2010GL046008/2010GL046008.pdf

Tropical Rainfall Measurement Mission Project (TRMM) (2011), Daily TRMM and Others Rainfall Estimate (3B42 V6 derived),
http://disc.sci.gsfc.nasa.gov/precipitation/documentation/TRMM_README/TRMM_3B42_readme.shtml

Tsihrintzis; V, John, D and Tremblay, P (1998), 'Hydrodynamic Modeling of Wetlands for Flood Detention', *Water Resources Management* vol. 12 no. 4 pp.251–269. Retrieved 25 May 2011 from
http://www.springerlink.com.ezproxy.uct.ac.za/content/u61367j3h0107871/fulltext.pdf

Tsihrintzis, V and Sidan, C (2008) 'ILLUDAS and PSRM-QUAL predictive ability in small urban areas and comparison with other models', *Hydrological. Processes* vol. 22 no. 17 pp.3321–3336. Retrieved 25 May 2011 from
http://onlinelibrary.wiley.com.ezproxy.uct.ac.za/doi/10.1002/hyp.6914/pdf

USGS (2004), Shuttle Radar Topography Mission, 3 Arc Second scene SRTM32S29E028, Filled Finished 2.0, Global Land Cover Facility, University of Maryland, College Park, Maryland, February 2000.

Van Rossum, G et al., Python Language Website, http://www.python.org/

Vecchiato, P (2011) *Floods may have caused R160bn-worth of damage*. Mail and Guardian. Retrieved 12 July 2011 from
http://mg.co.za/article/2011-01-24-floods-may-have-caused-r160bn-worth-of-damage

Villarini, G and Krajewski, W (2007) 'Evaluation of the research version TMPA three-hourly 0.25° × 0.25° rainfall estimates over Oklahoma' *Geophysical Research Letters* vol. 34 iss. 5, 5 pp. Retrieved 10 May 2010 from
http://www.agu.org/journals/gl/gl0705/2006GL029147/2006GL029147.pdf

Ward, A and Trimble, S (2004), *Environmental hydrology* 2nd ed., Lewis Publishers, Florida.

Whiteaker, T; Robayo; O, Maidment, D; Obenour, D (2006), 'From a NEXRAD Rainfall Map to a Flood Inundation Map' *Journal of Hydrologic Engineering*, vol. 11 iss. 1 pp.37–45. Retrieved 13 April 2011 from

http://www.sciencedirect.com.ezproxy.uct.ac.za/science/article/pii/S0301479705000228

Xie, J, Gray, P, Zettler, D and Yingling, B (1997) 'Modeling Fecal Coliform in Mill Creek', in James, William (ed.), *Advances in Modeling the Management of Stormwater Impact* Volume 5, Computational Hydraulics International, Guelph, Ontario pp.307–320.

Xiong, Y and Melching, C (2005), 'Comparison of Kinematic-Wave and Nonlinear Reservoir Routing of Urban Watershed Runoff', *Journal of Hydrologic Engineering* vol. 10 no.1, 11 pp. Retrieved 25 May 2011 from

http://web.ebscohost.com.ezproxy.uct.ac.za/ehost/pdfviewer/pdfviewer?sid=c7f78a44-92f4-44de-ba79-b83a1be41799%40sessionmgr104&vid=2&hid=111

Yang, D, Koike, T and Tanizawa, H (2004) 'Application of a distributed hydrological model and weather radar observations for flood management in the upper Tone River of Japan' *Hydrological Processes* vol. 18 pp. 3119–3132. Retrieved 27 January 2010 from

http://www3.interscience.wiley.com/cgi-bin/fulltext/109793786/PDFSTART

Ye, W, Jakeman, A and Young, P (1998) 'Identification of improved rainfall-runoff models for an ephemeral low-yielding Australian catchment' *Environmental Modelling & Software* vol. 13 no.1 pp.59–74. Retrieved 10 February 2010 from

http://www.sciencedirect.com/science?_ob=MImg&_imagekey=B6VHC-3TXD9HH-5-1&_cdi=6063&_user=635696&_pii=S1364815298000048&_orig=browse&_coverDate=12%2F31%2F1998&_sk=999869998&view=c&wchp=dGLzVlz-zSkzV&md5=0c9dc407063b0cff34d1398bb0b28d28&ie=/sdarticle.pdf

Appendix A – Soil infiltration characteristics

Table 25 below shows the HWSD mapping units that overlap this project's study area, their soil composition and the infiltration parameters based on these textures and percentages. Literature values for the field capacity come from James et al. (2008), p.734. Literature values for the porosity, suction head and hydraulic conductivity (K_s) come from Mays (2001), p.241. The initial deficit is the porosity minus the field capacity.

Table 25: Soil infiltration characteristics for study area derived from the HWSD

Mapping unit	Soil composition					Porosity (ratio)	Field capacity (ratio)	Suction head (mm)	K_s (mm/h)	Initial deficit (ratio)
	Sandy clay loam	Loam	Sandy loam	Clay	Clay loam					
28323	91%	9%	0%	0%	0%	0.39566	0.24292	271.636	1.671	0.15274
28112	0%	0%	88%	12%	0%	0.45564	0.21256	134.844	9.628	0.24308
28338	91%	9%	0%	0%	0%	0.39566	0.24292	271.636	1.671	0.15274
28340	21%	62%	0%	0%	17%	0.44763	0.24778	582.899	2.593	0.19985
28363	16%	14%	65%	0%	5%	0.44471	0.21052	230.211	7.851	0.23419
28415	0%	20%	0%	0%	80%	0.46380	0.29440	328.820	1.480	0.16940
28433	75%	0%	0%	0%	25%	0.40775	0.26050	216.075	1.375	0.14725
28262	75%	0%	25%	0%	0%	0.4050	0.23050	191.400	3.850	0.17450
28920	16%	14%	70%	0%	0%	0.44416	0.20452	225.276	8.346	0.23964

Appendix B – Manning's *n* values

The following sources were used to determine the land cover in the study area:

- DWA dams (GIS vector)
- DWA rivers (GIS vector)
- CD:NGI inland water (GIS vector)
- CD:NGI land use (GIS vector)
- CD:NGI roads (GIS vector)
- a MODIS 12Q1 land cover type global 500 m grid image (GIS raster)

The following procedure was followed:

1. Buffer rivers to a width of 10 m.
2. Buffer roads to 7.4 m for national routes, 7 m for secondary roads and 6 m for streets (Vleggaar, C, 2010, pers. comm. 28 July).
3. Assign a Manning's *n* value to each land cover type based on literature values. Table 26 below shows the land cover types present in all these layers and the values chosen from literature for each.
4. Convert vectors to rasters.
5. Overlay rasters in the order of the bulleted list above so that the values in the first raster take precedence over the following rasters. This means that the CD:NGI high-resolution data took precedence over the low resolution MODIS data.
6. Convert the final product to a vector layer with Manning's *n* as an attribute.

Table 26: Manning's n *values for overland flow*

Land cove type	Manning's *n*	Source	MODIS land cover code
Aerodrome	0.24	Mays (2001), dense grass in Table 15.4.3 p.617.	NA
Apron	0.01	Mays (2001), asphalt in Table 15.4.3 p.617.	NA
Arterial route	0.01	Mays (2001), asphalt in Table 15.4.3 p.617.	NA
Cemetery	0.01	Mays (2001), gravelled surface in Table 15.4.3 p.617.	NA
Clinic	0.01	Mays (2001), concrete in Table 15.4.3 p.617.	NA
College	0.01	Mays (2001), concrete in Table 15.4.3 p.617.	NA
Cultivated land	0.04	Mays (2001), average of cultivated areas in Table 5.1.1 p.92.	NA
Dam	0.06	Mays (2001), maximum of Major streams Regular section in Table 5.1.1 p.92.	NA
Eroded area	0.01	Mays (2001), bare clay loam eroded in Table 15.4.3 p.617.	NA
Golf course	0.24	Mays (2001), dense grass in Table 15.4.3 p.617.	NA

Land cove type	Manning's *n*	Source	MODIS land cover code
High urban density	0.01	Mays (2001), asphalt in Table 15.4.3 p.617.	NA
Holiday resort	0.13	Mays (2001), 50% dense grass, 50% concrete Table 15.4.3 p.617.	NA
Hospital	0.01	Mays (2001), concrete in Table 15.4.3 p.617.	NA
Hotel	0.01	Mays (2001), concrete in Table 15.4.3 p.617.	NA
Lake	0.06	Mays (2001), maximum of Major streams Regular section in Table 5.1.1 p.92.	NA
Landing strip	0.01	Mays (2001), asphalt in Table 15.4.3 p.617.	NA
Large building	0.01	Mays (2001), concrete in Table 15.4.3 p.617.	NA
Large reservoir	0.06	Mays (2001), maximum of Major streams Regular section in Table 5.1.1 p.92.	NA
Low urban density	0.13	Mays (2001), 50% dense grass, 50% concrete Table 15.4.3 p.617.	NA
Main road	0.01	Mays (2001), concrete in Table 15.4.3 p.617.	NA
Marsh vlei	0.45	Kadlec and Wallace (2009), average of values, p. 40.	NA
National route	0.01	Mays (2001), asphalt in Table 15.4.3 p.617.	NA
Non-perennial pan	0.06	Mays (2001), maximum of Major streams Regular section in Table 5.1.1 p.92.. In summer most likely to have water	NA
Open urban land	0.24	Mays (2001), dense grass in Table 15.4.3 p.617.	NA
Orchard vineyard	0.04	Mays (2001), average of cultivated areas in Table 5.1.1 p.92.	NA
Other access	0.01	Mays (2001), bare clay loam eroded in Table 15.4.3 p.617.	NA
Perennial pan	0.06	Mays (2001), maximum of Major streams Regular section in Table 5.1.1 p.92.	NA
Place of worship	0.01	Mays (2001), concrete in Table 15.4.3 p.617.	NA
Plantation	0.1	Mays (2001), trees, 4. Heavy stand of timber in Table 5.1.1 p.92.	NA
Recreation area	0.19	Mays (2001), 80% dense grass, 20% concrete, in Table 15.4.3, p.617.	NA
Rifle range	0.01	Mays (2001), bare clay loam eroded in Table 15.4.3 p.617.	NA
River	0.05	Mays (2001), average for natural streams in Table 5.1.1 p.92.	NA
Runway	0.01	Mays (2001), concrete in Table 15.4.3 p.617.	NA
School area	0.07	Mays (2001), 50% concrete, 25% bare clay loam eroded, 25% dense grass	NA
Secondary road	0.01	Mays (2001), concrete in Table 15.4.3 p.617.	NA
Sewerage works	0.06	Mays (2001), maximum of Major streams Regular section in Table 5.1.1 p.92.	NA
Street	0.01	Mays (2001), concrete in Table 15.4.3 p.617.	NA
Track footpath	0.01	Mays (2001), bare clay loam eroded in Table 15.4.3 p.617.	NA
Woodland	0.1	Mays (2001), brush, 5. Medium to dense brush in summer in Table 5.1.1 p.92.	NA
Water	0.06	Mays (2001), maximum of Major streams Regular section in Table 5.1.1 p.92.	1
Evergreen needle leaf forest	0.1	Mays (2001), trees, 4. Heavy stand of timber in Table 5.1.1 p.92.	2

Land cove type	Manning's *n*	Source	MODIS land cover code
Evergreen broadleaf forest	0.1	Mays (2001), trees, 4. Heavy stand of timber in Table 5.1.1 p.92.	3
Deciduous broadleaf forest	0.1	Mays (2001), trees, 4. Heavy stand of timber in Table 5.1.1 p.92.	4
Mixed forest	0.1	Mays (2001), trees, 4. Heavy stand of timber in Table 5.1.1 p.92.	5
Closed shrub lands	0.1	Mays (2001), brush, 5. Medium to dense brush in summer in Table 5.1.1 p.92.	6
Open shrub lands	0.06	Mays (2001), brush, 3. Light brush and trees in summer in Table 5.1.1 p.92.	7
Woody savannas	0.13	Mays (2001), range (natural) in Table 15.4.3 p.617.	8
Savannas	0.13	Mays (2001), range (natural) in Table 15.4.3 p.617.	9
Grasslands	0.13	Mays (2001), range (natural) in Table 15.4.3 p.617.	10
Permanent wetlands	0.45	Kadlec and Wallace (2009), average of values , p. 40	11
Croplands	0.04	Mays (2001), average of cultivated areas in Table 5.1.1 p.92.	12
Urban and built up	0.01	Mays (2001), asphalt in Table 15.4.3 p.617.	13
Cropland/natural vegetation mosaic	0.02	Mays (2001), average of cropland and savannas	14
Snow and ice	0.01	Mays (2001), concrete in Table 15.4.3 p.617.	15
Barren or sparsely vegetated	0.01	Mays (2001), bare clay loam eroded in Table 15.4.3 p.617.	16